UNIVERSITÀ DEGLI STUDI DI PADOVA

UNIVERSITA' DEGLI STUDI DI PADOVA

Department of Industrial Engineering DII

Master's Degree in Energy Engineering

Numerical Simulation of CO_2 Reduction to Carbon Monoxide in an Electrochemical Flow Cell

Supervisor: Prof. Anna Stoppato

Co-supervisor:

Dr. Tanja Vidakovic-Koch

Dr. Antonio Sorrentino

Monisha Sivasankaran

Max Planck Institute for Dynamics of Complex Technical Systems

Student

Alireza Akbari, 2043080

Academic Year

2023/2024

Acknowledgements

I express heartfelt gratitude to my parents, brother, and partner for their unwavering support throughout my academic journey, despite the physical distance separating us. Their encouragement and belief in me have been indispensable.

Furthermore, I extend my sincere appreciation to Dr. Vidakovic-Koch, Dr. Sorrentino, and Monisha Sivasankaran for their continual support and invaluable guidance in navigating the complexities of electrochemistry. Their mentorship has not only provided me with inspiration but also deepened my understanding of the subject.

A special acknowledgment is reserved for my supervisor, Professor Anna Stoppato, whose imperturbable availability and guidance have been instrumental in shaping my academic pursuits. Her expertise and willingness to address any queries have been truly invaluable.

To all those mentioned above, and to countless others who have contributed to my journey in myriad ways, I offer my deepest thanks.

Abstract

The primary concern of many nations in recent years has been the rise in CO_2 levels in the atmosphere brought on by the energy sectors' heavy reliance on fossil fuels. Many strategies have been put out to lower the amount of CO_2 in the atmosphere, but because of its high efficiency and scaling potential, the electrochemical CO_2 reduction technique (ERC) has received the most attention. This cutting-edge technique offers the dual benefit of reducing greenhouse gas emissions and promoting the development of renewable energy sources by converting the gas into useful chemicals and fuels. The attractive feature of the process is its capacity to incorporate renewable energy sources, which improves sustainability and reduces the carbon footprint of the energy industry.

Like other technologies, electrochemical cells also possess areas for improvement and potential upgrades. In ERC, where CO_2 becomes a carbon source for the production of renewable fuels/feedstocks there are some limitations in terms of mass transfer. Therefore, this work investigates the electrochemical reduction of CO_2 to CO, with a primary emphasis on examining the impact of mass transfer and the distribution of reactants on the selectivity of the products under different flow cell designs. To acquire such results, COMSOL Multiphysics® software is employed for the simulation, which provides the ability to combine fluid dynamics and electrochemistry meticulously, thereby enabling a comprehensive exploration of a wide parameter space at reduced costs compared to physical experiments. In this thesis, COMSOL Multiphysics® is used to study the effect of flow conditions on ERC at different cell constructions.

Sommario

La preoccupazione principale di molte nazioni negli ultimi anni è stata l'aumento dei livelli di CO2 nell'atmosfera causato dalla pesante dipendenza dei settori energetici dai combustibili fossili. Sono state proposte molte strategie per ridurre la quantità di CO2 nell'atmosfera, ma a causa della sua alta efficienza e del potenziale di scalabilità, la tecnica di riduzione elettrochimica del CO2 (ERC) ha ricevuto la maggior parte dell'attenzione. Questa tecnica all'avanguardia offre il doppio vantaggio di ridurre le emissioni di gas serra e promuovere lo sviluppo di fonti di energia rinnovabile convertendo il gas in sostanze chimiche e combustibili utili. La caratteristica attraente del processo è la sua capacità di incorporare fonti di energia rinnovabile, migliorando così la sostenibilità e riducendo l'impronta di carbonio dell'industria energetica.

Similmente ad altre tecnologie, anche le celle elettrochimiche possiedono aree di miglioramento e potenziali sviluppi. Nell'ERC, dove il CO2 diventa una fonte di carbonio per la produzione di combustibili/materie prime rinnovabili, ci sono alcune limitazioni in termini di trasferimento di massa. Pertanto, questo lavoro indaga la riduzione elettrochimica della CO2 a CO, con un'enfasi primaria sull'esame dell'impatto del trasferimento di massa e della distribuzione dei reagenti sulla selettività dei prodotti sotto diversi disegni di celle a flusso. Per acquisire tali risultati, viene impiegato il software COMSOL Multiphysics® per la simulazione, che ha la capacità di combinare la dinamica dei fluidi e l'elettrochimica consentendo così un'esplorazione comprensiva di un ampio spazio dei parametri a costi ridotti rispetto agli esperimenti in laboratorio. In questa tesi, COMSOL Multiphysics® è utilizzato per studiare l'effetto delle condizioni di flusso sull'ERC in diverse costruzioni delle celle.

Contents

List of Figures

List of Tables

Nomenclature

Abbreviations

CCS	Carbon Capture and Sequestration
ERC	Electrochemical Reduction of CO_2
FE	Faradaic Efficiency
FEM	Finite Element Method
HER	Hydrogen Evolution Reaction
OER	Oxygen Evolution Reaction
CD	Primary Current Distribution
SCD	Secondary Current Distribution
TCS	Tertiary Current Distribution
SHE	Standard Hydrogen Electrode
PDE	Partial Differential Equation
IE	Instant Equilibrium Case
GDE	Gas Diffusion Electrode
RDE	Rotating Disc Electrode
MEA	Membrane Electrode Assembly
TDS	Transport of Dilute Species

CE	Counter Electrode
WE	Working Electrode
PMMA	Polymethylmethacrylate
RE	Reference Electrode
I/O	Inlet and Outlet
EE	Energy Efficiency
RE	Reynolds Number
SHE	Standard hydrogen Electrode

List of Common Symbols

A	Geometric area of the electrode	[m^2]
D	Diffusivity of Species	[m^2 /s]
C	Concentration	[mol/m^3]
α	Anodic Transfer Coefficient	[-]
E	Applied Voltage	[V]
E_{eq}	Equilibrium Potential	[V]
F	Faraday's constant	[C/mol]
i_a	Anode Exchange Current Density	[A/m^2]
i_c	Cathode Exchange Current Density	[A/m^2]
η	Overpotential	[v]

I	Current	[A]
ρ	Density	[kg/m^3]
μ	Dynamic Viscosity	[N.s/m^2]
σ_m	Membrane Conductivity	[S/m]
u_0	Inlet Velocity	[m/s]
T	Temperature	[K]
V_{cell}	Cell Potential	[V]
w_m	Membrane Thickness	[mm]
H	Henry constant	[M/bar]
$\Delta G^0_{reaction}$	Gibbs energy change for the complete reaction	[J/mol]
F	Body Force	[N/m^3]
j	Current Density	[A/m^2]

1

Introduction

Fossil fuels have been the backbone of economic development since the beginning of the Industrial Revolution. They provide most of the world's electricity, power vehicles, ships, and airplanes, and provide energy for industrial processes. This interdependence of economic expansion and fossil fuel consumption has historically led to a parallel increase in greenhouse gas emissions, marking a significant phase in modern economic history. Over the past century, our industrial advancements have perfected the extraction of carbon from the Earth, only to release it as carbon dioxide (CO_2) into the atmosphere. This endless cycle has pushed atmospheric CO_2 levels beyond 422 ppm, Figure 1.1, [1] a figure that cannot be overlooked given its profound implications: rising sea levels, shifting weather patterns, and the daunting challenge of reversing climate change within several hundred years. As CO_2 is a major contributor to greenhouse gas emissions, accounting for about 76% [2] of the total, the attempt to mitigate these emissions has become a global imperative. This is crucial not only to curb the global warming crisis but also to meet the world's escalating energy demands, primarily fed by fossil fuel combustion.

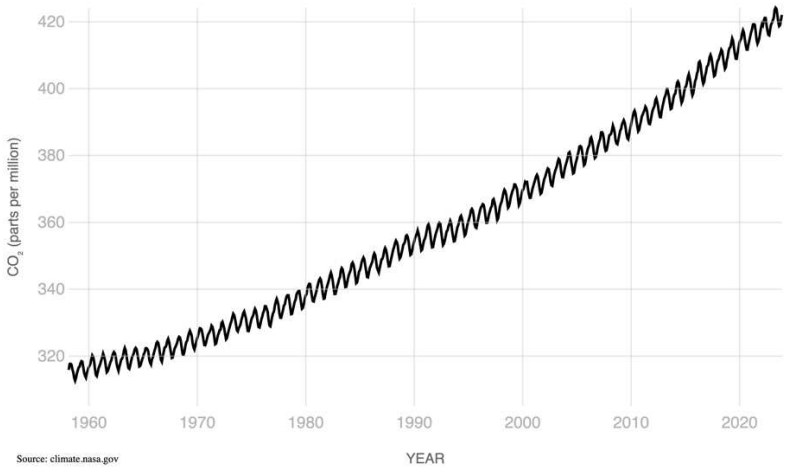

Figure 1.1: Atmospheric CO_2 Concentrations (Parts per Million) from 1960 to 2022 [1]

We are moving away from fossil fuels and toward more sustainable energy sources at this critical juncture. This shift involves reevaluating our attitude toward energy, our economy, and our way of life on the planet rather than merely switching out one energy source for another. It pushes us to be creative, work together worldwide, and envision a future in which environmental sustainability is not sacrificed for progress. To put it plainly, we are learning how to develop in balance with our environment and ensure that the advancements we make today do not jeopardize our future viability.

In response, a myriad of technological solutions has emerged, ranging from Carbon Capture and Sequestration (CCS) to boosting renewable energy usage and enhancing process efficiencies. These solutions reflect our growing recognition of the urgent need to address climate change and the role technology can play in this battle. From the development of more efficient energy systems that minimize waste to the adoption of renewable energy sources that reduce our carbon footprint, each innovation represents a step forward in our efforts for sustainability. These technologies are not just about reducing emissions; they are about changing the way we produce and consume energy, making it cleaner, more sustainable, and more aligned with the needs of our planet.

Amid all the technological solutions popping up to tackle climate change, Electrochemical Reduction of CO_2 (ERC) really catches the eye. It is not just about getting a handle on emissions; it is about reversing conventional views and transforming CO_2, traditionally regarded as waste, into valuable resources. Think about it: all that CO_2 from factories and cars, which is heating up our planet, could be transformed into fuels and chemicals. It is like hitting the jackpot in the world of recycling, turning a big problem into an even bigger opportunity.

ERC works by using some smart science electrochemistry to break down CO_2 into stuff we can actually use, like fuel or even the building blocks for plastics. And the best part? It can run on renewable energy. So, when the sun's shining or the wind's blowing, we can store that extra energy by turning CO_2 into something useful. In addition, it is thermodynamically feasible at near ambient temperatures and pressures. This could mean we do not need to dig up as much oil or coal, which is a win for the planet.

But ERC is not just attractive because it can help us cut down on emissions or because it is a clever way to store renewable energy. It is a game-changer because it represents a whole new way of thinking about how we can live and work without harming the earth. It is about making sure that our solutions to climate change do not just put a band-aid on the problem but get us to a place where the way we make and use things is actually good for the planet [3].

This innovative method uses electrocatalysis at electrode surfaces to convert CO_2 into valuable reduced compounds such as carbon monoxide (CO), formic acid (HCOOH), methane (CH_4), ethylene (C_2H), and various alcohols. Among the various products of electrochemical CO_2 reduction, carbon monoxide (CO) holds a particularly significant role due to its critical function as an intermediary in the synthesis of numerous valuable chemicals and fuels. CO's importance extends beyond its simplicity; it serves as a foundational building block in the industrial chemistry sector, facilitating the creation of complex molecules ranging from hydrocarbons to alcohols. This versatility makes CO an essential feedstock for the chemical industry, enabling the production of methanol, synthetic fuels, and a variety of polymers and fine chemicals through well-established processes such as Fischer-Tropsch synthesis. [4],[5].

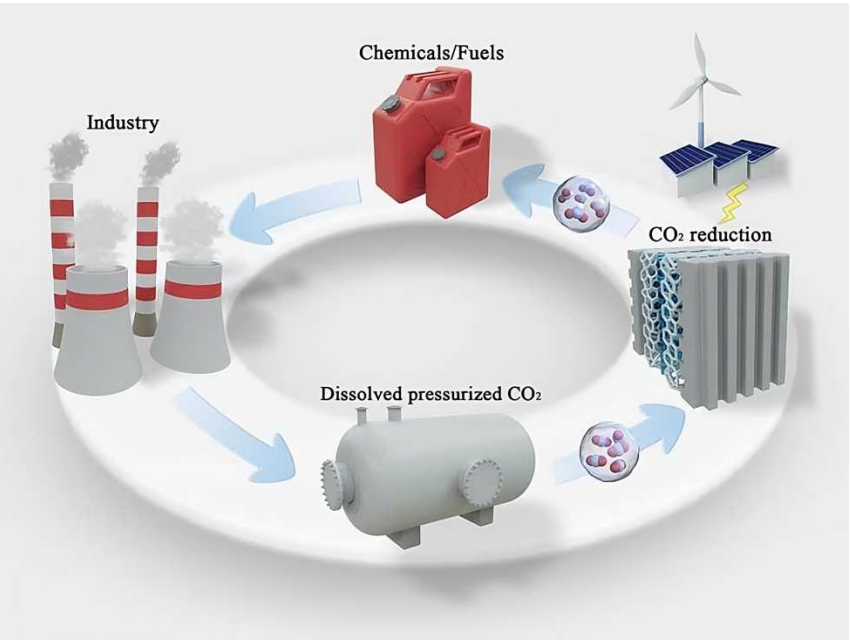

Figure 1.2: A general system level overview of electrohemical CO2 reduction, and its role as carbon neutral cycle[6], [7].

The transformation of CO_2 into CO via electrochemical means represents a pivotal step towards a sustainable industrial ecosystem. By utilizing renewable energy sources to power the conversion, this process aligns with the broader goals of reducing fossil fuel dependence and minimizing carbon footprints. The vision of harnessing CO as a renewable resource is a testament to the transformative potential of electrochemical CO_2 reduction. It not only addresses the immediate challenge of mitigating CO_2 emissions but also lays the groundwork for a future where carbon utilization is optimized within a circular economy framework.

This approach underscores the potential to revolutionize how we perceive and utilize CO_2, transitioning from viewing it as a problematic byproduct of industrial processes to a valuable resource that can be efficiently recycled into useful products. In doing so, it contributes to a more sustainable and carbon-neutral future, where the cycle of carbon is closed through innovative technological solutions, thereby reducing the overall impact on the climate. [8]

1.1. Electrochemical Reduction of CO_2

In the heart of an electrochemical cell, three key players are found: the anode, the cathode, and the membrane. This trio works together in a fascinating dance of chemistry and electricity. One such cell configuration is shown in Figure 1.3. at one end, there is the cathode, and at the other, the anode, with the electrolyte nestled in between. It is here that electrochemical transformations take the spotlight, with ions moving through the electrolyte, bridging the membrane between the anode and cathode. This is not just any setup; it is where carbon dioxide (CO_2) molecules get a makeover at the cathode. Due to the application of an external electric potential, these CO_2 molecules undergo a reduction process, transforming itself chemically.

Meanwhile, over at the anode, water molecules (H_2O) are being oxidized, split into oxygen gas and hydrogen ions (H^+). These hydrogen ions then diffuse through the electrolyte, a crucial pathway to maintain electrical balance across the cell. This whole process is an example of nature's balance. The anode's responsibility is to generate electrons and protons through the oxidation process, while the cathode plays the role of the consumer, eagerly accepting these electrons and protons during the reduction of CO_2. Electrons do not just move around in these cells, their flow is the key to the cell's magic. It lets them change stuff and keep track of energy all at the same time.

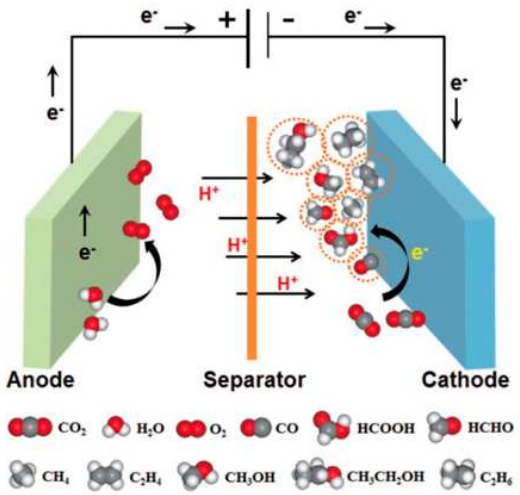

Figure 1.3: A schematic representation of a typical electrochemical cell showing ERC [9]

Figure 1.3 shows that when we look into ERC, we can end up with different products. But, the energy we need to put in can change a lot depending on the product. Table 1.1 gives us a peek at how CO_2 can be broken down, whether in a basic or acidic environment. It shows E_0, which is nothing but the minimum amount of voltage needed for a chemical reaction, measured against a standard called the Standard Hydrogen Electrode at a neutral pH of 7. Even though E_0 tells us the minimum voltage needed, in reality, we usually have to use more potential than what E_0 suggests. This is mainly because CO_2 molecules are stable and the carbon in them do not have any valance electrons. This stability makes breaking CO_2 apart into a high energy demanding process. This energy barrier is further enhanced by the competing Hydrogen Evolution Reaction.

Product	**Cell reaction**	$E^0 VS\ SHE$
	$CO_2 + e^- \dashrightarrow {}^*CO^-_2$	-1.9
Formic Acid/Formate $HCOOH/HCOO^-$	$CO_2\ (aq) + 2\ (H^+ + e^-) \dashrightarrow HCOOH(l)$	-0.61
	$CO_2(aq)+H_2O+2e^- \dashrightarrow HCOO^-(aq)+OH^-$	-0.43
	$CO_2\ (aq) + 2\ (H^+ + e^-) \dashrightarrow CO(g) + H_2\ O(l)$	-0.53

Carbon Monoxide CO	$CO_2(aq)+H_2O+2e^- \longrightarrow CO(g)+2OH^-$	-0.52
Formaldehyde (HCHO)	$CO_2\ (aq) + 4\ (H^+ + e^-) \longrightarrow HCHO(l) + H_2\ O(l)$	-0.48
	$CO_2(aq)+3H_2O+4e^- \longrightarrow HCHO(l)+4OH^-$	-0.89
Methanol (CH_3OH)	$CO_2\ (aq) + 6\ (H^+ + e^-) \longrightarrow CH_3\ OH(l) + H_2\ O(l)$	-0.38
	$CO_2(aq)+5H_2O+6e^- \longrightarrow CH_3OH(l)+6OH^-$	-0.81
Methane (CH_4)	$CO_2\ (aq) + 8\ (H^+ + e^-) \longrightarrow CH_4\ (l) + 2\ H_2\ O(l)$	-0.24
	$CO_2(aq)+6H_2O+8e^- \longrightarrow CH_4(g)+8OH^-$	-0.25

Table 1.1: Some of the possible products of ERC with their respective reduction reactions [56]

As we delve deeper into the fine differences of ERC, it is crucial to understand the efficiency of these electrochemical conversion systems. One key aspect that significantly impacts the performance of these systems is the Faradaic Efficiency (FE), which measures the efficiency with which electrons are converted into desired chemical products.

In this thesis, a relatively understudied dimension is explored: fundamental fluid flow effects on the electrochemical CO_2 reduction reaction (ERC) on a polycrystalline silver catalyst. The focus narrows on the hitherto overlooked influence of mass transport on product distribution and, by extension, product selectivity, a critical yet underexplored area. To better understand these dynamics, flow cell reactor over the traditional rotating disc electrode (RDE) setup was chosen as the model system. As known from the literature, RDE systems have defined mass transport conditions compared to flow cell reactors. Yet, the flow cell reactor possesses enhanced efficiency and scalability, making it more suited for practical applications. This is because of the flow cell reactor's design to accommodate electrons with larger geometric

surfaces which facilitate the attainment of high current densities. For the above reasons, it was of greater interest to study the effect of fluid flow pattern in ERC in a flow cell reactor.

To further this investigation, the capabilities of COMSOL Multiphysics software was used, a robust platform for simulating and analyzing the physics-based interactions within complex systems. This innovative approach marks a pioneering step in considering cell geometry modifications to influence fluid distribution and consequently, mass transport phenomena along the catalyst surfaces. By investigating into the fine differences of how cell geometry affects fluid dynamics, this research aims to shed light on new ways for optimizing electrochemical CO_2 reduction processes. This exploration is not only a testament to the complexity of the challenges at hand but also to the innovative spirit that guides our pursuit of sustainable solutions in the battle against climate change. The novelty of this work emerges from its concentrated examination of the complex interplay between cell design and electrochemical performance.

For the latter, polycrystalline silver foil with planar structure is the chosen catalyst material, because of the idealized surface and exclusion of pore diffusion effects. Bicarbonate 0.1M solution, a common choice in previous studies, was selected as the electrolyte.

The simulation methodology consists of Geometry Simplification, Fluid Dynamic Analysis, Concentration Analysis, and Electrochemical Analysis which is further elaborated in Chapter 4.

2

Literature Review

The interdisciplinary approach of Electrochemical Reduction of CO_2 (ERC) has attracted insights and advancements from diverse research fields. The subsequent section provides an overview of its present state. It systematically categorizes the existing research into critical aspects such as catalysts, electrolytes, and membrane design configurations, which collectively impact the performance of CO_2 reduction processes.

2.1. Catalyst

The work of Abhishek Dey, Sk Amanullah, and Paramita Saha has made a substantial contribution to our understanding of the complex interactions between catalysts' electronic structures and product selectivity in the carbon dioxide reduction reaction (ERC) in the field of chemical catalysis [10]. Their work clarifies the basic connection between catalyst electronic properties and the preferred production of particular products during ERC. They found that catalysts with metal centers rich in electrons tend to produce carbon monoxide (CO), whereas catalysts with metal centers lacking in electrons have a tendency to produce formic acid (HCOOH).

This distinction is essential to improving the selectivity and efficiency of CO_2 conversion processes. However, optimizing CO_2 reduction at modest potentials—that is, enhancing energy efficiency—presents several formidable obstacles. The tendency of many effective CO_2-binding and reducing catalysts to additionally promote the hydrogen evolution process (HER) is one of them. The CO_2 reduction process is put into a competitive dynamic by this simultaneous catalytic activity, which may have a negative impact on the yield of the intended electrochemical reduction of carbon dioxide (ERC) products. This phenomenon emphasizes how difficult it is to create selective and effective catalysts in the context of ERC, emphasizing

the necessity for creative solutions to reduce competing reactions and increase the total yield of useful products.

Further insights from their research highlight the role of the electronic arrangement in the intermediates formed during CO_2 reduction, especially with iron- and cobalt-based complexes. Understanding how these intermediates, particularly the M−COOH intermediate's spin state and electronic structure, affect product formation is crucial. This understanding not only sheds light on the reaction mechanisms but also has profound implications for catalyst design. By designing the electronic structure of these intermediates, it is possible to develop more efficient catalysts that selectively produce desired ERC products, thereby optimizing the process towards more sustainable and energy-efficient outcomes [10].

Building on the momentum of exploring innovative solutions to enhance the efficiency and selectivity of ERC, a groundbreaking study by Rongzhong Jiang, Vijay S. Parameshwaran, Jonathan Boltersdorf, and David R. Baker presents a novel catalyst design that merges the best of both worlds: silver nanoparticles and copper nanowires. This hybrid catalyst, boasting a composition of 37% copper and 63% silver, is adeptly layered onto a gas diffusion layer serving as the cathode electrode in a CO_2 reduction reaction setup. Employed within a zero-gap electrolyzer, this catalyst composition demonstrates notable Faradaic and energy efficiencies, shining across a spectrum of operational temperatures.

This pivotal research reveals the complex dynamics of operating parameters such as temperature and cell voltage on the CO_2 reduction reaction's efficiency and selectivity. Noteworthy is the catalyst's robust stability and the remarkable effect of operational pauses on product yields. Introducing breaks in electrolyzer activity, notably a rest day, resulted in a significant shift in product distribution, favoring C-C coupling reactions and thereby enhancing the yield of desired products. This observation underscores the potential of operational strategies to influence electrochemical pathways and product outcomes.

Delving deeper, the study articulates two critical advancements in the realm of CO_2 electroreduction: the development of ideal electrochemical catalysts and the optimization of electrochemical reactors. The proposed network of nanomaterials, with their expansive active

surfaces and distinctive nanostructures, facilitates swift mass, electron, and ion transfers, while ensuring heightened electrochemical activity and stability. Moreover, the adoption of a zero-gap cell configuration, characterized by its ultra-thin electrolyte membrane (less than 40 µm), emerges as a highly efficient reactor design, poised to meet the electrolysis rates demanded by industrial-scale production. [11]

In another work also Sichao Ma, Yangchun Lan, Gaby M. J. Perez, Saman Moniri, and Paul J. A. Kenis used the silver supported on titania (Ag/TiO2) as a catalyst for the electrochemical reduction of carbon dioxide (CO_2). The challenge identified in the research was the high overpotential and insufficient current density observed in most electrocatalysts used for CO_2 reduction, which results in reduced energy efficiency. To address this, the study proposed the use of Ag nanoparticles supported on TiO_2, which was shown to have better performance compared to Ag supported on carbon black (Ag/C). They also discussed the synthesis of Ag/TiO_2 and compares its electrochemical performance for CO_2 reduction to CO with that of well-studied Ag nanoparticle catalysts. They highlighted the significant finding that 40 wt % Ag/TiO2 demonstrates a twofold higher current density for CO production compared to Ag/C. The catalyst boasted over 90% Faradaic efficiency for CO with a notably high mass activity, suggesting that TiO_2 not only supports but also possibly facilitates CO_2 reduction by serving as a redox electron carrier. [12]

2.2. Membrane

In a compelling study, Lien-Chun Weng, Alexis T. Bell, and Adam Z. Weber delve into the potential of membrane-electrode assemblies (MEAs) for the electrochemical reduction of CO_2, highlighting their advantages in terms of low ohmic losses and enhanced energy efficiency. The research identifies how full-MEAs encounter limitations due to ohmic resistance, particularly as membranes dehydrates with rising cell temperatures, thus affecting water mass transport.

The paper underscores the necessity for high current densities (above 100 mA cm^2) and minimized power input for the commercial viability of CO_2 reduction, with gas-diffusion electrodes (GDEs) offering promising solutions by concentrating CO_2 locally and reducing mass-transfer resistances. MEAs, by eliminating aqueous electrolyte compartments and employing an ionomer as both separator and electrolyte, effectively decrease the ohmic

overpotential, showcasing their superiority over planar cells in efficiency and performance at high current densities. Additionally, this study not only highlights the technological advancements in MEA designs for CO_2 reduction but also addresses the challenges and potential solutions, marking a significant step forward in the development of efficient, scalable electrochemical CO_2 reduction technologies. [13]

In another study Morgan M Monroe, Peter Lobaccaro, Yanwei Lum, and Joel W Ager introduced a membraneless laminar flow cell designed for efficient product separation in electrochemical processes. The innovative aspect of this cell lies in its utilization of a co-laminar flow regime, where CO_2 saturated electrolyte (catholyte) and anolyte streams flow adjacently in a single channel without the need for a membrane, thus avoiding physical barriers. The cell's design, featuring a co-laminar flow and a strategic Y-split at the channel's end, ensures that separation of reduction products and anolyte occurs efficiently, leveraging the laminar flow's nature to prevent turbulence and mixing. The membraneless approach offers multiple advantages, including reduced ohmic losses, lower costs, simpler design and operation, improved scalability, enhanced product purity, and ease of product collection, alongside increased durability, and longevity.

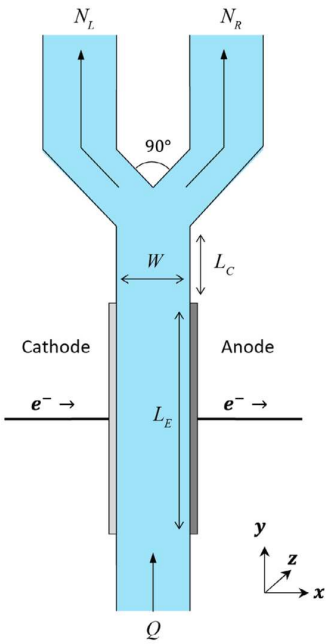

Figure 2.1. Cross section view of the Y-channel geometry of the laminar CO2 reduction flow cell. CO2 saturated water enters at the bottom of the device at flow rate Q. Liquid products are generated at the cathode and O2 is generated at the anode via water oxidation. The Y-split at the top of the figure divides the flow into two channels; reduced products are concentrated in the left-hand (cathode) channel. [14]

2.3. Electrolyte

Aqueous electrolytes containing K+, Na+ cations and HCO−3, OH− anions cover a vast majority of the literatures. The presence of electrolyte lowers the CO_2 solubility in water due to "salting-out" effect [15] [16] the effect of cation and anion solvation which leaves lesser water molecules for dissolving CO_2. On the other hand, more recently, ionic liquids have been found not only to have higher CO_2 solubility and electrical conductivity but also to reduce the reaction overpotentials [17]. However, their production cost limits their widespread usage [18].

Alvarez et al extensively reviewed the usage of ionic liquids in electrochemical processes [19]. Apart from improving the conductivity, electrolytes have been shown to act as a co-catalyst, consequently altering the product selectivity. Electrolytes modulate the selectivity through their composition, concentration [20]. In addition to this, it was Murata et al. [21] who have shown that the choice of cation between Li+, Na+, K+, Cs+ remarkably alters the product selectivity on Cu electrodes. Similar results have been reported on Ag electrode showing higher selectivity towards CO with heavier cations [22].

2.4. Cell design

In an effort to enhance the efficiency and selectivity of electrochemical CO_2 reduction processes, our discussion has primarily focused on the importance of catalyst composition, operational parameters, and the innovative design of membrane. Although Michael Filippi and his colleagues designed the catholyte compartment, Linear wide, Shifted, Serpentine, and Linear, in which the bubble formation and local PH level is controlled by changing velocity, they missed an important part, to design the cell with different inlets and outlet configurations.

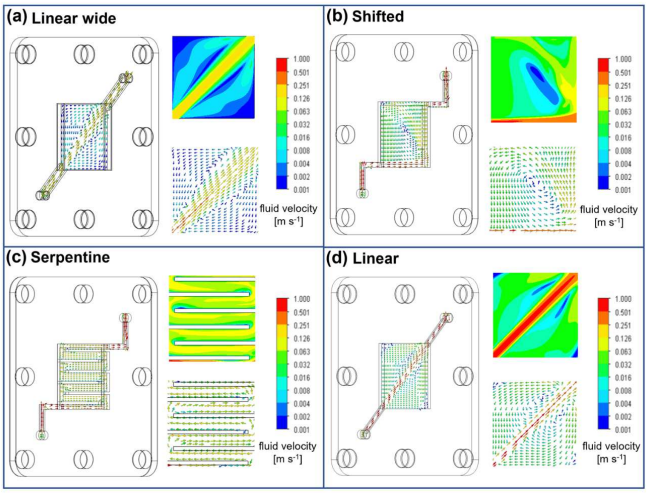

Figure.2.2- CFD simulation results of studied flow compartment geometries.

Yet, it is crucial to acknowledge that these elements operate within a broader ecosystem of factors influencing the outcome of electrochemical reactions. One such axial aspect that often goes underexplored is the role of fluid distribution and mass transport dynamics across the catalyst surfaces along with laminar and turbulent fluid dynamics. The geometry of the electrochemical cell, far from being a mere structural consideration, has a profound impact on how reactants are delivered to, and products are removed from the active sites of the catalyst. This, in turn, significantly affects the selectivity of the reaction and the efficiency with which electrons are utilized in forming desired products [23].

3

3.1. Theory

This chapter emphasizes several key concepts and equations from electrochemistry, homogeneous chemical reactions, and fluid dynamics that are crucial for realizing the subtleties of electrochemical flow cells. These foundational elements are vital for the subsequent simulation, development, and examination of models.

3.1.1 Thermodynamics

Thermodynamics serves to characterize the properties of electrode reactions when in equilibrium, enabling the prediction of a reaction's probability and the amount of energy it will emit or consume. The standard Gibbs free energy change of a reaction is an important parameter in electrochemistry that can be used to determine whether a reaction is spontaneous. A spontaneous reaction is one that will occur on its own without the need for any external input of energy. The standard Gibbs free energy change of a reaction is expressed using equation 3.2. This can be conveniently related, using Faraday's constant (F), to the standard electrode potential (E0), as shown in equation 3.3. The Gibbs free energy determines the minimum required potential to initiate the electrode reaction. When the value is positive it means that the reaction is non-spontaneous ($\Delta G^0_{reaction} > 0$) while when its value is negative, it indicates that the reaction is spontaneous ($\Delta G^0_{reaction} < 0$).

$$O + ze^- \rightarrow R \tag{3.1}$$

$$\Delta G^0_{reaction} = \sum \Delta G^0_{f,R} - \sum \Delta G^0_{f,O} \tag{3.2}$$

$$\Delta G^0_{reaction} = -zFE^0 \tag{3.3}$$

Here we have,

ΔG^0 is Standard Gibbs Free Energy Change [J/mol]. z is Ionic Charge [-]

F is Faraday's Constant [C/mol] E^0 is Standard Potential [V]

O is Oxidizing Species [-] R is Reducing Species [-]

When the concentrations of the oxidized and reduced species are not both 1 M (non-standard conditions or different temperature or pressure), the standard electrode potential (E_0) needs to be adjusted using the Nernst equation 3.4:

$$E_{eq} = E^0 + \frac{RT}{zF} In \frac{a_O}{a_R} = E^0 + \frac{RT}{zF} Ln \frac{\gamma_o c_o}{\gamma_R c_R} \quad 3.4$$

Here we have,

E_{eq} is Equilibrium Potential [V] a is Species Activity $[mol/m^3]$

R is Gas Constant [J/(mol-K)] γ is Activity Coefficient [-]

T is Temperature [K] c is Species Concentration $[mol/m^3]$

Overcoming the energy barrier for ERC often demands exceeding the equilibrium potential (E_{eq}). This excess voltage($E - E_{eq}$), referred to as overpotential (η), is commonly described as follows by equation 3.5, and 3.6:

$$\eta = E - E_{eq} = \eta_{act} + \eta_{conc} \quad 3.5$$

$$\eta_{conc} = \frac{RT}{zF} In \frac{c^s}{c^*} \quad 3.6$$

Here we have,

E is Applied Voltage [V] η is Overpotential [V]

η_{act} is Activation Overpotential [V] η_{conc} is Concentration Overpotential [V]

c^s is Species Concentration near the Electrode $[mol/m^3]$ $c^*$is Species Concentration in the Bulk $[mol/m^3]$

The total overpotential (η) consists of two parts: activation overpotential (η_{act}), associated with the initial electron transfer, and concentration overpotential (η_{conc}), associated with maintaining enough reactants at the electrode surface [24]. A high η_{conc} signifies sluggish electron transfer, while a high ηconc indicates limitations in reactant supply. Both lead to increased energy input, and ideally, we try to minimize the overall overpotential for optimal efficiency [24].

To understand how the double layer properties, interface between electrode surface and electrolyte, influence the overpotential of an electrode reaction, we can employ the equation 3.7, which accounts for factors like charge distribution and ion transport within the double layer:

$$\eta = (\Delta\emptyset_1 - \Delta\emptyset_2) - E_r \qquad 3.7$$

Here we have,

$\Delta\emptyset_1$ is the interfacial potential of the electrode [V]

$\Delta\emptyset_2$ is the interfacial potential of a reference electrode [V]

E_r is the equilibrium potential between the electrode and the same reference electrode [V]

3.1.2. Kinetics

As previously explained, initiating an ERC frequently necessitates the application of overpotential. Notably, the reaction rate of this electrochemical process exhibits a strong dependence on the applied potential magnitude [24]. Fundamentally, under the applied potential every non-spontaneous electrode reaction, equation 3.1, can proceed in forward (reduction) or backward (oxidation) direction, often producing a net current 3.8:

$$i = i_c - i_a = zFA[k_o c_O^s - k_b c_R^s] \qquad 3.8$$

Here we have,

i is Net Current [A]

i_a is Anodic Current. [A]

i_c is Cathodic Current [A]

k_o is Heterogeneous Rate Constant (forward reaction) [m/s]

k_r is Heterogeneous Rate Constant (backward reaction) [m/s]

Electrode kinetics explains how net current density depends on applied potential and species concentrations. The forward (k_o) and backward (k_r) rate constants from equation 3.8 reflect this, incorporating the impact of both potential and overpotential. Following the approach in Bard and Faulkner [51], we reach the Butler-Volmer equation, 3.9:

$$j = j_0 \left[\exp\left(\frac{-a_c F}{RT}\eta\right) - \exp\left(\frac{a_a F}{RT}\eta\right) \right] \quad 3.9$$

Here we have,

j is Current Density $[A/m^2]$ j_0 is Exchange Current Density $[A/m^2]$

a_c is Cathodic Charge Transfer Coefficient [-] a_a is Anodic Charge Transfer Coefficient [-]

Equation 3.9 links current density (current per unit area) to overpotential, but it ignores the impact of reactant concentration. This simplified equation assumes αc + αa = 1 [51]. In reality, most ERC face concentration limitations, so to account for them, we use the more complex "concentration-dependent Butler-Volmer equation. 3.10:

$$j = j_0 \left[\frac{c_O^S}{c_O^*} \exp\left(\frac{-a_c F}{RT}\eta\right) - \frac{C_R^S}{C_R^*} \exp\left(\frac{a_a F}{RT}\eta\right) \right] \quad 3.10$$

In the above equation there are two notable variables. First, j_0, which represents the exchange current density, is measured when the overpotential is zero ($E = E_{eq}$) and the net current, (from equation 3.9) is zero. This equilibrium is the reflection of balanced faradaic activity.

Second, α ,which is the indicator of relative distribution of the applied potential between cathodic (forward) and anodic (backward) process, gets the value ranging from 0 to 1 as the minimum and maximum respectively.

Expanding upon the fundamental framework provided by the Butler-Volmer equation, explore deeper into the behavior of electrochemical systems under diverse overpotential conditions. Enter the Tafel equation, a critical extension that offers a sophisticated insight on electrochemical kinetics. It quantitatively describes the exponential relationship between overpotential (η) and the observed current density (j). For instance, in the case of low current

density (j_0) a high overpotential is required to extract the net current, which cause irreversible electron transfer. This irreversible electron transfer is quantified by Tafel equation, which can be driven from equation 3.11:

$$\eta = \frac{RT}{aF} In\, j_0 - \frac{RT}{aF} Inj \qquad 3.11$$

Beyond the above description regarding the Tafel equation, this expression also is used to fit experimental data in a logarithmic scale. This fitting helps to determine the exchange current density j_0 and the charge transfer coefficient α as well as to evaluate the number of electrons transferred in the reaction.

In this report the main focus is to find the relationship between the concentration distribution of reactants along the catalyst and the exchange current density. Thus, the mass transfer resistant has to be taken into account, especially when there is a significant change in concentrations at the electrode surface due to reaction.

Restricting transportation solely to diffusion, the molar flux $\dot{N}_R$ of the reactant can be written as 3.12: [25]

$$\dot{N}_R = k_b\left(c_{R,b} - c_{R,s}\right) \qquad 3.12$$

This equation states that the molar flux ($\dot{N}_R$) is a product of the reaction rate constant (k_b) and the difference in concentration of the reactant in the bulk ($c_{R,b}$) and at the surface ($c_{R,s}$). Since the molar flux ($\dot{N}_R$) is directly proportional to the current density the relationship can be described by equation 3.13:

$$j_{R,diff} = nFk_b\left(c_{R,b} - c_{R,s}\right) \qquad 3.13$$

3.1.3. Cell Potential

Within the operational framework of electrochemical flow-cell technologies, the applied voltage is specifically defined by the electric potential difference established between two critical components: the cathode and the anode. This differential is recognized as the cell potential, denoted by V_{cell}. The distribution of this cell potential across the entirety of the electrochemical cell is not arbitrary but follows a deliberate and structured allocation strategy.

This strategic distribution ensures that the flow-cell operates efficiently, with the electric potential being systematically divided to meet the operational requirements and enhance the performance of the cell. This nuanced approach to the management of cell potential is a foundation in the functionality of electrochemical systems, underscoring the importance of precision in the application and distribution of voltage within these advanced technological setups, which can be described by the following equation 3.14:

$$V_{cell} = (E_a{}^0 - E_c{}^0) + (\eta a + \eta c) + \eta_{ohm} \quad 3.14$$

Here we have:

V_{cell} is Cell Potential [V] η_{ohm} is Ohmic Drop [V]

ηa is Anodic Overpotential [V] ηc is Cathodic Overpotential [V]

3.1.4. Current Distribution

The main objective when simulating an electrochemical cell is to determine the distribution of current. This parameter is crucial for describing the performance of electrochemical cells. Its significance lies in its immediate association with the total ionic movement (N), which predominantly arises from three phenomena: the diffusion, migration, and convection of ions. Specifically, for electrochemical CO_2 reduction in an aqueous solution, when presuming Transport of Dilute Species (TDS), the ionic movement (N_i) for a given species i can be calculated using the Nernst-Planck equation.3.15:

$$N_i = -D_i \nabla c_i - z_i u_{m,i} F c_i \nabla \phi_1 + c_i u \quad 3.15$$

Here we have:

N is Total Ionic Flux [mol/$m^2 - s$] u is the velocity [m/s]

D is Species Diffusivity u_m is Species Mobility [$m^2/V - s$]

ϕ_1 is Electrolytic Potential [V]

In the modeling approach the mobility (u_m)is given by Nernst-Einstein relation 3.16:

$$u_{m,i} = \frac{D_i}{RT} \quad 3.16$$

The overall density of the electrolytic current is directly linked to the cumulative effect of the flux of individual ions, 3.17:

$$j_1 = F \sum_i z_i N_i \qquad 3.17$$

Here we have:

j_1 is Electrolytic Current Density $[A/m^2]$

The assumption holds that the solution remains electrolytically neutral throughout, except in the vicinity of the electrode surface. Here, electrical attraction induces the formation of a thin layer, compelling ions to migrate and congregate in this region, 3.18:

$$\sum_i c_i z_i = 0 \qquad 3.18$$

Correlating equation 3.18 and the Nernst Planck equation 3.15 the electrolytic current density given by equation 3.17 reduces to 3.19:

$$j_1 = -F \sum_i z_i D_i \nabla c_i - k \nabla \phi_1 \qquad 3.19$$

Here we have:

k is Electrolytic Conductivity [S/m]

Therefore, the charge conservation has to be:

$$\nabla . i_1 = 0 \qquad 3.20$$

The Equation 3.20 facilitates the derivation of electrolyte potential, with current density formulations from section Current Distribution establishing the boundary constraints. Consequently, it is acknowledged that electrode kinetics significantly affect the current distribution. Notably, even though velocity is omitted from Equation 3.19 due to the electroneutrality principle (Equation 3.18); however, it impacts the distribution of current via the mechanism of species transport, encompassing diffusion, migration, and convection processes, which is given by:

$$\frac{\partial c_i}{\partial t} = -\nabla . N_i + R_i \qquad 3.21$$

Here we have:

R_i is the homogeneous source or sink of species

In the case of ERC, it is recommended to assume $R_i = 0$ as long as the homogeneous reactions are not considered as rate dependent. Thus, substituting flux N_i from equation 3.15 we get:

$$\frac{\partial c_i}{\partial t} + (u.\nabla)c_i = D_i\nabla.(\nabla c_i) + Fz_i u_i c_i \nabla.(\nabla \emptyset_1) \qquad 3.22$$

We have i unknowns, including i values for c, $\emptyset_1$, and u. To solve for these, we have three equations: the above equation (1.21), the electroneutrality equation (1.17), and the momentum equation which will be explained in the next following discussions. Solving this system of equations will reveal the current distribution.

In COMSOL Multiphysics, current distribution is categorized into Primary Current Distribution (cd), Secondary Current Distribution (scd), and Tertiary Current Distribution (tcd) models, each representing increasing complexity: cd assumes rapid electrode kinetics (for example very high j_0) and constant concentration; scd incorporates finite reaction rates but disregards concentration changes similar to cd; while tcd captures both finite kinetics and concentration variations, offering the most comprehensive yet computationally demanding analysis. For further detail regarding the current distribution, it is recommended to refer to the electrochemistry book by West [26].

It is crucial to acknowledge that exceeding a certain overpotential threshold the (ERC) mass-transfer becomes mass transfer limited. Above this critical point, further increases in overpotential no longer impact current density, signifying the system has attained its limiting current density ($\boldsymbol{j_{lim}}$). The limiting current density is given by:

$$j_{lim} = \frac{zFDCO_2 c^*_{CO_2}}{\delta_{conc}} \qquad 3.23$$

Here we have:

δ_{conc} is Concentration Boundary Layer $[m]$

3.1.5. Chemical Reactions

The complex interactions of CO_2 in water, forming the uniform carbonic acid ($KHCO_3$) buffer system, have been the subject of extensive research. There are some similarities between modeling ERC and CO_2 dissolution in seawater - both necessitate the estimation of CO_2 solubility in saline solutions. Therefore, this section briefly introduces relevant concepts from CO_2 dissociation studies, specifically the reactions (homogeneous reactions).

Several factors influenced our choice of $KHCO_3$ as the electrolyte medium in our simulation:

- High conductivity is essential for efficient electrochemical reactions because it allows for the easy transfer of ions between the electrodes, and regarding this point, $KHCO_3$ is highly soluble in water, which ensures good ionic conductivity in the electrolyte solution.
- As part of the bicarbonate buffer system, $KHCO_3$ helps maintain a stable pH in the electrolyte solution during the CO_2 reduction process. This is crucial because significant changes in pH can alter the kinetics and selectivity of the electrochemical reactions.
- In CO_2 reduction systems, bicarbonate ions (HCO_3^-) can act as a source of CO_2. When a potential is applied, HCO_3^- can release CO_2, which is then reduced at the cathode. This means the system can operate effectively even with lower concentrations of dissolved CO_2.
- $KHCO_3$ does not undergo decomposition under typical electrochemical CO_2 reduction conditions, which means it does not introduce impurities into the system that could interfere with the reaction or degrade the electrodes.
- The nature of the electrolyte can significantly affect the product distribution in CO_2 electroreduction. Silver catalysts, in particular, are sensitive to the electrolyte composition. $KHCO_3$ can help steer the reaction towards the desired products by affecting the intermediate species' stability and the surface chemistry of the silver catalyst.

When we bubbled CO_2 into water the following reactions are taking place: [27], [57]

$$CO_2 + H_2O \leftrightarrow H_2CO_3^- \quad 3.24$$

$$HCO_3^- \leftrightarrow H^+ + CO_3^{2-} \quad 3.25$$

$$CO_2 + OH^- \leftrightarrow HCO_3^- \quad 3.26$$

$$HCO_3^- + OH^- \leftrightarrow CO_3^{2-} + H_2O \quad 3.27$$

Based on the above reactions, reaction 3.24 and 3.25 can be combined as follows:

$$CO2 + H_2O \leftrightarrow H^+ + HCO_3^- \quad 3.28$$

To calculate the equilibrium constants (K) for the reactions in the bicarbonate buffer system we need to determine the concentration of all species at equilibrium. The equilibrium constant corresponding to equation 3.27 and 3.28 are given as follows:

$$K_{B_1} = \frac{[H^+][HCO_3^-]}{[CO_2][H_2O]} \qquad K_{B_2} = \frac{[CO_3^{2-}][H_2O]}{[HCO_3^-][OH^-]} \quad 3.29$$

Note: The concentration of water is often considered constant and omitted in dilute aqueous solutions, assuming it does not change significantly.

These equilibrium constants of CO_2 dissociation reactions are well-known for the dissolution of CO_2 in pure water. However, as mentioned in chapter 1, ERC is rarely carried out in pure water. Moreover, $K_{B_1}$and K_{B_2} are influenced by the presence of electrolyte as well as temperature. Millero et al. [28] have provided explicit parametric expressions for calculating equilibrium constant for CO_2 dissolution in sea water at different temperature. To use these expressions in this study, two terminologies need to be introduced. First, the ionic strength (I), it is given by 3.30:

$$I = \frac{1}{2}\sum_j c_{ion,} z_j^2 \quad 3.30$$

Here we have:

I is Ionic Strength $[mol/m^3]$

c_{ion} is Concentration of ion $[mol/m^3]$

In the case of ERC, c_{ion} would represent the concentration of cation/anion present in the electrolyte. The second terminology is salinity (S) which is related to ionic strength as follows:

$$I = \frac{19.924S}{1000 - 1.005\,S} \tag{3.31}$$

Table 3.1 shows pK_i (= $\log K_i$) values calculated from expressions given in Millero et al.[28] along with forward and reverse reaction rates of different CO_2 dissociation reactions in pure water at room temperature (298.15 K). The predominant dissociation pathways in acidic environment are denoted by 'a' and those in basic environment by 'b'. In addition, water dissociation reaction is represented by table 3.1:

i	Equilibrium Reaction	k_f^i	k_r^i	pK_i
a1	$CO_2 + H_2O \leftrightarrow H^+ + HCO_3^-$	$3.71 * 10^{-2} s^{-1}$	$83.33 * 10^3 M^{-1} S^{-1}$	6.35
a2	$HCO_3^- \leftrightarrow H^+ + CO_3^{2-}$	$2.34\ S^{-1}$	$5 * 10^7\ M^{-1} S^{-1}$	10.33
b1	$CO_2 + OH^- \leftrightarrow HCO_3^-$	$2.23 * 10^3\ M^{-1}\ S^{-1}$	$4.99 * 10^{-5}\ S^{-1}$	-
b2	$HCO_3^- + OH^- \leftrightarrow CO_3^{2-} + H_2O$	$6 * 19^9\ M^{-1}\ \ S^{-1}$	$1.28 * 10^6\ S^{-1}$	-
w	$H_2O \leftrightarrow H^+ OH^-$	-	-	14

Table 3.1: Reaction rates and equilibrium constants for the dissociation of CO2 in water at 25°C [58]

* The pK values are calculated from parametric relations provided in Millero et al. [28]; please note: these values are accurate for temperature 273.15 K - 313.15 K and salinity 0 - 50

** Values adapted from Schulz et al. [29]

Besides temperature and ionic concentration, the pH level of a solution also plays a crucial role in determining the equilibrium concentrations of CO_2, HCO_3^-, and CO_3^{2-}. The balance between these species is sensitive to pH changes, which can shift the equilibrium positions of the related chemical reactions. A more acidic pH typically favors the formation of dissolved CO_2 and HCO3−, while a more basic or alkaline pH tends to increase the proportion of CO_3^{2-}ions. This influence is represented in Figure 3.1. Increasing the electrolyte concentration (or salinity) or temperature, increases the equilibrium constants of CO_2 dissociation, or in other words it reduces the corresponding pK values (see dashed/dotted lines).

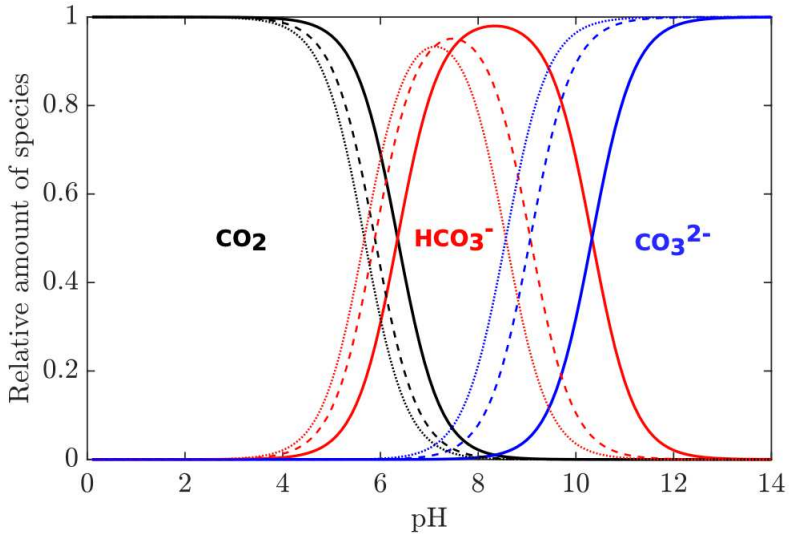

Figure 3.1: The influence of temperature, ionic strength and pH on CO2 dissociation reactions in (solid lines) pure water 298.15 K, (dashed lines) aqueous solution of 0.5 M KHCO3 at 298.15 K and (dotted lines) aqueous solution of 0.5 M KHCO3 at 313.15 K [32]

In this thesis, Potassium Hydroxide ($KHCO_3$) as our working electrolyte. There are many reasons behind this methodology:

- Potassium ions are larger than other alkali metal ions like sodium (Na^+), which can influence their solvation shell in water. A larger ion like K^+ typically has a less tightly bound solvation shell, which can make it easier for the electrolyte to participate in the CO_2 reduction process because it may not hold onto the water molecules as tightly. This can potentially increase the availability of water molecules for the reaction.

- Potassium ions have a good electrochemical compatibility with silver electrodes. They do not interfere with the electrocatalytic activity of the silver and can support the formation of the desired reduction products.
- K^+ has high ionic mobility in aqueous solutions, which contributes to the electrolyte's overall conductivity. High conductivity is vital for efficient electron transfer during the electrochemical reduction process.
- $KHCO_3$ provides a buffering action due to the bicarbonate ion (HCO_3^-), but the presence of K^+ also contributes to the overall ionic strength of the solution, which can help maintain a stable pH during electrolysis. A stable pH is essential for the predictability and control of the reaction's kinetics and selectivity.

3.1.6. Single Phase Laminar Flow

The following section offers a brief theoretical framework for simulating an electrochemical cell with single-phase laminar flow. The modeling of such flow is effectively accomplished through the application of the Navier-Stokes equations. Many publications explore the derivation and application of these equations, including the seminal work by Batchelror [30]. These resources clarify the comprehensive mathematical principles that govern fluid dynamics and provide the necessary foundation for accurately predicting the behavior of a fluid under laminar flow conditions within a single-phase system. This is pivotal for designing and analyzing systems like flow-cells, where precise control and understanding of fluid movement are essential for their operation and efficiency. The Navier-Stokes equations serve as a foundation in fluid mechanics, offering a robust model for a wide range of fluid flow scenarios, including those with complex boundary conditions and varying flow velocities that are characteristic of single-phase laminar flow within a flow-cell environment. For incompressible flow the Navier-Stokes equations read:

$$\nabla . u = 0 \tag{3.32}$$

$$\rho \frac{\partial u}{\partial t} + \rho(u.\nabla)u = -\nabla P + \mu \nabla^2 u + F \tag{3.33}$$

Here we have:

∇ is the divergence operator, which calculates the net flow of fluid

u is the velocity vector field of the fluid [m/s]

ρ is the density of the fluid $[kg/m^3]$

F is the body force vector field acting on the fluid per unit volume $[N/m^3]$

P is Pressure [pa]

μ is Dynamic Viscosity $[N.s/m\text{^}2]$

To demonstrate the practical application of these equations within the context of flow-cells, we can refer to a two-dimensional model of a flow-cell as depicted in Figure 3.2. In this model, the flow is introduced into the channel with an even velocity distribution and a specific concentration gradient. It is posited that the exit point of the channel maintains a steady pressure level. Additional boundary conditions, which are crucial for a complete description of the flow behavior, are detailed within the figure. This simplified representation allows for the examination of fluid dynamics within the flow-cell, providing insight into how the flow interacts with the cell's geometry and how it might be influenced by various input parameters. Such a model is instrumental in optimizing the flow-cell design for uniform distribution of reactants and efficient operation.

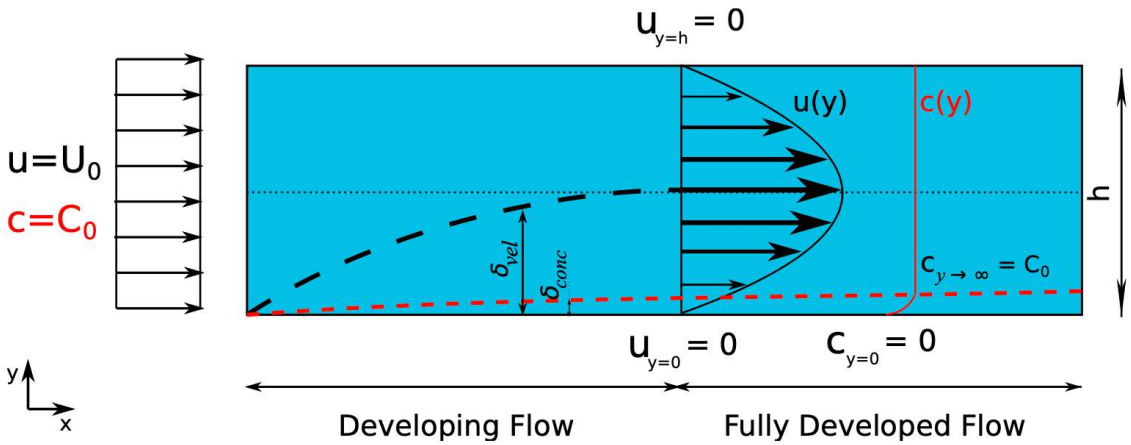

Figure 3.2: The interplay between concentration boundary layer and velocity boundary layer in relation to flow-cells [31]

As we can see from the Figure 3.2, we have two kinds of flows, developing flow and Fully Developed flow. Let's begin with a brief explanation about these two types of flow. Developing Flow, also known as entrance flow, occurs at the region near the entrance of a pipe or duct where the flow is adjusting to the confines of the channel. In this region, the velocity profile is not uniform and changes along the length of the pipe. It typically starts with a relatively flat profile at the entrance (assuming a uniform inflow) and develops into a parabolic profile (for laminar flow) or a flatter, plug-like profile (for turbulent flow) as it moves downstream.

Fully Developed Flow on the other hand, refers to the region where the velocity profile is fully developed and does not change in the streamwise direction (along the length of the pipe). In fully developed laminar flow, the velocity profile is typically parabolic across the pipe's cross-section. For turbulent flow, it is more uniform across the center and drops near the walls.

Back to the Figure 3.2, we can see that the developing flow corresponds to a part of channel in which the velocity boundary layer thickness (δ_{vel}) is increasing (black dashed line). At a certain point downstream, it remains constant. The flow after that is called fully developed flow. The fully developed flow profile has a distinct parabolic shape (solid black curve) which remains unchanged along the x-direction. The parabolic flow profile can be obtained by solving equation 3.33 with above-mentioned boundary conditions. This derivation can be found in Batchelor [52] here, only the final result is provided. The fully developed velocity profile is given by:

$$u(y) = \frac{6U_0}{h^2}(yh - y^2) \tag{3.34}$$

Comparable to the velocity boundary layer (δ_{vel}), we can observe the concentration boundary layer depicted by a red dotted line in the same figure. This boundary layer emerges due to the current density being at its limiting value, denoted a j_{lim} along the bottom surface of the wall. At this rate of current density, the consumption rate of species c is such that its concentration diminishes when moving toward the bottom wall (indicated by the solid red line), reaching zero right at the wall. The illustration reveals that the concentration boundary layer thickness, δ_{conc}, is notably less than that of the velocity boundary layer, δ_{vel}. This suggests that, unlike

the velocity profile which has reached a fully developed state, the concentration profile is still evolving. The validity of this observation is contingent upon the fulfillment of a specific condition:

$$Pe = \frac{U_0 h}{D} \gg 1 \tag{3.35}$$

Where Pe is a well well-known parameter, Peclet number.

Indeed, this scenario is similar to the traditional Graetz problem [32], which presupposes a concentration profile that is in the process of development alongside a velocity profile that has already reached a fully developed state. The central concept of the Graetz problem is to determine δ_{conc}, which, in reality, changes as one moves along the channel. Within a two-dimensional channel under steady-state conditions, the transport of species can be reduced to a more simplified form (refer to equation 3.22):

$$u_x \frac{\partial c}{\partial x} u_y \frac{\partial c}{\partial y} = D \left(\frac{\partial^2 c}{\partial x^2} + \frac{\partial^2 c}{\partial y^2} \right) \tag{3.36}$$

The velocity profile varies only in y direction; therefore, $u_x = u(y)$equation 1.33 and $u_y = 0$. Moreover, at high Peclet number convection is the dominant mode of transport. Consequently, the axial diffusion can be neglected. These replacements simplify the equation 1.36 to:

$$\left(\frac{6U_0}{h^2} (yh - y^2) \right) \frac{\partial c}{\partial x} = D \frac{\partial^2 c}{\partial y^2} \tag{3.37}$$

So, now if $\delta_{conc}(X) \ll h$, the velocity profile can be considered as a linear. This assumption is known as the Leveque approximation. Using this approximation in the above equation we can reduce it to:

$$\left(\frac{6U_0 y}{h} \right) \frac{\partial c}{\partial x} = D \frac{\partial^2 x}{\partial y^2} \tag{3.38}$$

The equation is addressed with the concentration boundary conditions outlined in Figure 3.2. Employing a similarity transformation, the methodology for which is detailed in West [33], yields the thickness of the concentration boundary layer, denoted as δ_{conc}, to be as follows:

$$\delta_{conc}(x) = 1.022\sqrt[3]{\frac{hDx}{U0}} \quad 3.39$$

3.1.7. Single Phase Turbulent Flow

The following section extends the theoretical framework to include the simulation of flow-cells with single-phase turbulent flow.

The turbulent flow model is complex and typically relies on statistical methods to predict the behavior of a fluid because the flow is chaotic and three-dimensional. The primary difference between laminar and turbulent flow modeling is the treatment of velocity fluctuations and their effect on momentum transfer. For the turbulent model, the RANS equations are commonly used. They decompose the instantaneous velocity into a mean and fluctuating part, allowing for the calculation of the average effect of the turbulence on the flow.

Turbulence significantly affects momentum transfer, and its statistical behavior is captured by decomposing the instantaneous velocity into a mean and fluctuating component. The seminal work by Wilcox [34] and other resources provide in-depth analysis and derivation of the RANS equations, which are crucial for understanding the principles of turbulence and its impact on fluid dynamics.

For incompressible flow, the RANS equations are:

$$\nabla . \bar{u} = 02.31 \quad 3.40$$

$$\rho\left(\frac{\partial \bar{u}}{\partial t} + \bar{u}.\nabla\right)\bar{u} = -\nabla\bar{P} + \mu\nabla^2\bar{u} + \bar{F} - \nabla.(u'u')2.32 \quad 3.41$$

Here we have:

∇ is the divergence operator

u is the Reynolds-averaged velocity field $[m/s]$

ρ is the fluid density $[kg/m^3]$

P is the Reynolds-averaged pressure $[Pa]$

μ is the dynamic viscosity $[N.s/m^2]$

F is the body force per unit volume $[N/m^3]$

$u'u'$ represents the Reynolds stress tensor, which accounts for the turbulent momentum transfer.

The RANS equations are typically closed with a turbulence model, such as the $k-\epsilon$ or $k-\omega$ model, which provides additional equations to determine the turbulent kinetic energy (k) and its rate of dissipation (ε) or specific dissipation rate (ω).

Just as with laminar flow, the practical application of these equations in flow-cell modeling involves setting appropriate boundary conditions that reflect the physics of turbulent flow. In a typical flow-cell, turbulence might be generated at the inlet and affected by the channel's geometry. The boundary layer for turbulent flow starts with a relatively uniform profile and develops a velocity deficit near the wall due to the increased momentum transfer from the fluctuating components of the velocity.

For fully developed turbulent flow, the velocity profile tends to be flatter in the center and exhibits a sharp decline near the wall, described by the logarithmic law of the wall. This profile can be derived from the RANS equations and appropriate wall functions that account for the effects of turbulence near solid boundaries.

The turbulent transport of species is governed by an advection-diffusion equation similar to equation 3.36, but with additional terms to account for the turbulent mixing: (3.42)

$$\bar{u}_x \frac{\partial c}{\partial x} + \bar{u}_y \frac{\partial c}{\partial y} = D\left(\frac{\partial^2 c}{\partial x^2} + \frac{\partial^2 c}{\partial y^2}\right) + \frac{\partial}{\partial y}\left(-u_y' c'\right)2.35 \qquad 3.42$$

Here we have:

$-u_y' c'$ represents the turbulent diffusive flux, which is typically modeled using a gradient diffusion.

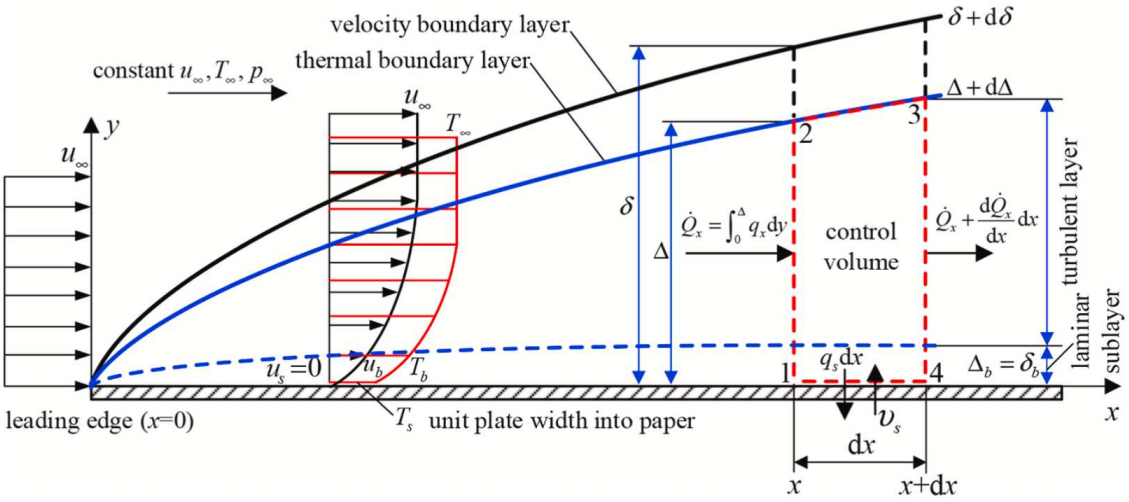

Figure3.3: Sketch of turbulent boundary layer flow over a flat plate and differential control volume analysis [35]

3.2 Finite Element Method

In this study, COMSOL Multiphysics software is employed to construct both two-dimensional (2D) and three-dimensional (3D) models of a flow-cell. While the 3D model serves as the basis for comprehensive fluid dynamics, concentration, and current distribution analyses, a 2D model is utilized for product concentration analysis to reduce computational demands and streamline the simulation process.

COMSOL Multiphysics uses the Finite Element Method (FEM) as its principal numerical technique for solving systems of equations that describe complex physical phenomena. This section offers a brief introduction to FEM, outlining its fundamental principles and terminologies that are recurrently referenced throughout this report. The section aims to introduce readers to the basic ideas of FEM, such as mesh generation, boundary conditions, and the discretization of continuous variables, which enable COMSOL to model and analyze complex scenarios with precision and accuracy. This introductory guide is intended to deepen the reader's comprehension of the computational tactics that form the foundation of the simulations discussed in this document.

In mathematics, FEM is celebrated for its strength in using the minimization principle a technique that aims to reduce the total energy of a system to its least possible value. To clarify the underlying mechanism of FEM, consider a partial differential equation (PDE) that includes the momentum equation 3.33. [36] This equation arises from an integration of the forces present within an infinitesimally small volume of fluid. The resulting equation covers terms

that are integral over volumes, holding the amounts that exist within the area, and terms integral over surfaces, which specify the domain's interactions with adjacent domains or the external environment.

The application of the Gauss divergence theorem innovatively transforms the surface integrals into volume integrals, effectively transmuting the integral form of the momentum equation into its differential counterpart (PDE). In the complicated working of FEM, this differential form often referred to as the 'strong form' is transformed into what is known as the 'weak form'. This transformation is facilitated using shape functions that are skilled at capturing the behavior of the system within each element of the domain. By so doing, FEM simplifies complex problems into a series of manageable calculations, paving the way for the simulation and analysis of physical phenomena with remarkable precision.

In the FEM, the initial step involves partitioning the domain of interest into smaller, manageable subdomains known as elements, through a process known as meshing. This crucial step allows for a more localized and detailed analysis of the domain by breaking it down into elements that can be individually analyzed. Subsequently, the weak forms of the governing equations, as previously discussed, are applied and solved within these discrete elements. It is important to note that the complexity and the computational resolution of each element are determined by its order, which directly influences the number of nodes it contains. For illustrative purposes, consider Figure 3.4, which contrasts linear elements, having a simpler structure, with quadratic elements that exhibit a higher level of complexity due to their increased node count. Although our discussion here is focused on one-dimensional (1D) elements for the sake of clarity, the underlying principles and methodologies of FEM are equally applicable and extend seamlessly to domains of higher dimensions. This multidimensional applicability underscores the versatility and the broad utility of the Finite Element Method in engineering and scientific analyses.

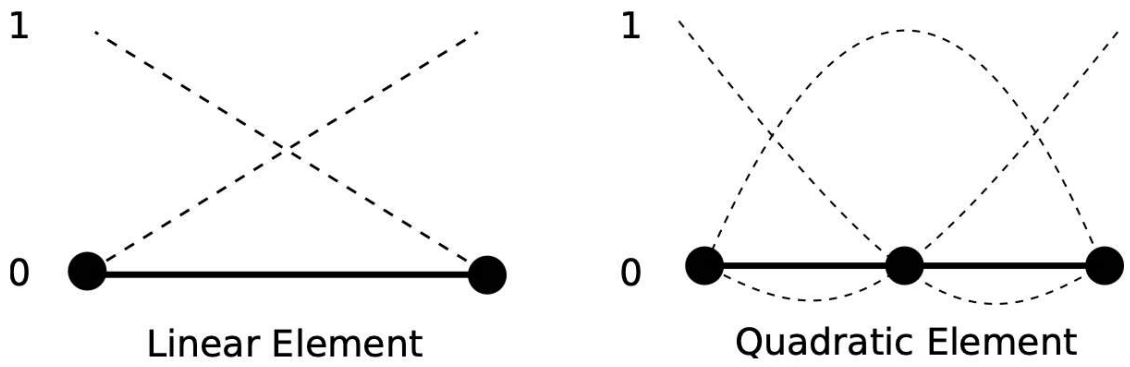

Figure 3.4: A schematic showing a 1D linear and a quadratic element and their shape functions [31] [37]

One of the most notable distinctions between linear and quadratic elements within the context of Finite Element Method (FEM) is the number of nodes each possesses; notably, a quadratic element incorporates an additional node at its center. This differentiation is crucial because the weak forms of the governing equations are solved at these nodes. By computing solutions at each node, FEM enables the assembly of a comprehensive solution through the process of interpolation between nodes.

The method of interpolation is graphically represented in illustrations, often with dashed lines, to depict the transition of solutions across the nodes for different element orders. Specifically, linear elements utilize linear interpolation functions to bridge solutions between nodes, while quadratic elements employ quadratic interpolation functions for this purpose. Commonly, Lagrange polynomials are employed as these interpolation functions, also referred to as shape functions in the realm of FEM.

The use of shape functions is a pivotal aspect of FEM, serving as the mathematical backbone that facilitates the estimation of unknowns within the element. Importantly, the process of mesh refinement increasing the number of nodes and consequently the shape functions plays a dual role. On one hand, it significantly enhances the accuracy of the solution by offering a more granular simulation of the physical behavior across the domain. On the other, it proportionally escalates the computational demand and time. This trade-off between solution precision and computational efficiency is a key consideration in the application of FEM, underscoring the importance of judicious mesh design in achieving optimal analysis outcomes.

4

4.1. Modeling

In this section, three models that are connected to the objectives of this study are explored, providing an in-depth exploration of their practical applications and the core assumptions upon which they are built. Initially, the cell geometry is simplified for enhanced analytical clarity, a modification based on the work previously conducted within the group by Christoph Blümner [38]. This simplification serves as a foundation for the subsequent stages of investigation. Following this, a comprehensive 3D fluid dynamic, concentration analysis are undertaken, examining the effects of varying geometries to glean insights into their impacts. Finally, ERC is incorporated into the analysis, applying these principles to the preliminary stages to enhance the understanding and findings. This structured approach allows us to systematically address the complexities of the study, ensuring a thorough examination of the models in question.

Given the multidisciplinary nature of ERC, COMSOL Multiphysics is selected for modeling a 3D electrochemical cell. This software stands out for its integrated electrochemistry interface, designed specifically for modeling applications, providing instant and crucial specialized features. It offers a graphical user interface (GUI) that allows for easy setup of the simulation scenario, including geometry creation, meshing, physics definitions, and boundary conditions. This contrasts markedly with alternatives such as Fluent or OpenFOAM, where the integration of similar features is absent, underscoring COMSOL's superiority in addressing the specific needs of electrochemical modeling. [39]

This chapter proceeds under the assumption that the reader is familiar with the predefined equations in Chapter 3. Consequently, for the sake of conciseness and as required, references to these equations are made directly.

4.1.1 Geometry Modification

Based on the fundamental research that has already been conducted, this project examines the impact of mass transport within the cell, employing both turbulent and laminar fluid flow physics. This innovative approach aims to dissolve the complexities of how varying velocities influence species transport across different cell geometries. By integrating these distinct fluid dynamics perspectives, the study seeks to provide a more comprehensive understanding of the electrochemical CO_2 reduction process and product distribution on a polycrystalline silver 2D idealized catalyst. This work not only extends the scope of the initial investigation that has been done by [38] but also introduces a unique analytical simulation, highlighting its innovative contribution to the field by combination of fluid dynamics and electrochemistry using both laminar and turbulent flow for simulation.

4.1.2 Geometry Simplification

In the original cell geometry, [38] began by specifying the dimensions of the Ag electrode as 25x25x1 mm. To create an electrochemically non-active border for sealing, a 30x30 mm compartment was selected, leaving a 2.5 mm border around it. The aim was to make the electrolyte compartment as thin as possible, minimizing ohmic drop, which is particularly important for the larger area electrode expected to generate higher currents. Therefore, the compartment's thickness was determined to be 4 mm. This thickness ensured that there is sufficient housing material outside the compartment for two main purposes: a) to provide the necessary mechanical strength when the cell body is assembled and compressed, and b) to accommodate a 1 mm Luggin capillary and a 1 mm thick inlet channel, both surrounded by housing material.

For the design of the inlet and outlet sections [38] decided to guide the flow in the desired direction, which was achieved by connecting them to a flow promoter between the membrane and electrode surface, which helps reduce pressure drop, and then dividing the flow into one or multiple directions. The representation of this setup is illustrated in Figure 4.1. and 4.2. Additionally, the thickness of the simulated fluid domain includes a 0.5 mm

separator gasket, contributing to the total thickness and ensuring an effective separation within the device.

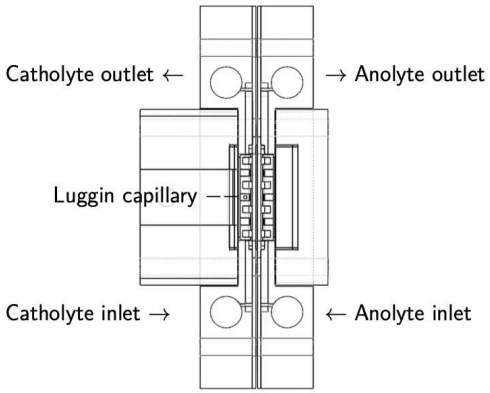

Figure 4.1 Cross section through the layers of the CAD flow cell, in the assembled state [38]

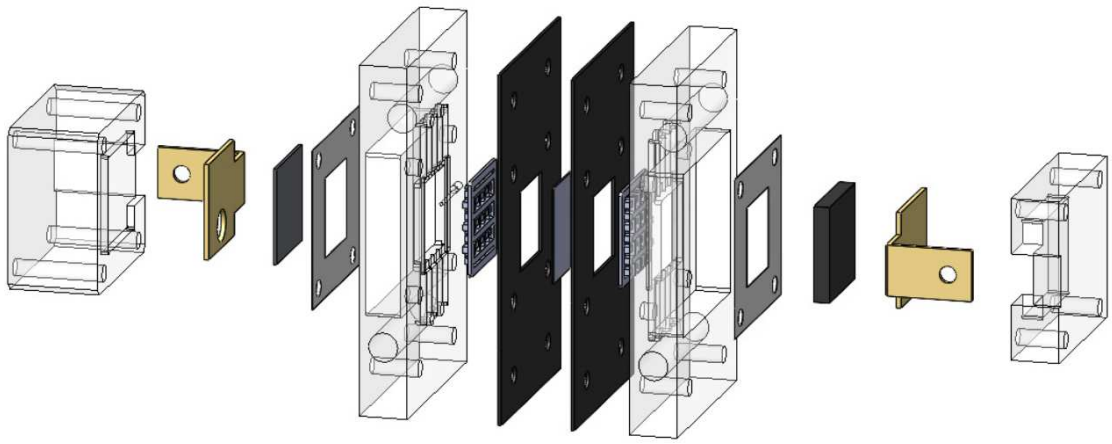

Figure 4.2 Exploded view of the flow cell assembly [38]

In the development phase of the study, the cell geometry was innovated by engineering it to a sandwich structure, incorporating strategically designed channels for both inlet and outlet flows as depicted in Figure 4.3 This novel design features both single and multiple inlets and outlets, a deliberate choice aimed at analyzing the influence of fluid flow patterns on electrolyte current density and product concentration. This approach enables an investigation into the fluid dynamics within the cell, specifically examining how different flow configurations affect the selectivity and distribution of electrochemical reactions. By optimizing the geometry for enhanced mass transport and reduced ohmic losses, this design is pivotal in advancing our understanding of ERC, potentially leading to improved cell performance and energy efficiency.

These models were selected after considering a tradeoff between their implementation complexity, computational requirements, and accuracy.

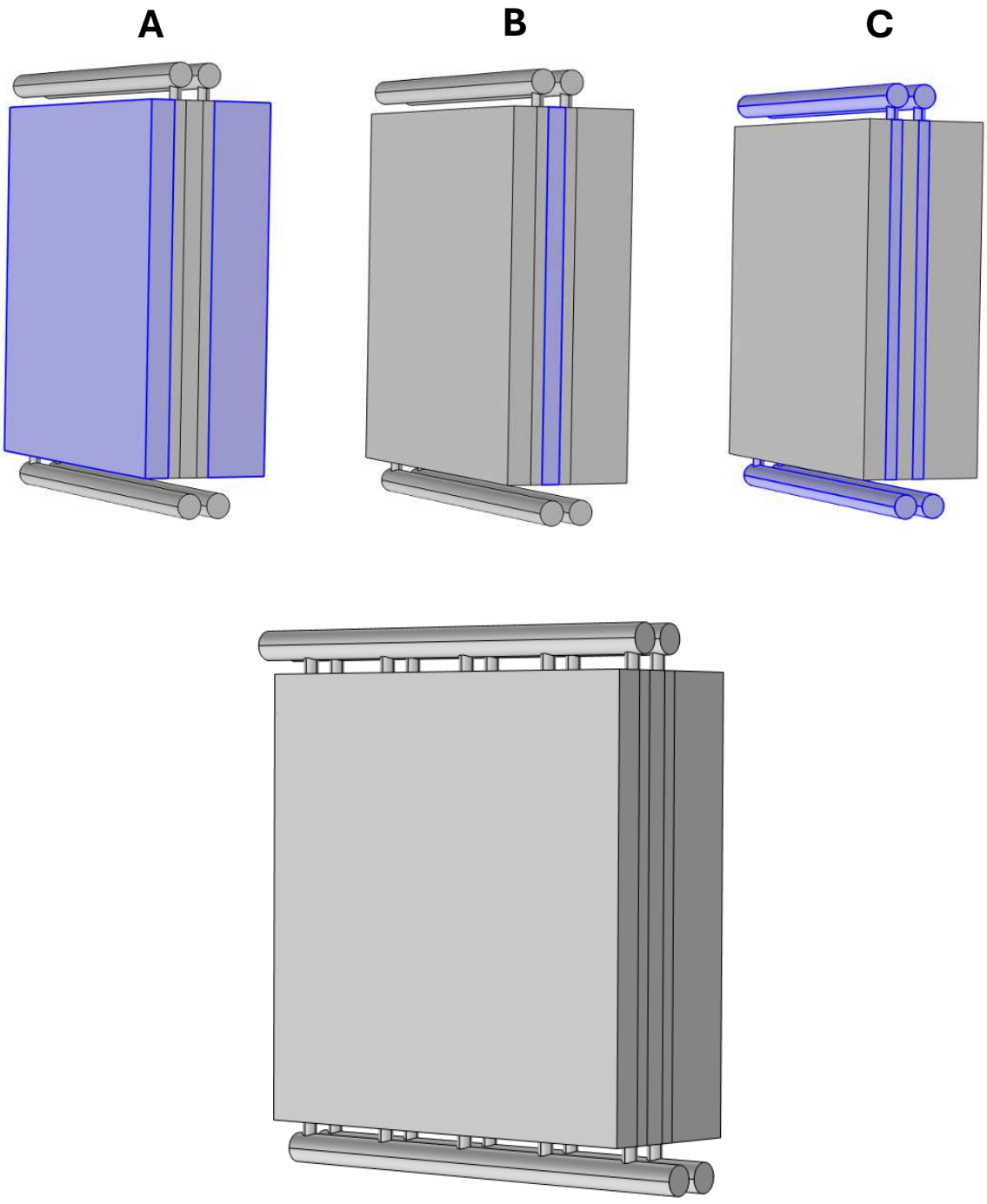

Figure 4.3 The Final Simplified Representation of the Flow Cell Geometry

The geometric configurations of the cell have been constructed and simulated using only the COMSOL Multiphysics software suite, Geometry Section. A comprehensive breakdown of the detailed specifications is listed in Table 4.1:

	Name	Size [mm]	Material
A	Anode Electrode	30*30*5	Glassy Carbon
A	Cathode Electrode	30*30*2	Silver
B	Membrane	30*30*1.5	Nafion
C	Electrolyte Channels	30*30*1	Polymethyl Methacrylate

Table 4.1 Geometry Details, presenting the specific details of the flow cell's simplified geometry.

The anode catalyst is considered Glassy carbon due to its high conductivity, chemical inertness, corrosion resistance, and broad electrochemical window, which collectively enhance the efficiency and durability of the reduction process.

On the other side, the polycrystalline silver is considered as the reduction catalyst due to its superior catalytic efficiency in selectively converting CO_2 to carbon monoxide (CO), coupled with their excellent electrical conductivity and stability under the specific conditions required for CO production.

Nafion is utilized as the membrane because of its ability for proton conductivity, high chemical stability, selective permeability to ions over gases, and durability under acidic and oxidative conditions, facilitating efficient ion transport while maintaining separation between the electrodes.

Polymethyl Methacrylate (PMMA) is selected as the channel material due to its chemical resistance, optical clarity for reaction observation, excellent electrical insulation, mechanical strength, and ease of fabrication, which collectively enhance the cell's operational efficiency and durability.

4.2. 3D Fluid Dynamic Analysis

Continuing the investigation, the study extends into a simulation of fluid dynamics within the electrochemical cell, emphasizing the importance of achieving homogeneous electrolyte flow across the catalyst layer. This uniform distribution is critical not just for enhancing product selectivity but also for ensuring the long-term stability and performance of the cell, thereby addressing key operational challenges, and optimizing the cell's overall effectiveness.

Due to the lack of ability to calculate Reynolds number in COMSOL software, for example, if your flow is turbulent but you use the Laminar Flow interface, the results may not accurately represent the physical phenomena occurring within the flow. Discrepancies arise because the laminar model does not capture the effects of turbulence, such as mixing, increased momentum diffusion, and energy dissipation. Consequently, before proceeding to the next step, the Reynolds numbers were calculated manually to see whether the considered flow rate is laminar or turbulent.

For this project, three flow rates are considered and given in table 4.2:

Flow rate	Unit
200	mL/min
350	mL/min
430	mL/min

Table 4.2: Selected Flow Rates for Modeling Analysis

To calculate the Reynolds number, necessitating the fluid's velocity, we can derive this velocity by utilizing the flow rate and the cross-sectional area of the channel.

$$\upsilon = \frac{Q}{A} \tag{4.1}$$

Here we have:

Q is flow rate $[m^3/s]$

A is surface are $[m^2]$

υ is velocity $[m/s]$

Given a channel with a diameter of 1 mm, we can calculate the surface area as follows:

$$A = \pi r^2 => 3.14 * (0.001)^2 = 3.14 * 10^{-6} \quad 4.2$$

Given a flow rate of 200 mL/min, the corresponding velocity can be calculated as follows:

$$\upsilon = \frac{3.33*10^{-6}}{3.14*10^{-6}} = 1.06\ [m/s] \quad 4.3$$

Following the same procedure for the next two flow rates, I obtain the velocities as follows:

$$\upsilon = \frac{5.83*10^{-6}}{3.14*10^{-6}} = 1.85\ [m/s] \quad 4.4$$

$$\upsilon = \frac{7.17*10^{-6}}{3.14*10^{-6}} = 2.28[m/s] \quad 4.5$$

With the velocities already determined, we can now calculate the Reynolds numbers [40]:

$$Re = \frac{\rho \upsilon L}{\mu} \quad 4.6$$

Here we have:

ρ is Fluid Density $[kg/m^3]$

υ is Velocity $[m/s]$

L is Linear Dimension $[m]$

μ is Dynamic Viscosity. $[ps.s]$

Taking water as the working fluid to evaluate the velocity field within the cell the Reynolds number for three velocities were calculated as follows:

Water	**Density** $[\boldsymbol{kg/m^3}]$	**Dynamic Viscosity**$[\boldsymbol{pa.s}]$
H_2O	1000	$1.002 * 10^{-3}$

Table 4.3 Physical Properties of Water at Standard Conditions

Velocity	1.06	1.85	2.28
Reynolds Number	2116	3694	4552

Table 4.4 Relationship Between Flow Velocity and Reynolds Number

To determine that whether our velocity is laminar or turbulent, we have the compare the results with literature [41]:

$$Re < 2300 \rightarrow Laminar\ Flow \quad 4.7$$

$$2300 \leq Re \leq 4000 \rightarrow Transition \quad 4.8$$

$$Re > 4000 \rightarrow Turbulent\ Flow \quad 4.9$$

4.2.1 Laminar Flow

With the above specifications, began by simulating laminar flow in two cell designs: a singular input/output configuration and a multiple input/output setup.

From modeling perspective, it is often necessary to develop a simplified model for quick but accurate estimation of the results, therefore, number of assumptions are taken into account as follows:

1- The electrode surface is considered completely flat.
2- The temperature is fixed at 293.15 K.
3- To obtain the most optimal fluid field distribution the fluid is considered water.
4- The cell operates in isobaric condition.

To calculate the fluid field the Navier stokes equation, already mentioned in chapter 3 equation 3.33, from Laminar Flow interface in Fluid Flow module at COMSOL Multiphysics software is used. The 3D model is developed based on the details listed in table 4.5:

Name	Value	unit
Temperature	293.15	K
Pressure	1	atm
Density	1000	kg/m^3
Dynamic Viscosity	$1.002 * 10^{-3}$	$Pa.s$
Velocity	1.06	mL/min

Table 4.5 Working parameter in the simulation.[53]

Note: as it has already mentioned COMSOL does not take into whether the input velocity is laminar or turbulent and it solves the system based on the applied physics interface. Therefore, I decided to simulate the Laminar flow physic only with the velocity of 1.06 [m/s], which we found it as the laminar velocity in our system, then compare the fluid distribution in different cell geometries.

4.2.2. Turbulent Flow

Moving forward to the Turbulent Flow analysis, the foundational assumptions laid out for the Laminar Flow simulations remain applicable. The motivation behind exploring a turbulent model from a desire to putting together the effects of different flow regimes on the electrochemical cell. By comparing laminar and turbulent flows, it is aimed to explain how varying velocities and the nature of flow—whether Laminar or Turbulent—affect the distribution and efficiency of the electrolyte flow. This comparison is crucial for a deeper understanding of the operational dynamics within the cell, thus enabling us to fine-tune its design and operational parameters for enhanced performance and selectivity.

Following this base, the Turbulent Fluid Flow, $k-\epsilon$ interface from Fluid Flow physics at COMSOL Multiphysics is utilized. The 3D turbulent model is developed based on the details listed in table 4.6:

Turbulence model type	*RANS*
Turbulence model	*k-∈*
Turbulent dissipation rate	$spf.epinit^*$
Turbulent intensity	*Medium 0.05*
Turbulence length scale	*Geometry based*
Velocity 1 [m/s]	*1.85*
Velocity 2 [m/s]	*2.28*

Table 4.6 Turbulent Flow Simulation Parameters in COMSOL Multiphysics [60]

- $spf.epinit^*$ refers to the initial turbulent dissipation rate. It is a key parameter in turbulence models, especially in models like the k-ε (kappa-epsilon) model, where it helps in determining how quickly turbulence will dissipate in the flow.

Note: according to Equation 4.8, the velocity of 1.85 corresponds to a Reynolds number of 3694, which falls within the transitional range. Given its proximity to the turbulent regime, this velocity has been categorized as turbulent for the purposes of this analysis.

4.3. Meshing

In the Mesh section, a mesh configuration is developed and precisely captures the complex shapes and behaviors within the electrochemical cell. There are two main approaches to setting up the mesh in COMSOL software: the User-defined mesh, where the user specifies mesh sizes for different parts of the system according to computational needs, and the Physics-controlled mesh, which COMSOL automatically adjusts based on the involved physics. The latter also allows for customization of element sizes fitted to our geometry. Given the variety of physics interfaces in this project, a Physics-controlled mesh with a normal mesh size is preferred, ensuring a tight integration with the specific physics of this study. The illustration of the generated mesh is given in figure 4.4.

This constructed mesh guarantees the accuracy of the simulations by effectively capturing the critical physical phenomena, such as fluid flow patterns, species transport, and electrochemical reactions. By optimizing the mesh size and density, a balance between computational efficiency and the need for detailed is maintained. This optimization is crucial

for analyzing the interactions in 3D fluid dynamics and concentration analysis, thereby enabling a deeper understanding and increased predictability of the cell's performance under various operational conditions.

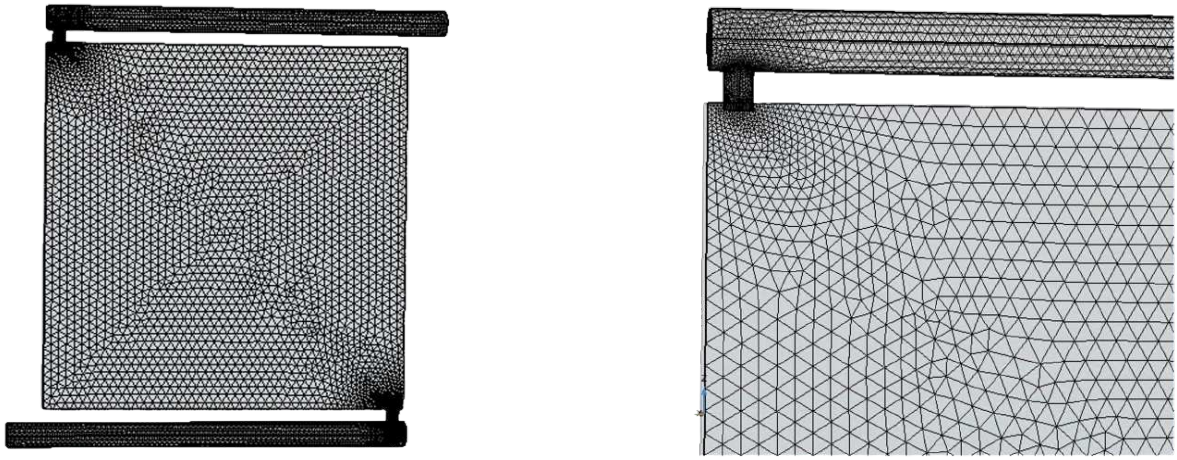

Figure 4.4 Mesh Generation for Computational Model

4.4. Concentration Analysis

The main reactant in the system is CO_2; thus, the distribution of CO_2 is one of the most important factors in this system, so in this chapter the correlation between the velocity/flow rate and CO_2 distribution alongside of the silver catalyst are simulated. CO_2 properties are given in table 4.7:

Dynamic viscosity	14.8	µPa.s
Density	1.977	kg/m³
Diffusion coefficient	1.6×10^{-5}	m²/s
Mean molar mass	44.01	g/mol
Velocity	0.0135	m/s

Table 4.7, Physical Properties of CO_2 for Velocity and Concentration Correlation Analysis

To acquire the concentration variation in cell geometries the Nernst-Planck equation which has been already described in chapter 3 is utilized. In this stage of simulation only the relationship between the fluid velocity and species concentration (CO_2) is taken into account, therefore the reaction coefficient in the Nernst-Planck is equal to zero, there is no production

or consumption of the species due to chemical reactions, and the reformed Nernst-Planck equation account only for the diffusion and convection. Thus, the simplified equation is given in equation 4.10:

$$\frac{\partial c}{\partial t} + \nabla.(-D\nabla c + uc) = 0 \qquad 4.10$$

Here we have:

c is Concentration Species $[mol/m^3]$

t is time [s]

D is Diffusion Coefficient $[m^2/s]$

u is Velocity Field $[m/s]$

4.5. Electrochemical Study

Having validated the suitability of the geometry for achieving homogeneous distribution of fluid and concentration, now electrochemical principles are applied to the specified geometry. Electrochemistry is a field where multiple mechanisms operate together to produce the interest product, as such, it is important that the cell not only supports but also enhances reactions controlled by convection, diffusion, and migration. In the previous passages the convection and diffusion were modeled by analyzing fluid dynamics and concentration variation, which paved the way for further exploration.

Since understanding migration is very important in electrochemistry studies due to its direct effect on uniform material deposition and removal, rate of electrochemical reaction on the electrode surfaces, charge transfer, and so on, in the following chapters, the current distribution in different conditions is going to be modeled, to validate the suitability of the cell.

4.5.1. Primary Current Distribution

In this chapter the Primary Current Distribution physics interface is employed to determine the current distribution within the cell's geometry.

The primary current distribution is designed to analyze and predict the distribution of electric current in electrochemical systems under steady-state conditions. Thus, in this stage the cell

geometry, applied potential, and electrolyte conductivity play a crucial role in determining the current distribution inside the cell. To do so, there are some assumptions, which have to be taken into account:

1- Electrode kinetics is neglected.
2- Mass transport is neglected.
3- Electrode potential is uniform.
4- There is only one equilibrium potential on the cathode side, CO_2 reduction.
5- There is only one equilibrium potential on the anode side, O_2 evolution.

Understanding and predicting the primary current distribution is important for the early stage of electrochemical system design, since it helps identifying possible issues related to non-uniform current distribution, such as overheating, and uneven material deposition and dissolution. Therefore, by understanding these issues early on, we can improve the system's overall efficiency and durability.

It is of significant scientific interest that in COMSOL Multiphysics it is a common practice to model the system with two electrodes, contrary to the reality where we have working electrode, counter electrode, and reference electrode and the applied potential (V_{cell}) is adjusted based on the reference electrode potential.

In COMSOL, the external potential is applied to each electrode individually, and the equilibrium potentials of each electrode as well as the potential of standard hydrogen electrode (SHE), which serves as an imaginary reference, has to be taken into consideration.
In the table 1.3 the input parameters are given:

Name	Value	Unit
Polycrystalline silver catalyst electric conductivity	$6.3 * 10^7$	$[S/m]$
Glassy carbon electrical conductivity	$1 * 10^2$	$[S/m]$
Electrolyte Conductivity [KHCO3]	10	$[S/m]$
Cathode equilibrium potential	-0.17	[V]
Anode equilibrium potential	1.23	[V]
Cathode external potential	-0.2	[v]
Anode external potential	1.6	[V]
Temperature	293.15	[K]

4.8 table Input Parameters for Electrode Potential Simulation in COMSOL

4.5.2. Secondary/Tertiary Current Distribution

Based on the findings from the Primary Current Distribution, the aim is to simulate the system with Secondary and Tertiary Current Distribution. This progression is important for understanding the system, because it includes the electrode kinetics, Butler Volmer Equation 3.10, and mass transport phenomena, Nernst Equation 3.15, which was previously neglected. The Secondary Current Distribution takes into consideration the effect of electrode kinetics, which tells us about the reaction rates and their effects on current distribution. Tertiary Current Distribution goes one step further by also considering the effect of mass transport; thus, provides more detail and accurate image of real electrochemical processes. Therefore, for this simulation the Tertiary Current Distribution is employed.

Several assumptions have been made in this segment of the study to simplify the computational process:

1- We have two reactions on the cathode and one reaction on the anode side.
2- All eCO_2RR are assumed to be in instant equilibrium.
3- The electroneutrality is valid throughout the domains because the double-layer is not explicitly modeled in this work.
4- Both compartments are supplied with the same electrolyte composition.
5- All the reaction products (CO, H_2, H_2O and O_2) are assumed to remain in liquid phase.

6- The cell operates in isobaric condition.

7- The temperature is fixed at 298.15 K. Although, in reality, the overpotential losses can be dissipated as heat (for instance, ohmic heating).

8- The ERC is assumed to occur at neutral to alkaline pH.

9- All CO_2 chemical (homogeneous) reactions are assumed to be in instant equilibrium– the equilibrium is established instantaneously. In reality, this assumption may not be valid, as the reaction rate depends on pH [42]. However, implementing the rate-dependent reaction is found to be numerically challenging – it is difficult to achieve solution convergence.

10- The electroneutrality is valid throughout the domain, due to the presence of HCO_3 and OH^-.

11- The exchange of only H^+ ions is assumed through the cation exchange membrane (Nafion), because Nafion allows to conduct only H^+.

To enhance our understand regarding the working mechanisms, I developed a 2D model that incorporates the reaction processes and inputs outlined in table 4.8 and showed in Figure 1.5:

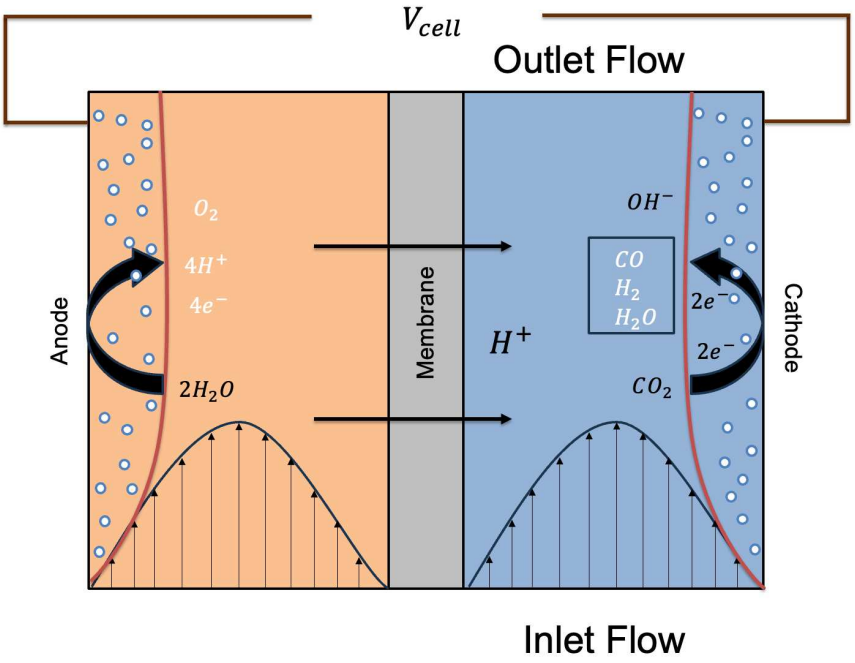

Figure 4.5 A schematic representing a 2D flow-cell for ERC to carbon monoxide.

The flow (consisting of electrolyte and the dissolved species) enters at bottom (inlet), as indicated by the flow distribution, and leaves the compartment from top (outlet). Moreover, the sides of the rectangular geometry represent the cathode (right) and the anode (left). Furthermore, the anodic and cathodic compartments are separated by a thin membrane.

Under the action of applied potential (V_{cell}) electrochemical reduction of CO_2 on cathode produces three products, CO, H_2, and H_2O as shown, whereas water oxidation at the anode produces O_2, H^+, and e^-.

On the anode side, the oxygen evolution reaction (OER) generates the required charges for subsequent reactions on the cathode side. Upon initiation of the reaction, electrons (e^-) migrate from an external circuit towards the cathode, while protons (H^+) also move across the membrane to the cathode. At the cathode, these charges interact with the reactant (CO_2), resulting in the production of CO, H_2O, and H_2 as by-products.

According to the above description the dissolved CO_2 enters the cathodic chamber. CO_2 solubility at given operating conditions is calculated using the method elaborated in chapter 3 table 3.1. With $KHCO_3$ as the electrolyte, the equilibrium concentrations of different species are calculated as follows:

$$k_{b1} = \frac{k_f^{b1}}{k_r^{b1}} = \frac{[CO_2][OH^-]}{[HCO_3^-]} \quad 4.11$$

$$k_{b2} = \frac{k_f^{b2}}{k_r^{b2}} = \frac{[HCO_3^-][OH^-]}{[HCO_3^-]} \quad 4.12$$

$$[k^+] + [H^+] = [OH^-] + [HCO_3^-] + 2[CO_3^{2-}] \quad 4.13$$

$$[k^+] + \frac{k_w}{[OH^-]} = [OH^-] + k_{b1}[CO_2][OH^-] + 2k_{b1}k_{b2}[CO_2][OH^-]^2 \quad 4.14$$

The value of k_f and k_r are calculated from table 3.1 chapter 3. In addition, equation 4.14 can be solved iteratively to get OH^- concentration, and subsequently that of the remaining species. To acquire such results from COMSOL software we must set number of inputs which are listed in table 4.8:

Name	concentration	Unit
Temperature	293.15	[K]
Pressure	1	atm
C_{OH^-}	1.0446*10^{-3}	$[mol/m^3]$
$C_{HCO_3^-}$	1485.4	$[mol/m^3]$
C_H^+	9.5731*10^{-6}	$[mol/m^3]$
C_{CO_3}	7.3	$[mol/m^3]$
C_k^+	1485.4	$[mol/m^3]$
CO evolution exchange current density (CO_{j_0})	4.71*10^{-4}	$[mA/cm^2]$
CO anodic and cathodic transfer coefficient (α_{CO})	0.33	$[-]$
H_2 evolution exchange current density(H_{2,j_0})	1.16*10^{-6}	$[mA/cm^2]$
H_2 anodic and cathodic exchange current density(α_{H_2})	0.36	[-]
O2 evolution exchange current density (O_{2,j_0})	6.21*10^{-5}	$[mA/cm^2]$
O2 anodic and cathodic transfer coefficient (α_{O_2})	0.5	[-]

Table 4.9 lists the necessary input parameters for the COMSOL software. [61]

Another important input parameter is the species diffusivity. The diffusivity directly alters the diffusive flux, and indirectly the migrational flux, through the Nernst-Einstein relation (equation 3.16). Table 4.10 lists the diffusivities of different species involved in the model. These tabulated values are taken from the real experiment [38]. Although, these values are

temperature dependent, viscosity dependent, and vary slightly between different sources, in the present work these are kept constant.

Species	Diffusion Coefficient	Unit
(D_{OH})	$5.27e-9$	$[m^2/s]$
$\left(D_{HCO_3^-}\right)$	$9.23e-10$	$[m^2/s]$
(D_H^+)	$9.31e-9$	$[m^2/s]$
(D_{CO_3})	$1.19e-9$	$[m^2/s]$
(D_k^+)	$1.96e-9$	$[m^2/s]$
$\left(D_{H_2}\right)$	$5.13e-9$	$[m^2/s]$
(D_{CO})	$2.03e-9$	$[m^2/s]$

Table 4.10 presents the diffusivities of various species used in the model, which are critical in determining both diffusive and migrational fluxes via the Nernst-Einstein relation.

As already mentioned, ERC in aqueous electrolyte using silver electrode produces mainly three products as shown in figure 4.5. Table 4.11 lists the electrochemical reactions used in this study. The kinetic parameters (α and j_0) for cathodic reactions are fitted using Tafel equation 3.11 on the experimental data by [38]:

	Electrode reaction	a	$E^0(vs\ SHE\ at\ PH=7)[V]$
Cathode	$CO_2 + 2H^+ + 2e^- \rightarrow CO + H_2O$	0.5	-0.719
	$2H^+ + 2e^- \rightarrow H_2$	0.5	-0.609
Anode	$2H_2O \rightarrow O_2 + 4H^+ + 4e^-$	0.5	1.23

Table 4.11 kinetic parameters for the electrode reactions

In COMSOL, the modeling of both cathode and anode sections employs a tertiary current tcd approach, complemented by a dilute-species transport mechanism. This approach is adopted because concentration overpotential (η_{conc}), activation overpotential (η_{act}), and ohmic losses are all significant factors that must be considered, with none being consistently negligible. The assumption of dilute species posits an infinitely dilute aqueous electrolyte environment, implying that there is no interaction between the dissolved species. Cathode and Anode Compartments:

At the cathode only CO_2 is assumed to get reduced. Implying, other carbon containing species, for instance, HCO_3^- and CO_3 do not participate in the electrode reactions. In addition, the role of, HCO_3^- remains debatable: some researchers have observed that HCO_3^- can be directly reduced [54, 55], some others disagree [43] [44], and there are others, who claim that HCO_3^- is decomposed to CO_2 first, before it is reduced [45] [46] [47] . Therefore, due to this ambiguity over the role of, HCO_3^-, in the present work it is assumed that it does not undergo electrochemical reduction.

Regarding the anode reaction, it is assumed have a non-limiting reaction. Practically, this means using a catalyst which has extremely facile kinetics of water oxidation. However, in practice, oxygen evolution, in fact, has sluggish kinetics, and it is an energy intensive process [48]. Nevertheless, the assumption facile kinetics of anodic reaction allows for studying the ERC independent of the anodic reaction.

The 3D schematic of the cell is depicted, figure 4.6, To better understand how the COMSOL set the boundaries to solve the equations presented in chapter 3:

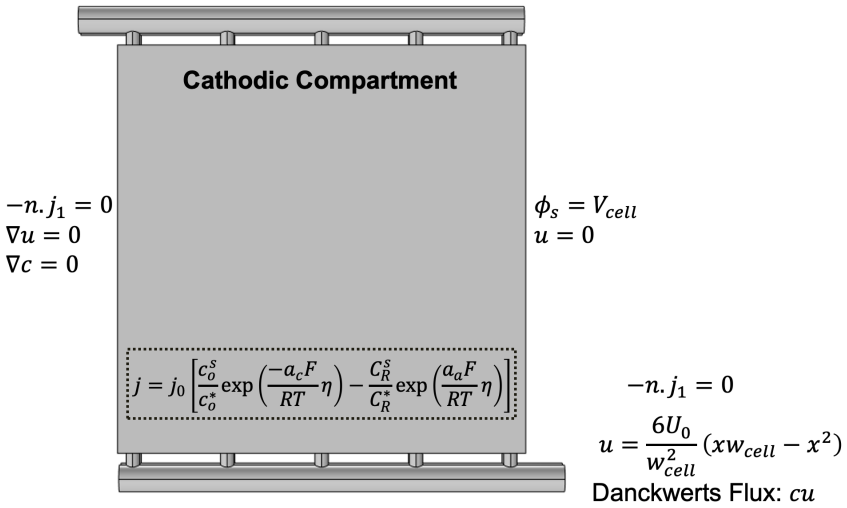

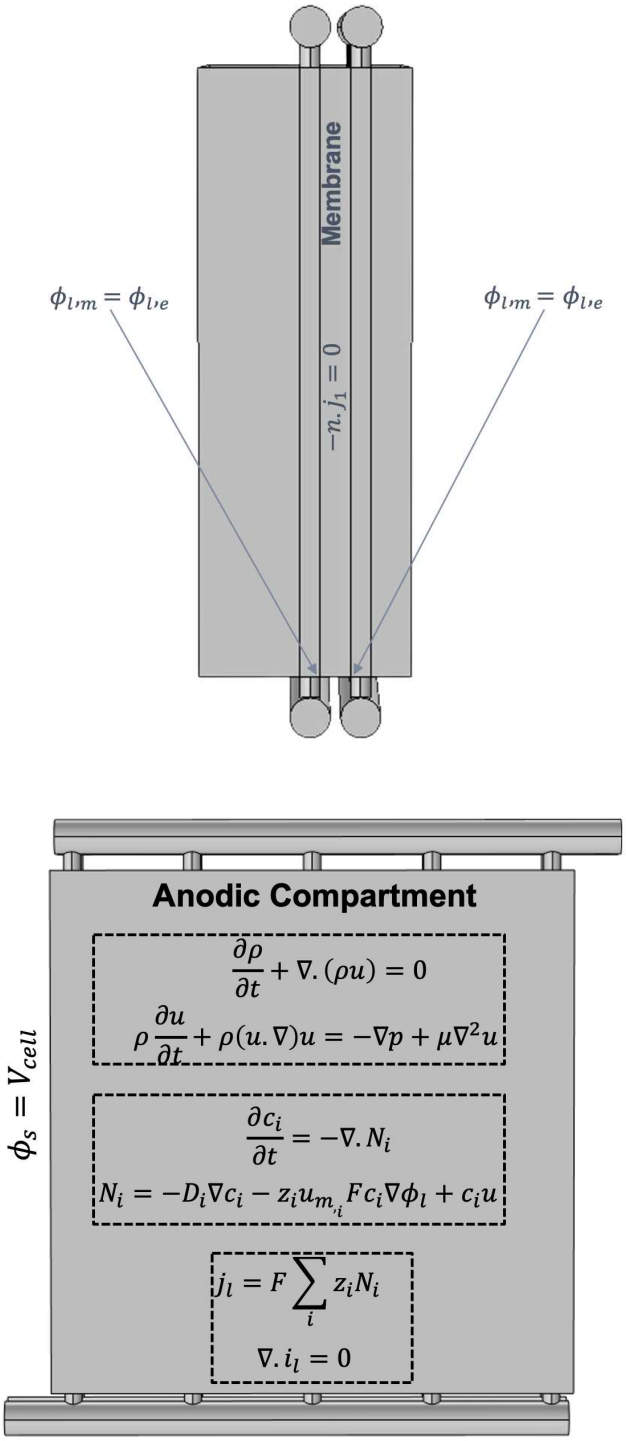

Figure 4.6 the boundary conditions for the 3D flow-cell model

These equations shown in the anodic compartment, and the boundary conditions shown on cathodic compartment are applicable to the other compartment as well. There are two remarks worth noting: First, Danckwert's flux is the inlet boundary condition selected for species transport. According to COMSOL knowledge base [49], any reaction – here cathodic reaction – which starts right from the inlet, causes unwanted negative concentrations in the

domain. By choosing Danckwert's flux condition this can be avoided [50]. Second, since both anode and cathode reactions are modelled, applied cell potential is assigned to both sides.

The underlying equations are grouped in three parts (dashed rectangles) as shown in the anodic compartment of Figure 1.6. The main purpose here is to explain how COMSOL treats these equations while solving the problem. The first rectangle shows the equations for obtaining the velocity field, the second represents the species transport and the third rectangle shows the equations for obtaining electrolytic potential. As it can be noticed, each rectangle contains a set of equations related to what COMSOL refers to as 'physics'. Moreover, given the nonlinear nature of these underlying equations, the solution is found iteratively using the Newton method. This procedure requires finding a Jacobian matrix. In COMSOL this Jacobian matrix can be formed in two ways: fully coupled approach and segregated approach. In the fully coupled approach one Jacobian matrix is created covering all the problem relevant 'physics'. Conversely, in the segregated approach the Jacobian matrix corresponding to each 'physics' is created separately. In other words, each 'physics' is solved separately. This means, for example, first solving for the velocity field, then for the species transport and lastly for the electrolytic potential, until the solution is converged.

Note that in COMSOL there two ways to study the behavior of the model, first stationary in which users are interested in finding a solution that does not change as time progresses. The results will give users information about the system's behavior under a set of conditions that are constant in time. This type of study is used when time is not a factor in the behavior of the modeled phenomena, or users are only interested in the final equilibrium state of the system. Second, time dependent study in which the user is interested in how the system evolves from an initial state to a final state over a series of time steps. This type of study is essential when the time factor is significant to the behavior of the modeled phenomena and user needs to analyze how the system responds over time, not just in its final steady state.

4.5.3. Meshing

As it is already mentioned COMSOL uses FEM for solving the given equations. To achieve this, a bigger domain is divided into smaller domains by meshing operation. Generally, the meshing philosophy is, generating a finer mesh where higher concentration/velocity gradients are

expected. However, creating a finer mesh improves the accuracy albeit at a higher computational cost.

In a flow-cell, higher concentration gradients are expected in the wall normal direction of the cathode/anode and membrane; also, near the inlet where the flow enters, and immediately undergoes an electrochemical reaction at the cathode/anode. High aspect-ratio quadrilateral mesh elements can meticulously capture these concentration/velocity gradients close to electrode surface and membrane. In addition to this, making the mesh finer at the inlet, and progressively coarser towards the outlet, for instance, as shown in Figure 4.6– can help in accurately resolving the desired physics.

Choosing a mesh size involves balancing the solution accuracy and its computational cost. The mesh size is selected through the mesh independence study, further details on which will be provided in Chapter 5.

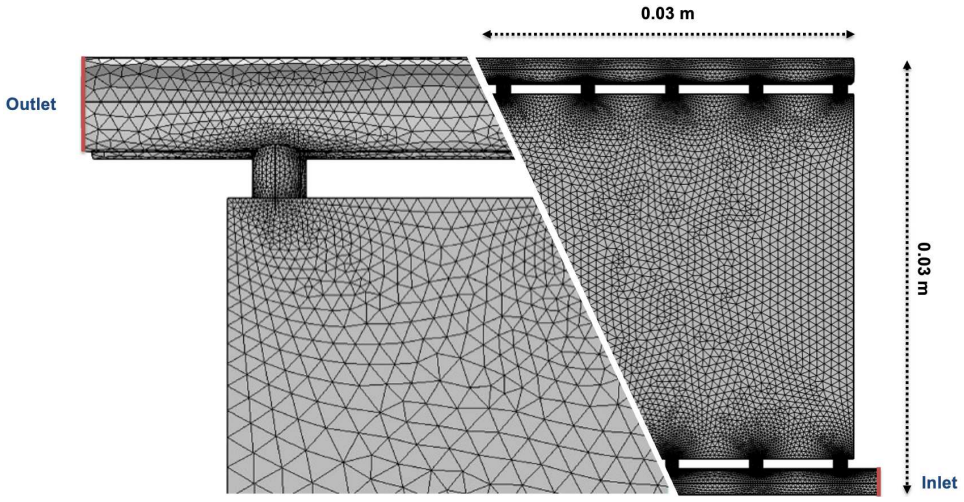

Figure 4.7 the flow cell geometry after meshing

To sum up, the flowchart that has been provided captures the systematic approach that was used in this investigation with the COMSOL software. Starting with the defining of geometry and material parameters, we analyze thermal conductivity, take mass transport and kinetic effects into account, and finally look at laminar flow conditions. We proceed to the study

phase after a computational mesh has been created, during which simulations are run and the outcomes are repeatedly improved. The aforementioned visualization highlights the methodical and interrelated procedures that constitute the foundation of our modeling methodology, ultimately leading to the resilient outcomes that enhance our comprehension of the concerned system.

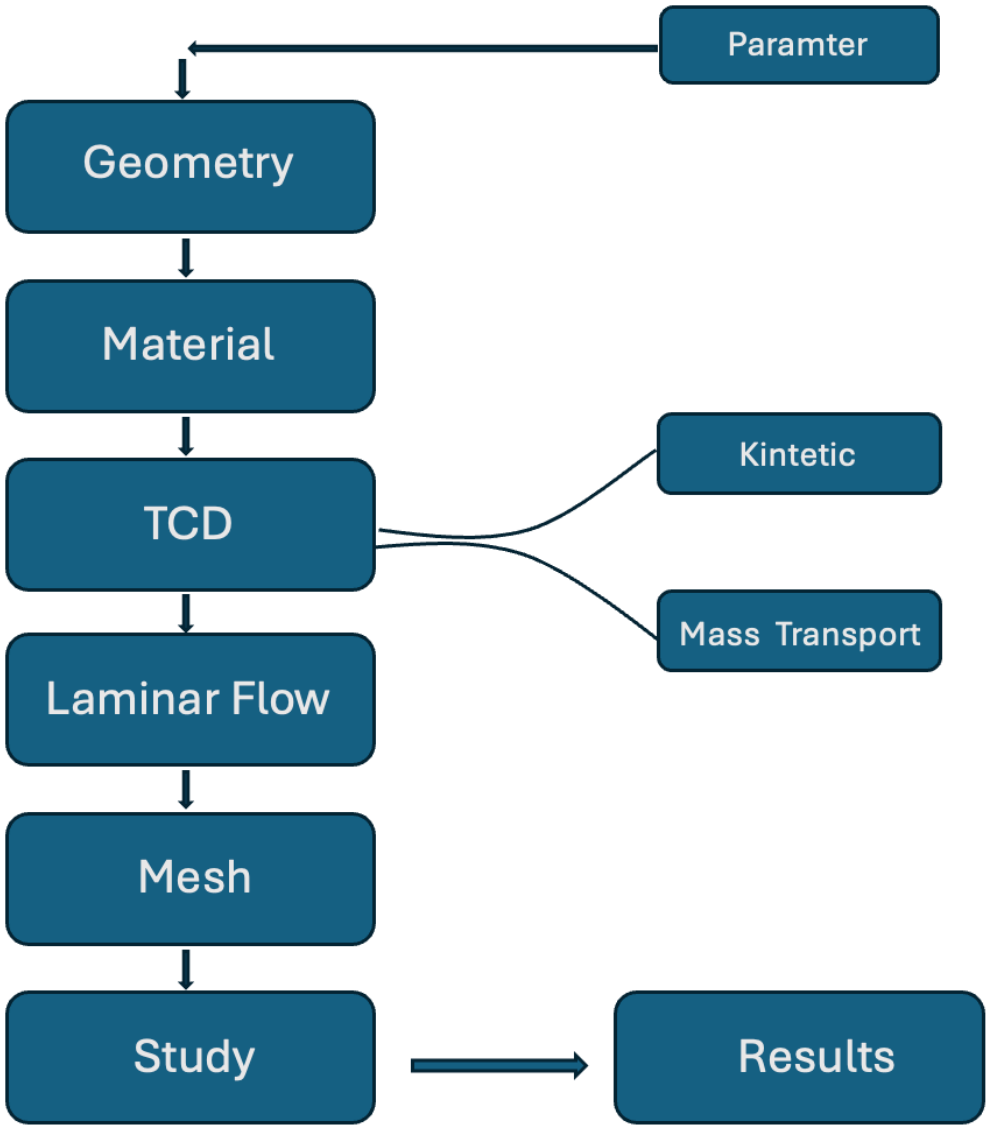

Figure 4.8 Schematic of the Modeling Workflow in COMSOL

5

Results and Discussion

This section presents the results of fluid dynamics simulations, including concentration analysis and electrochemical investigation within the cell. It emphasizes the effects of flow conditions on electrolyte distribution, product selectivity, and overall cell performance across various cell geometries. The analysis is grounded in the calculated Reynolds numbers, which guided the selection of flow conditions for the simulations, ensuring a rigorous examination of flow dynamics under varying operational scenarios. In the following, the findings from electrochemical reactions, including the current distribution and product concentration, are reported.

5.1. Laminar Flow Model Validation

Building on the conditions outlined in Chapter 3, a laminar fluid distribution within the cell have been achieved, as illustrated in Figure 5.1:

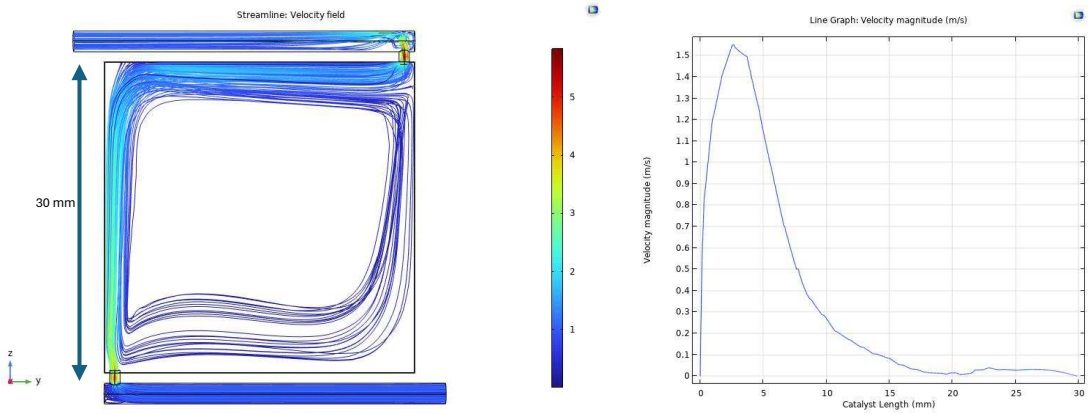

Figure 5.1: presents a visual representation of the flow field and corresponding performance metrics for the modified geometry with single inlet and outlet.

Referring to Table 4.4 in chapter 4 the velocity under consideration is 1.06 m/s. This velocity, when coupled with the physics of laminar flow, results in notably high velocities at both the inlet and outlet of the cell. Conversely, the cell's center exhibits regions of stagnation, which could detrimentally impact cell performance under reaction conditions.

Additionally, the simulations were conducted using the same velocity parameter but with a geometry featuring multiple inlets and outlets. The results of these simulations are presented to illustrate the impact of this altered configuration on flow distribution and cell performance:

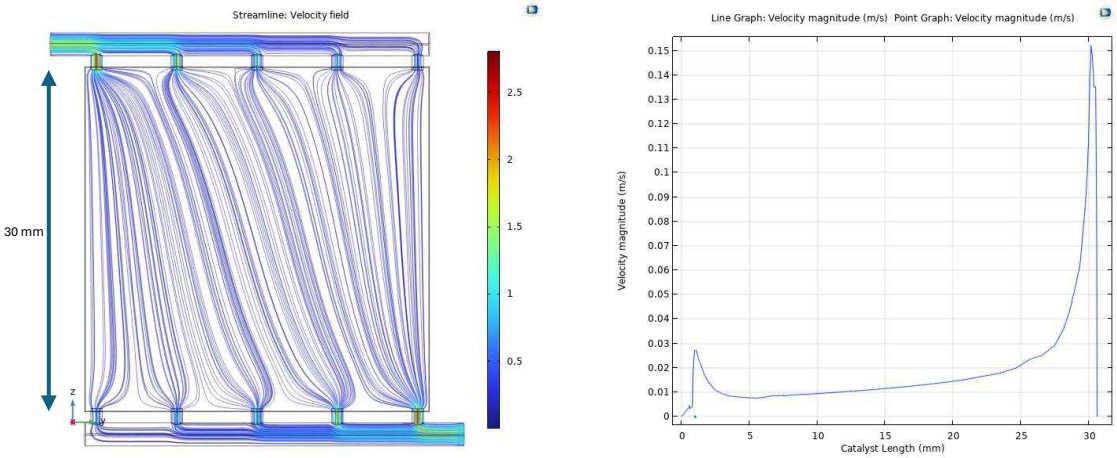

Figure 5.2: presents a visual representation of the velocity distribution on the ZY plane for the modified geometry with multiple inlets and outlets and laminar velocity.

The uniformity of the streamlines and the distributed gradient in velocity suggest that the fluid distribution is very uniform and predictable. Such conditions are often desired in processes where precise control over the flow and minimal disturbance are required. This laminar flow regime ensures that the cell avoids turbulence.

5.1.2. Turbulent Flow Model Validation

After examining laminar flow, the effects of turbulence within the cell were explored by simulating two different turbulent velocities, already defined table 4.4, using a turbulence model. These simulations help to see how turbulence changes the flow inside the cell and what changes occur in the velocity distribution. Thus, at the first step the results in single I/O geometry with the velocity of 1.85 [m/s] are illustrated in Figure 5.3:

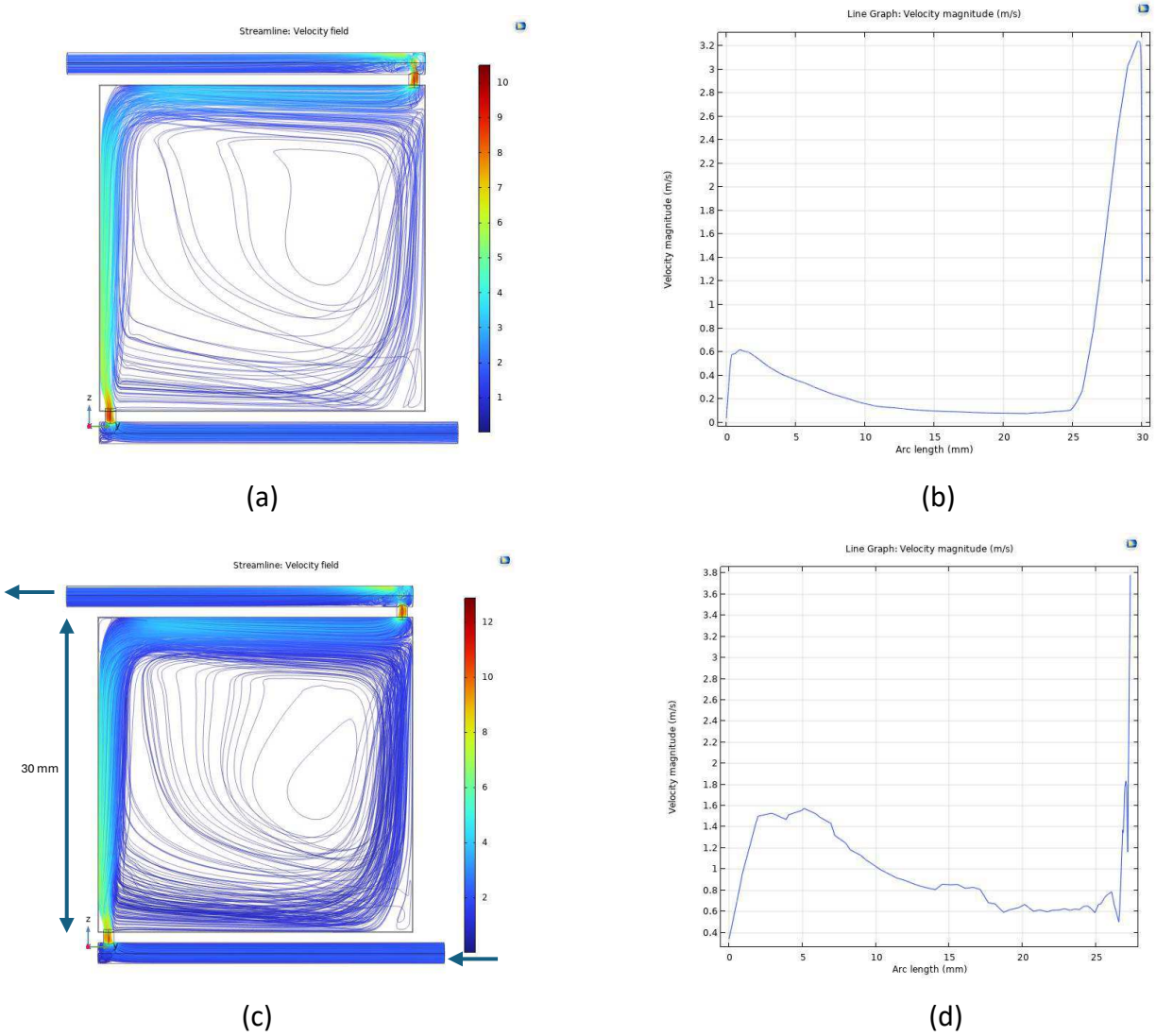

Figure 5.3: (a) and (b) represent the transition fluid flow velocity with single inlet and outlet cell geometry (c) and (d) represent the turbulent fluid flow velocity in the same configuration

The simulation shows that turbulent flow makes the streamlines twist and turn a lot and this effect is stronger in higher velocity (2.28 [m/s]), which is different from the straight lines seen with laminar flow figure [5.1, 5.2]. This mix-up means the liquid moves faster in some parts, especially where red is seen near the inlets and outlets and alongside the wall in front of inlet channel, and eddies are formed in the center resulting in poor mixing conditions. The different colors show that the velocity in the fluid spreads out more evenly.

After the observations of turbulent flow in a single inlet and outlet setup, the analysis is expanded to include simulations of turbulent flow within a cell configured with multiple inlets

and outlets. This will allow to assess the impact of a more complex entry and exit design on the fluid's velocity and mixing patterns. The results, are depicted in Figure 5.4:

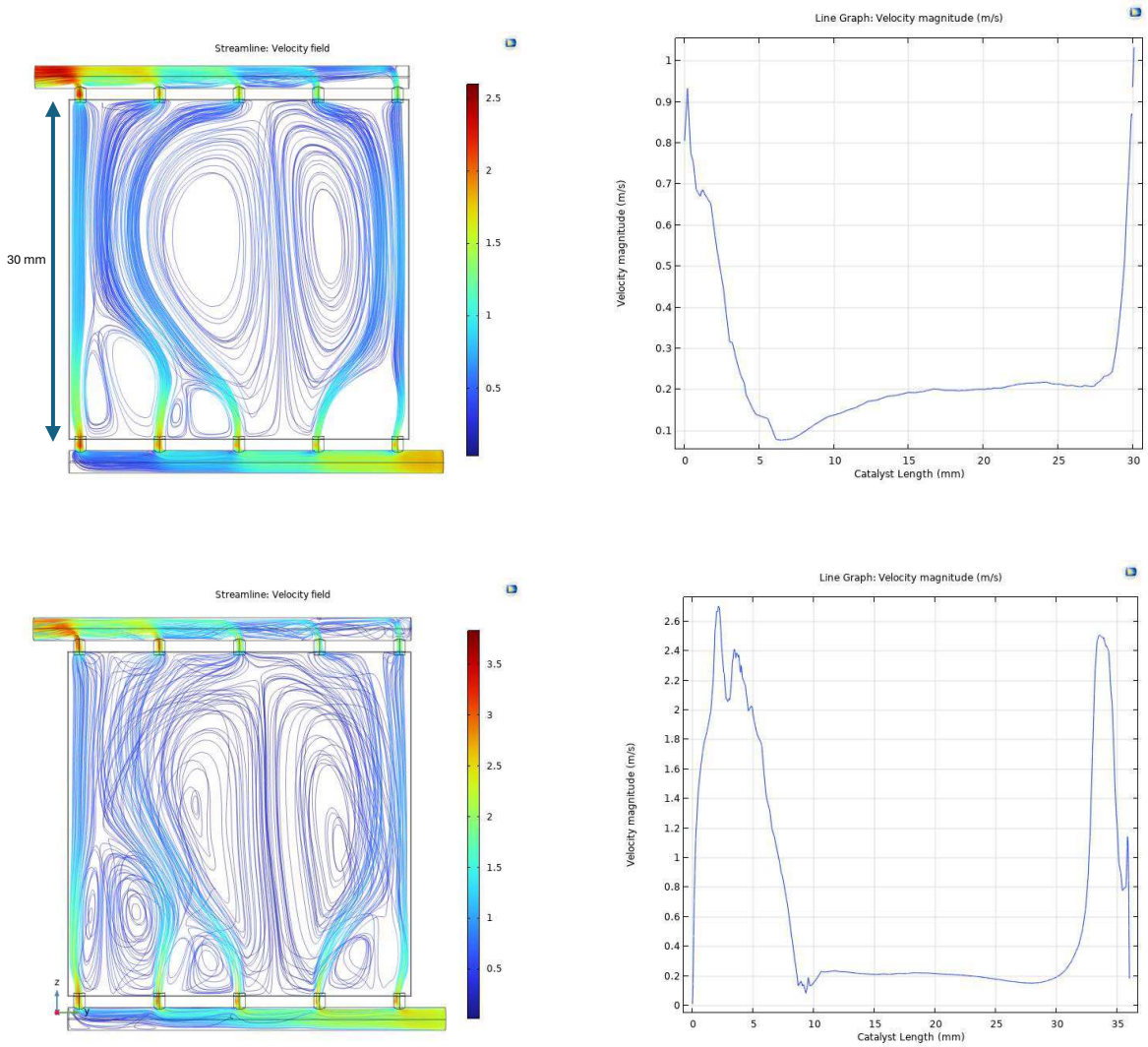

Figure 5.4 visual representation of fluid flow with multiple inlets and outlets cell geometry and transition and turbulent fluid velocities.

As shown in the figure, there is increased turbulence in the fluid distribution, especially at a velocity of 2.28 [m/s] in the bottom figure. This turbulent model with higher velocity leads to more mixing, which could be beneficial for mixing species in the electrolyte. However, the eddies in both compartments cause an uneven current distribution, which is an important factor in electrochemical CO_2 reduction cells. In contrast, with a more homogeneous fluid distribution, we will achieve better current distribution which is one the desire parameter in electrochemistry because it leads to uniform usage of catalyst surface. Subsequently, this could result in a more uniform electrochemical reaction near the catalyst, increasing faradaic efficiency and selectivity in producing CO.

Please note that these simulations were performed using the properties of water and did not take concentration into account. The aim was to observe how different cell configurations, physical properties, and velocities influence the velocity fields. As an optional configuration for further analysis, the cell configuration with multiple inlets and outlets with the laminar flow is taken into account for further investigation.

5.2. Concentration Analysis Validation

At this stage, the concentration gradient is incorporated into the fluid distribution analysis to observe how it influences the distribution of species in conjunction with velocity within the cell. Getting the most homogenous fluid distribution along the catalyst in multiple inlets and outlets cell configuration with laminar fluid flow, the concentration analysis also is only applied on that configuration. To evaluate the impact of concentration, the Transport of Diluted Species physics interface within COMSOL is utilized. This approach incorporates the Nernst-Planck equation (Equation 3.15, Chapter 3) for detailed analysis. Refer to Figure 5.5 for visual representation:

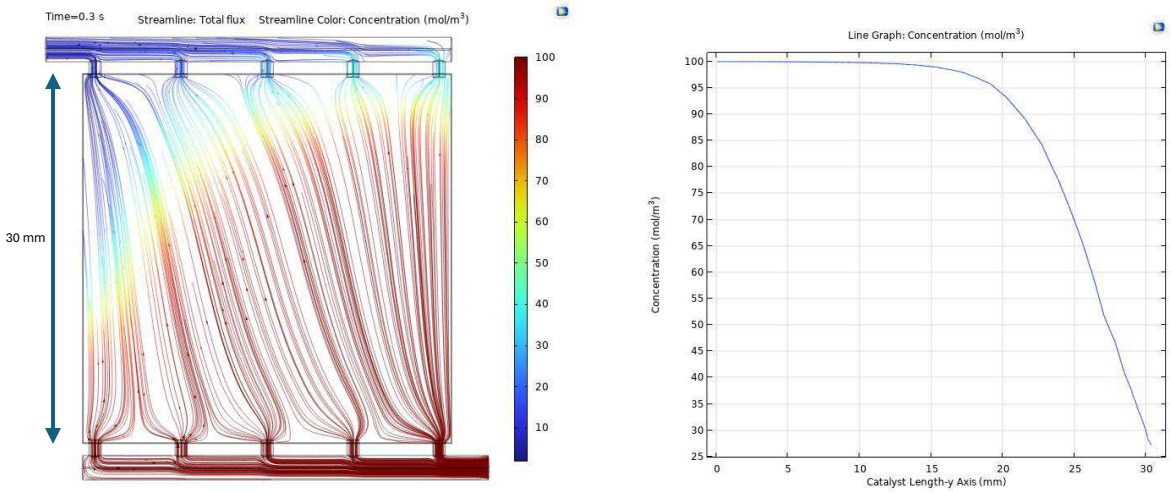

Figure 5.5: outcomes of incorporating a concentration gradient into the fluid distribution analysis within the multiple cell configurations.

The gradual shift in colors from warm (red) to cool (blue) indicates a concentration gradient, with the concentration decreasing further away from the initial inlets. This analysis was performed using a Time Dependent solver to illustrate how the concentration changes over

time as a result of velocity influences. Consequently, at time 0.3 seconds, the concentration near the outlets is lower, and as we approach the convergence time of 1 second, the concentration is expected to normalize throughout the entire cell.

5.3. Electrochemistry Validation

In the following subsections, a comprehensive validation process for the electrochemical models developed in this study will be embarked upon. This will involve a critical assessment of the primary current distribution, tertiary current distribution, and reaction kinetics against theoretical predictions and experimental data.

5.3.1. Primary Current Distribution Validation

In this chapter, the results from the simulation, which looked at how electric current spreads out in the cell design when it is in a steady state, are discussed. Details such as the speed of the reactions and the movement of materials were skipped over, with the focus instead being placed on the basics, such as ensuring an even distribution of current. This approach facilitated the early identification of potential problems, such as parts of the cell overheating, or materials not being laid down evenly. In the initial model, the potential is set in a way that uniformly applied across the surfaces of both electrodes via Potentiostatic control. Under this scenario, the conductivity of the electrodes becomes irrelevant, as the focus shifts towards considering the surface area of the electrodes for subsequent analyses, as illustrated in Figure 5.6:

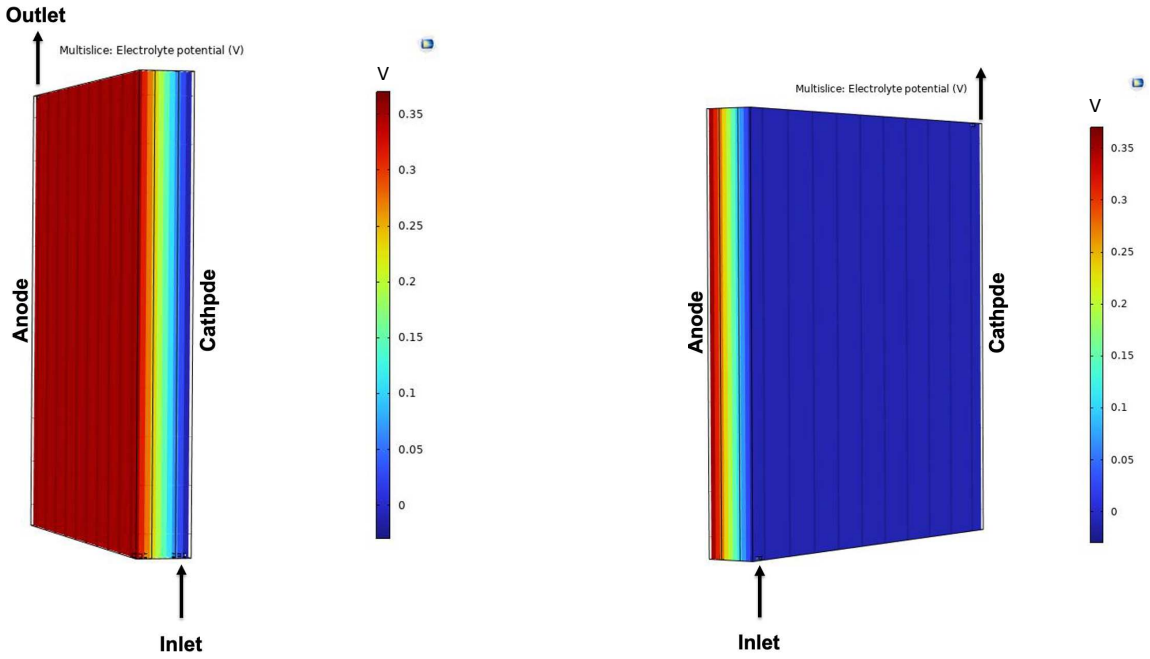

Figure 5.6 Representation of the potential distribution across the cell.

As indicated in figure 5.6 the electrolyte potential is higher on anode side where we have oxidation reaction and zero on the cathode side, with respect to anode, where we have reduction reaction. This gradient drives the migration of ions in the electrolyte to maintain charge balance as electrons flow through the external circuit from anode to cathode to power the cell's electrochemical reaction.

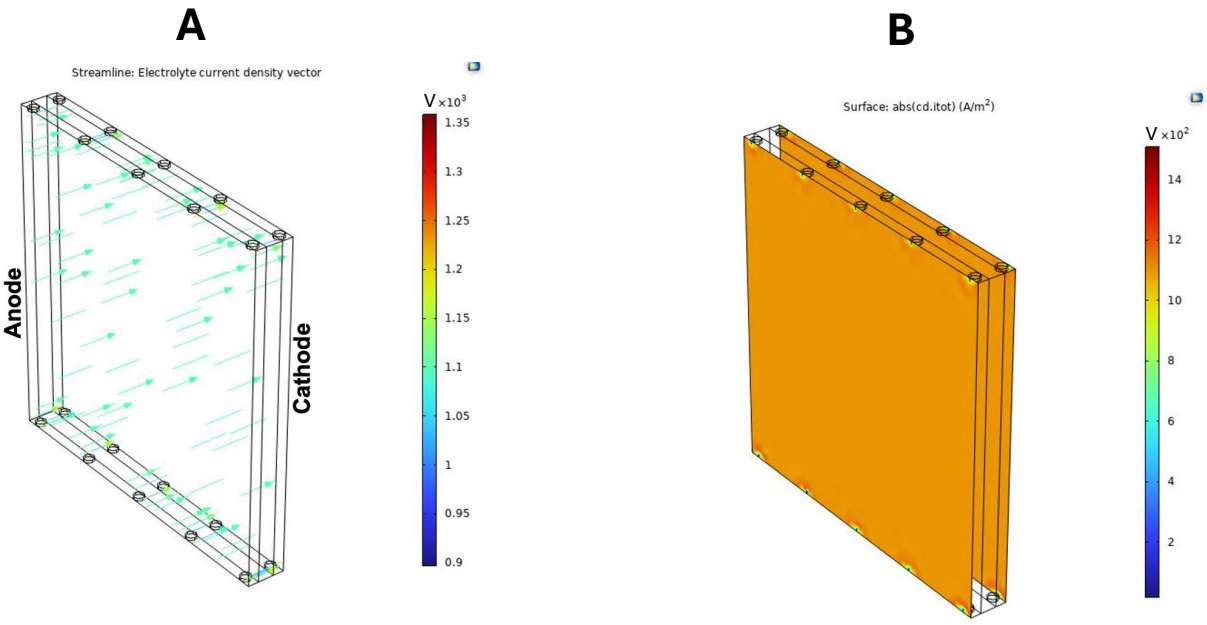

Figure 5.7 Representation of the electrolyte current density across the cell.

Figure 5.7 shows the three-dimensional nature of the cell with vectors representing the direction and magnitude of the electrolyte current density from the anode side toward cathode. The color and length of the arrows indicate the current density's magnitude at different locations within the cell, and at it is clear we have somehow the uniform magnitude except from the region around the inlets and outlets. The figure 5.7 B shows that the current density on the surface of the electrodes is consistent. Note that the use of the term "abs.cd.tot" in the title of the right-side image mean "absolute current density total," suggesting it is showing the total current density passing through the surface.

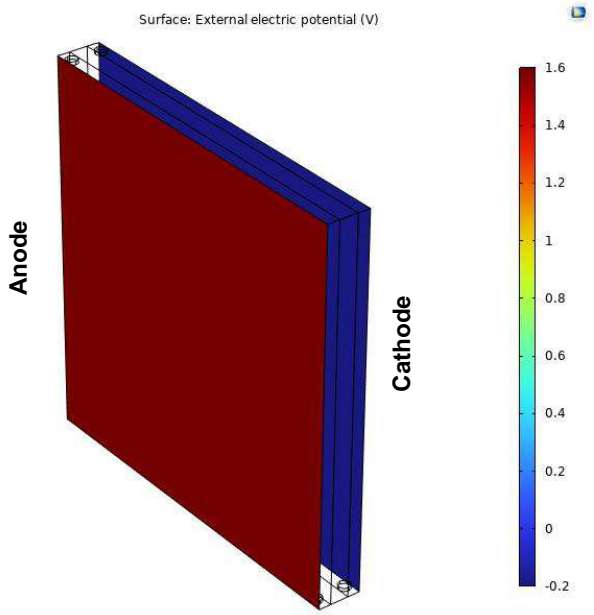

Figure 5.8 provides a visual representation of applied potential across cathode and anode surface.

Pointing out the discussion and the data presented in Table 4.8 of Chapter 4, figure 5.8 captures the external potentials at the anode and cathode as they are configured relative to the equilibrium potential. The cathode exhibits a negative value, reflecting the reduction reaction occurring there, while the anode displays a positive value, indicative of the oxidation reaction taking place.

In conclusion, the simulation results effectively validate the primary current distribution within the electrochemical cell, confirming a uniform electric current spread in steady-state conditions. The potentiostatic control application across the electrodes' surfaces ensured that the current distribution was not influenced by the electrodes' conductivity but was instead determined by the surface area. The simulation demonstrated a higher electrolyte potential at the anode due to the oxidation reaction and zero potential at the cathode where reduction

occurs, creating a potential gradient that drives ionic migration to maintain charge neutrality. The uniformity of the current density was confirmed, except in regions near the inlets and outlets, as depicted in the simulation visuals. Additionally, the consistency of the absolute current density total across the electrodes' surface was observed, aligning with the theoretical expectations. Lastly, the external electric potential profiles at the anode and cathode correlated with the respective oxidation and reduction reactions taking place, as anticipated from the cell's electrochemical principles. These findings underscore the reliability of the cell design and its operational efficacy, providing a strong foundation for further optimization and scale-up processes.

5.3.2. Tertiary Current Distribution

After confirming the accuracy of the cell geometry in terms of fluid flow and current distribution, the following aims to integrate electrochemical reactions to build upon the established findings. This involves assessing the impact of electrode kinetics and concentration gradients on the system.

Initially, this study sought to understand how variations in cell geometry and fluid dynamics influence product concentration, specifically CO and H_2, under consistent input conditions. To achieve this, the Tertiary Current Distribution method was employed, incorporating data from Chapter 4. The validation of fluid dynamics highlighted the optimal fluid flow for our scenario as being characterized by laminar physics with a laminar velocity profile. Consequently, subsequent analyses will exclusively focus on laminar flow to address the convection equations.

The analysis begins with modeling the product distribution in a configuration with a single inlet and outlet, so as the first result the electrolyte potential inside the cell is presented in Figure 5.9:

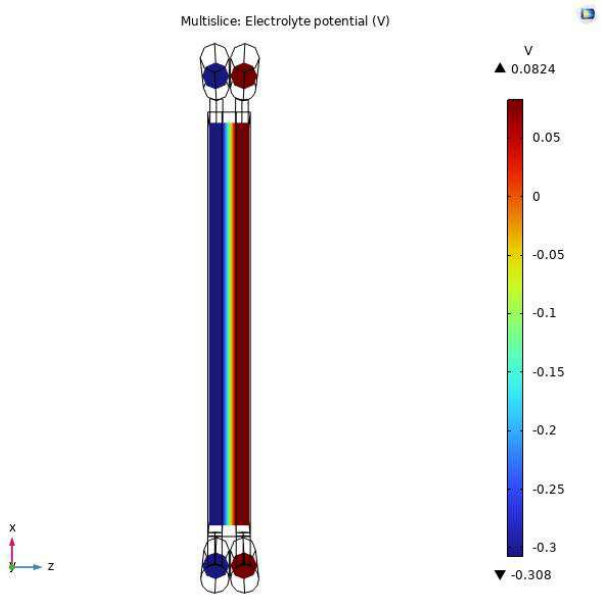

Figure 5.9 shows spatial distribution of electrolyte potential within an electrochemical cell.

The color gradient along the cell denotes the potential variations, with the anode region on the right exhibiting the highest electrolyte potential, as indicated by the warmer colors on the scale. This region is characterized by an oxidation reaction, which is typically associated with the loss of electrons. Conversely, the cathode region on the left, depicted in cooler colors, shows the lowest electrolyte potential, aligning with the site of the reduction reaction where the gain of electrons occurs. The central part of the cell is occupied by the membrane, which serves as a physical and ionic conductor between the two electrodes, allowing for ion exchange while maintaining electrical neutrality in the system. The observed potential gradient is a direct consequence of the electrochemical reactions occurring at the respective electrodes.

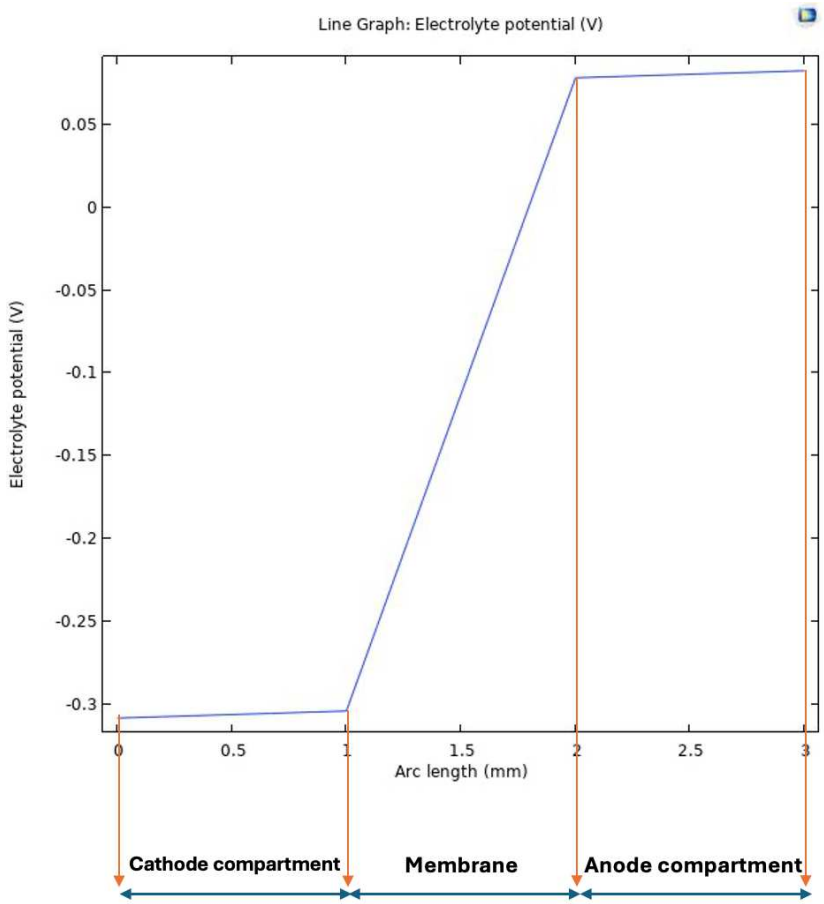

Figure 5.10 potential distribution across the different compartments of the electrochemical cell.

Based on the representation given by Figure 5.10, the oxidation reaction at the anode generates a surplus of positive charge, leading to a higher potential, while the reduction reaction at the cathode leads to an accumulation of negative charge, manifesting as a lower potential. This potential difference is the driving force for ion migration through the membrane, which sustains the cell's operation. The specific color in the membrane region indicates a relatively neutral potential, with neither the high nor low extremes present at the electrodes. This is consistent with its role as an intermediary in the electrochemical process, allowing ions to pass through while maintaining overall charge balance within the cell. In the pursuit of enhancing the overall efficiency and performance of the electrochemical cell, a thinner membrane is implemented in the subsequent simulation compared to the one used in this simulation, figure 5.10. This decision is supported by several key considerations. Firstly, a thinner membrane is expected to decrease the ionic resistance within the cell, potentially leading to an increase in power density. This modification could allow the cell to deliver a greater amount of power relative to its size, which is highly advantageous for applications

requiring lightweight and compact energy sources. Additionally, the reduction in membrane thickness improves the dynamics of ion transport, thereby accelerating the reaction rates and enabling a more rapid response to changing power demands. This is particularly relevant for devices that necessitate quick charging and discharging cycles. At the end, the simulation thus validates the fundamental principles of electrochemical cell behavior, providing a visual and quantitative representation of the potential distribution that is critical for the cell's functionality.

Please be aware that the electrolyte potential observed in the pipes in Figure 5.9 arises from the boundary conditions specified within the COMSOL Multiphysics software. The utilization of multiple physics modules necessitates that the boundary selections for each module conform to the requirements of the others, resulting in the pipes being included as components of the system. This is a constraint specific to 3D simulations; however, in 2D simulations, we have the capability to exclude these artifacts, thereby enhancing the accuracy of our model. In Graph 5.11, we observe the successful production of CO as the primary product of interest in this electrochemical cell, evidenced by the satisfying outcomes from the electrolyte potential measurements.

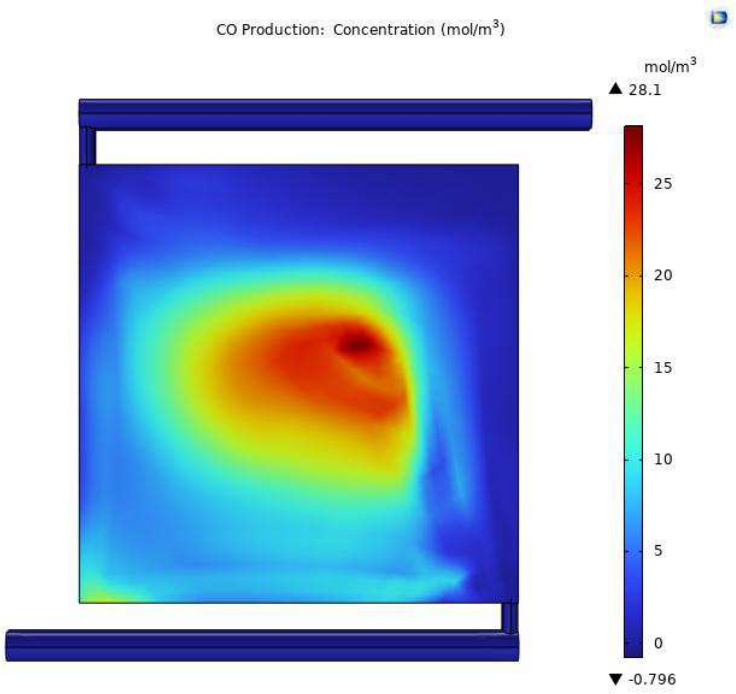

Figure 5.11 visual representation of the concentration gradient of carbon monoxide (CO) within the electrochemical cell.

From the fluid dynamic simulation, a pattern of steady streamlines is visible, Figure 5.1, which confirmed the laminarity of the flow, with a velocity set to 1.06. we figured out that an orderly flow pattern is crucial for our processes, as it allows for a stable environment where reactions can occur with predictability.

Turning to the CO concentration distribution, figure 5.11, a significant accumulation of CO in certain areas is noticeable, depicted by the red and orange hues. This pattern is indicative of where the CO concentration is the highest, away from the direct influence of the inlet and outlet flows. The correlation between these areas and the slower streamline velocities suggests that the reduced flow in these regions allows more time for the CO to form and concentrate.

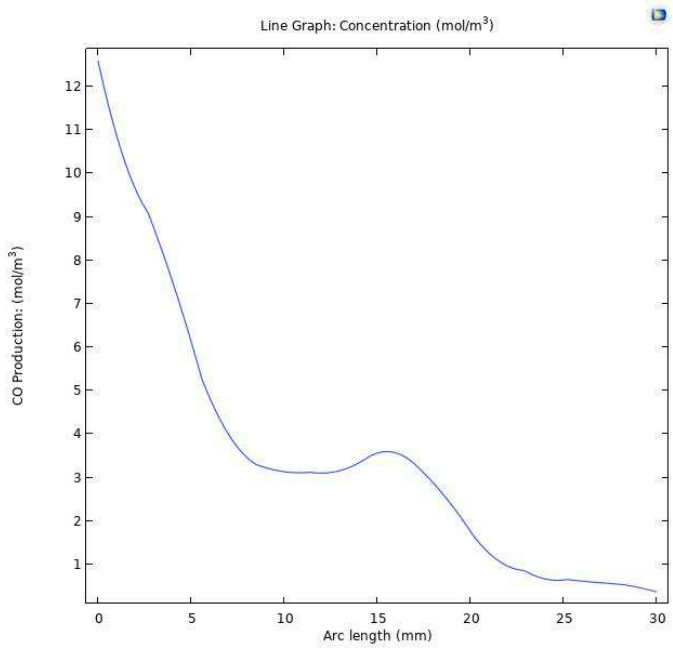

Figure 5.12 concentration of carbon monoxide (CO) production as a function of the arc length

Figure 5.12 illustrates that the concentration of CO is highest on the left side of the catalyst layer, corresponding with the area of reduced velocity field. This suggests that the slower flow facilitates a greater accumulation of CO in this region. As we traverse the length of the catalyst, there is a noticeable decline in CO concentration, indicating that the rate of accumulation of CO decreases with distance from this initial high-concentration zone due to the variation in velocity field.

These insights underscore the complicated relationship between fluid flow and reaction outcomes in the cell. The controlled flow conditions are evidently instrumental in achieving a desired concentration distribution of CO. By fine-tuning the flow characteristics, such as velocity and flow path, we can enhance the reaction efficiency and potentially improve the selectivity of our electrochemical processes. In addition, proper fluid distribution ensures that reactants are delivered evenly to the reactive surfaces. This uniformity is crucial for achieving consistent reaction rates across the entire electrode, which can affect the overall performance of the cell. These simulations are thus invaluable for guiding the optimization of our cell's design and operational parameters.

To better visualize the surface reaction, a 2D model with the same setup parameters has been developed. In this two-dimensional simulation of the electrochemical cell, the focused is on the detailed visualization of CO generation along the cathode surface. This approach allows for an enhanced view of product concentrations across the catalyst layer, providing valuable insights into the efficiency and distribution of the reaction. As depicted in figure 5.13, there is a clear gradient of CO concentration, which is particularly concentrated along the vertical span of the cathode.

Notably, the simulation assumes a uniform distribution of the applied potential across the catalyst due to its flat surface architecture. This assumption is critical as it ensures that the electrochemical reactions are evenly driven across the entire active area, thereby promoting consistent CO generation. The visualization highlights the bottom section of the plane, where the inlet is located, marking the entry point for reactants into the system. Here, the concentration of CO is observed to initiate and subsequently spread upward along the cathode, illustrating the trajectory and accumulation of the product as the reaction proceeds.

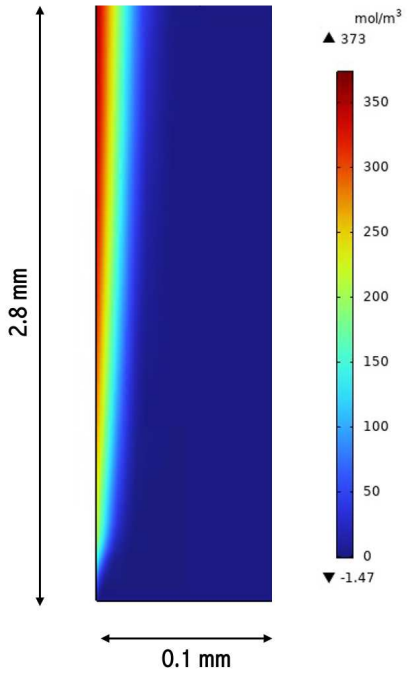

Figure 5.13 CO generation along cathode surface

Figure 5.14 illustrates the production of hydrogen, highlighting the occurrence of a secondary reaction—hydrogen evolution—at the cathode surface.

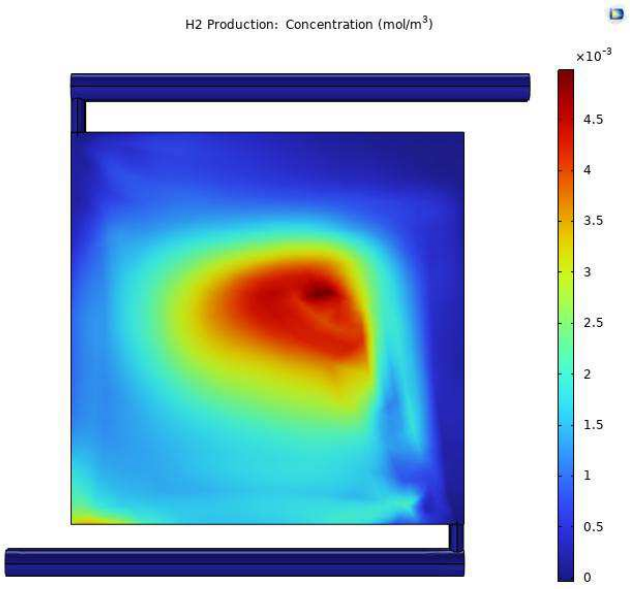

Figure 5.14 visual representation of the concentration gradient of hydrogen (H_2) within the electrochemical cell.

While the carbon monoxide concentration is a key focus in this ERC, the hydrogen production is secondary product produced on the cathode surface. Consequently, the hydrogen

concentration is lower, reflecting its ancillary role in the electrochemical processes at play. Figure 5.14 reveals a pronounced concentration of H_2 in the center-left region of the cell. While at first glance this may seem indicative of efficient production, it also raises concerns about uneven reactant utilization and the potential for localized concentration polarization. The high concentration areas may impede mass transport, leading to a reduction in reaction rates away from these hotspots.

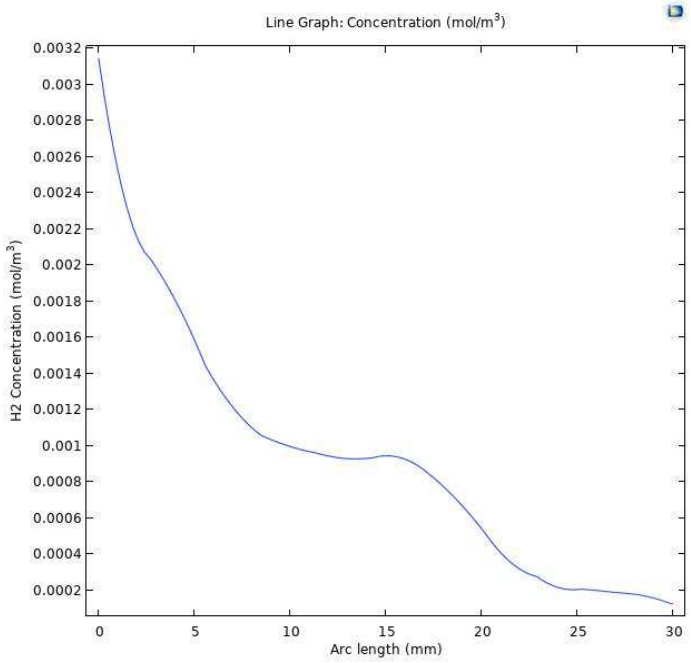

Figure 5.15 concentration of hydrogen (H2) production as a function of the arc length

Figure 5.15 shows the sharp decline in H_2 concentration along the arc length of the catalyst layer which is a sign of limitations in the diffusion and convection processes within the cell. The steep gradient indicates that H_2 production is not uniform across the catalyst layer, which could lead to an inefficient overall reaction process. Such an imbalance may not only affect the yield but also the purity of the produced H_2, as it can foster the occurrence of side reactions in areas of lower H_2 concentration.

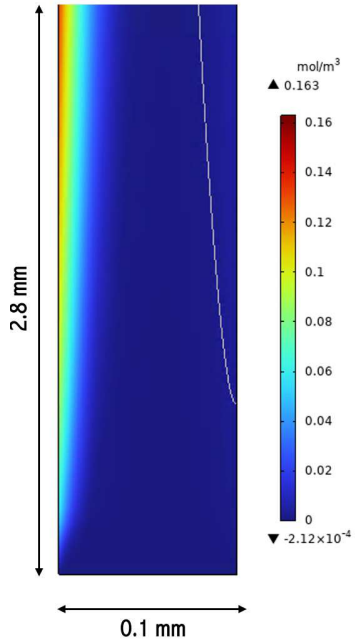

Figure 5.16 H_2 generation along cathode surface

The 2D cross-sectional view figure 5.16, further underscores the challenges posed by the observed concentration gradients. The high concentration of H_2 at the top, decreasing towards the bottom, suggests a stratification effect that could be detrimental to the cell's performance. If the heavier reactant species are not adequately mixed or are unable to reach the active sites due to this stratification, the reaction efficiency could be significantly prevented.

In the comprehensive analysis of this electrochemical cell's performance, special attention must also be given to the formation of H_2O as a byproduct, which emerges alongside carbon CO and H_2 production during the cathode side reactions. The production of H_2O is not only a critical indicator of the cell's efficiency in executing the desired reactions but also plays a pivotal role in maintaining the balance of reactants and products within the system. In figure 5.17 the concentration of H_2O on both sides, anode, and cathode, is illustrated:

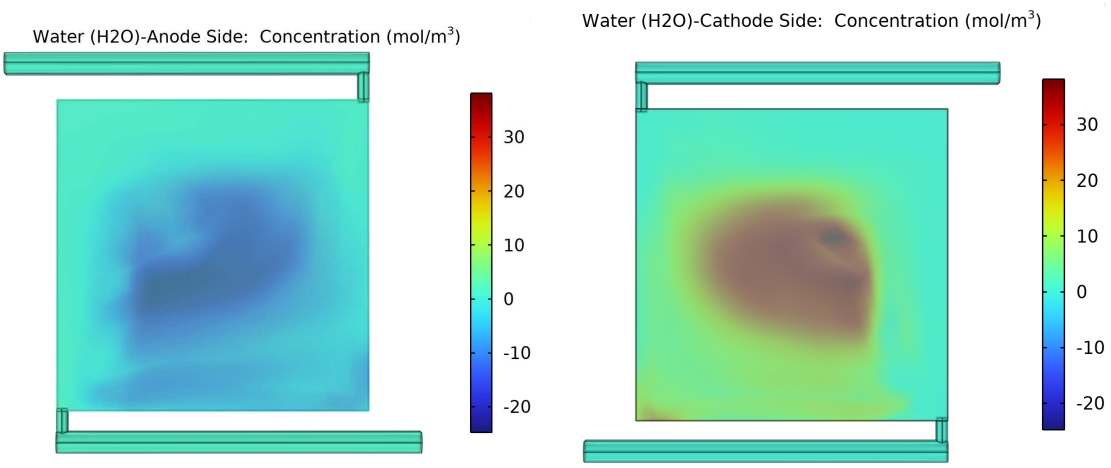

Figure 5.17 visual representation of water (H_2O) production and consumption on the cathode and anode respectively.

As illustrated on figure 5.17, on the cathode side, the areas of highest H_2O concentration appear to correlate with regions of lower velocity. This suggests that, similar to CO, the reduced flow rates provide more time for reactions to occur, leading to a localized increase in product concentration. However, these stagnant zones, while beneficial for concentration accumulation, can have deleterious effects on the selectivity of the reaction. The presence of H_2O in these zones might indicate that the water gas shift reaction is occurring more prominently, potentially reducing the efficiency of CO production, which is our primary interest. Additionally, stagnant regions can contribute to a non-uniform current distribution, as they may become areas where ionic species accumulate or are depleted more quickly than in areas with higher flow rates. This imbalance can lead to variations in the local current density, which in turn affects the overall efficiency and selectivity of the electrochemical reactions taking place within the cell.

On the anode side, the distribution of H_2O shows a different pattern, which is influenced by the different reaction mechanisms and the consumption of H_2O in the oxidation reactions. The concentration gradients are less pronounced than on the cathode side, suggesting a more uniform reaction rate across the electrode because here we are supplying the water as our electrolyte.

In both cases, it is crucial to optimize the flow to minimize these stagnant regions and promote a more uniform concentration and current distribution across the electrodes. This could

potentially improve the selectivity for the desired products and the overall performance of the electrochemical cell.

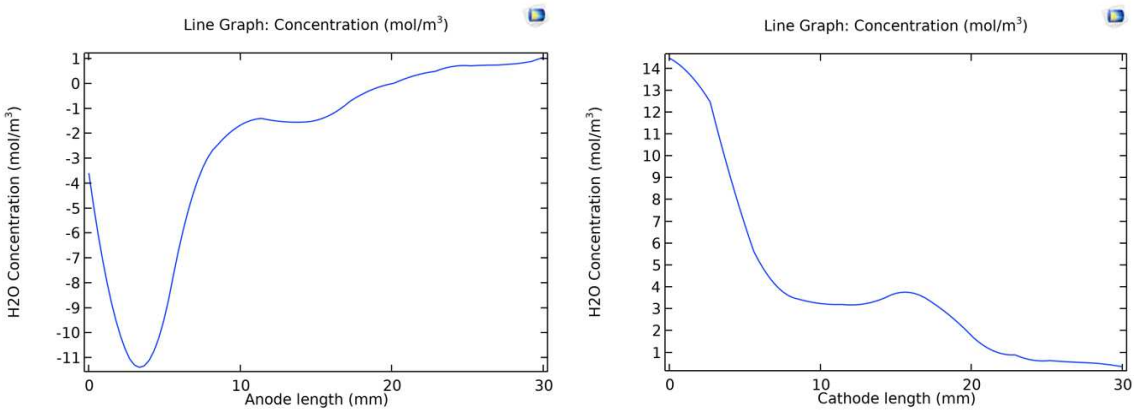

Figure 5.18-line graph production and consumption of water as a function of the arc length

As explained in the previous paragraph, H_2O acts as reactants on the anode side, while product on the cathode side, therefore, drawing the concentration gradient on the Y axis away from the inlets shows a descending gradient where we have consumption and ascending gradient where we have production of water.

As explained in the previous discussion, it becomes evident that H_2O serves a dual role within the electrochemical system, acting as a reactant on the anode side and as a product on the cathode side. This duality is manifest in the concentration gradients observed along the Y-axis, away from the inlets in figure 5.18. On the anode side, there is a discernible descending gradient, indicative of H_2O consumption, whereas the cathode side exhibits an ascending gradient, signifying the production of water. This distribution reflects the dynamic interplay between consumption and production processes, which are inherently influenced by the flow characteristics within the cell. Notably, stagnant regions can adversely affect the selectivity and current distribution, underlining the importance of optimizing fluid dynamics to ensure uniform reaction conditions and enhance the overall efficiency of the electrochemical reactions.

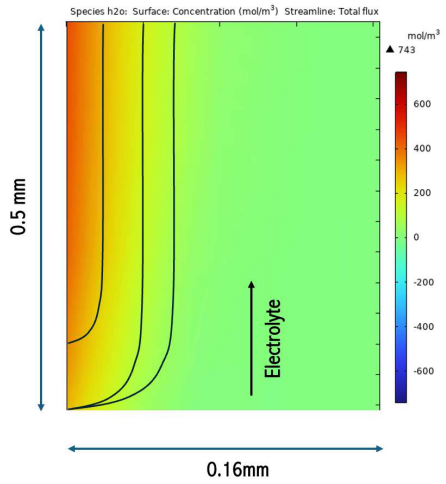

Figure 5.19 H_2O generation layer on the cathode surface

In accordance with the established understanding of our system's dynamics, figure 5.19 illustrates a marked concentration profile of species H_2O across the surface of the electrode. The depicted profile, with a width of 0.16 mm and a height of 0.5 mm, showcases a pronounced vertical concentration gradient, which aligns with the flow of the electrolyte. This gradient reveals a higher concentration of H_2O at the interface, suggesting a robust interaction between the electrochemical reactions and the fluid dynamics at play. The streamlines, which indicate total flux, run parallel and undisturbed, signifying a laminar flow regime that enhances the mass transport of reactants and products.

The gradation from warmer to cooler colors distinctly maps out a decreasing concentration of water as one moves away from the proximity of the catalyst layer. This gradient indicates a pronounced production of H_2O adjacent to the electrode surface, which systematically diminishes with increasing distance from the electrode, underscoring the critical influence of spatial positioning on the chemical dynamics at play within the electrochemical cell.

Although O_2 production is not the primary focus of the study, it is still informative to examine its distribution on the anode side. To this end, the observed results have been documented and can be reviewed in Figure 5.20:

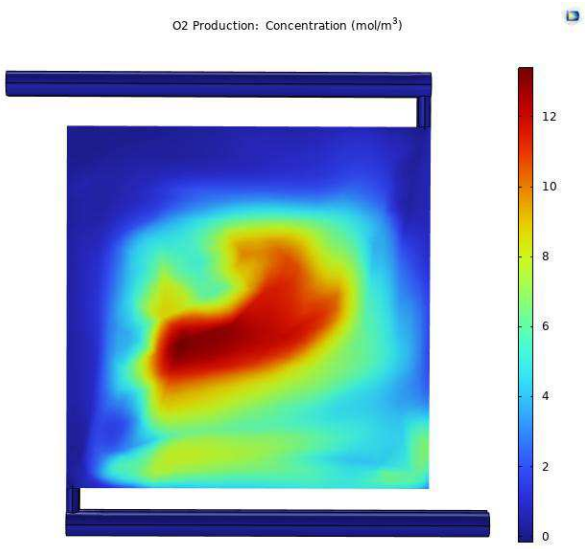

Figure 5.20 O_2 generated concentration along cathode surface

The O_2 production figure 5.20 reveals an accumulation of higher oxygen concentration towards the center and right corner of the catalyst surface, indicative of a stagnant velocity field in these regions. While this might initially seem beneficial for increased product formation, in the context of an electrochemical cell, such stagnation is typically undesirable. Stagnant regions can lead to uneven reaction rates and the potential for localized concentration polarization, which can negatively impact the cell's efficiency and longevity. These areas of diminished flow restrict the removal of produced products, which can create a barrier to the reaction front and impede the overall performance of the cell. This figure, therefore, underscores the necessity for improved flow dynamics to ensure uniform reaction conditions across the catalyst surface, which is essential for the optimal operation of electrochemical cells.

In the sophisticated interplay of reactions within the electrochemical cell, the proton (H^+) emerges as a pivotal component, primarily generated at the anode side based on the reaction mentioned in table 4.11. These protons exhibit a dynamic migration through the Nafion membrane, a material lauded for its proton exchange capabilities, towards the cathode, where they actively participate in reduction reactions. The kinetics of H^+ transport is critical; they are characterized by a concerted movement facilitated by the membrane's ionic conductivity and the electrochemical potential gradient across the cell. As such, the concentration of H^+ production and its subsequent migration towards the cathode is a dance

of precision, driven by the finely tuned kinetic parameters that dictate the rate and uniformity of proton availability at the site of reduction. In this simulation the reactions are assumed to be in equilibrium, therefore the rate of production and consumption is the same. In the figure 5.21 the 3D migration of H^+ from anode side toward cathode is depicted:

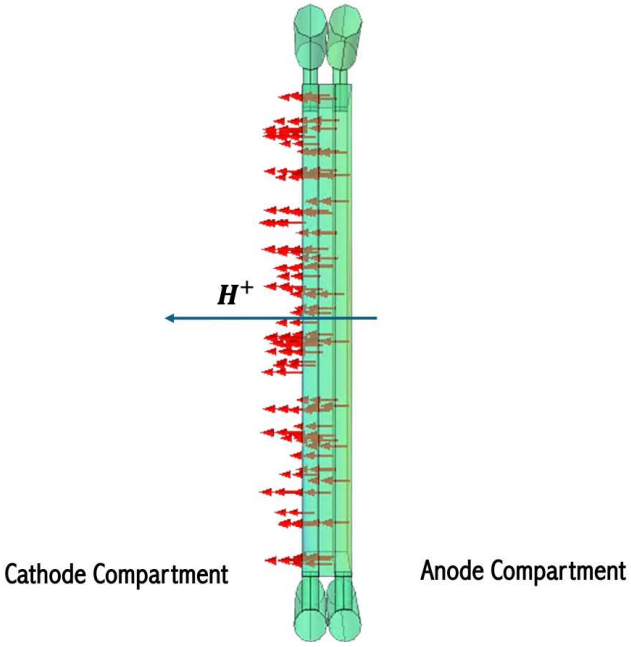

Figure 5.21 Proton migration from anode side toward the cathode through membrane

In figure 5.21 the H+ concentration gradient from anode side toward cathode side is shown, where we can trac the concentration as a function of the cell length:

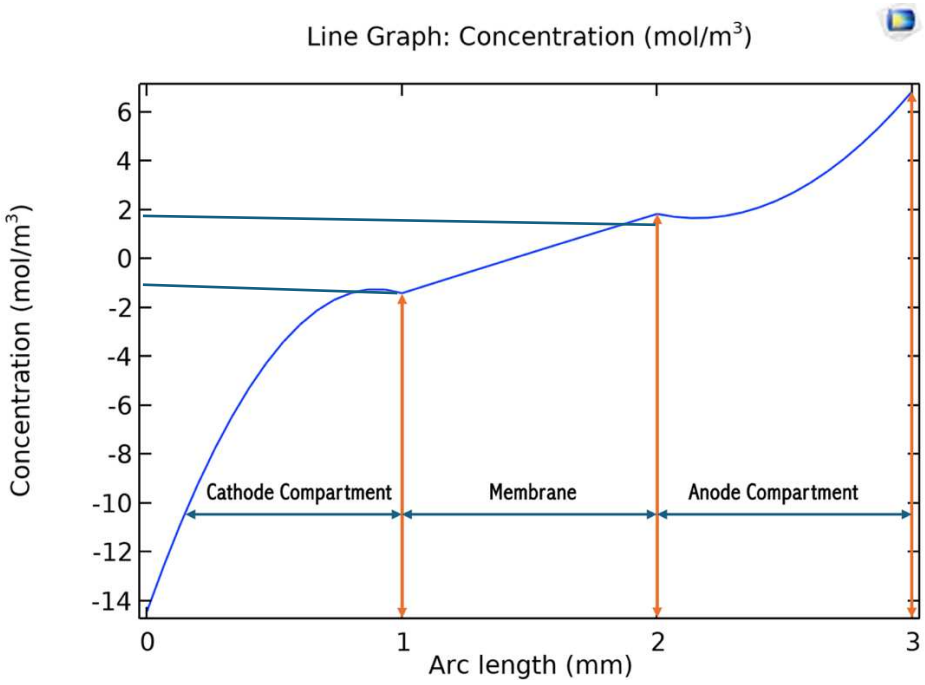

Figure 5.22 Proton concentration in the cell as a function of cell length

In Figure 5.22, there is a marked decrease in proton concentration within the Nafion membrane region. This decline suggests that the protons experience a significant resistance to transfer, which can be attributed primarily to the extended length of the membrane. Such a reduction in concentration across the membrane could be indicative of inefficiencies in proton exchange, potentially affecting the overall performance of the cell. Recognizing the profound impact of membrane length on proton transport, in the next stage of the simulation a membrane with a thinner length in multiple inlet and outlet cell configuration will be explored to enhance proton exchange efficiency and potentially improve the overall performance of the cell system.

Initially, a notable enhancement in the updated cell configuration simulation is the reduction of cell thickness from 1mm to 0.2mm. depicted in figure 5.23:

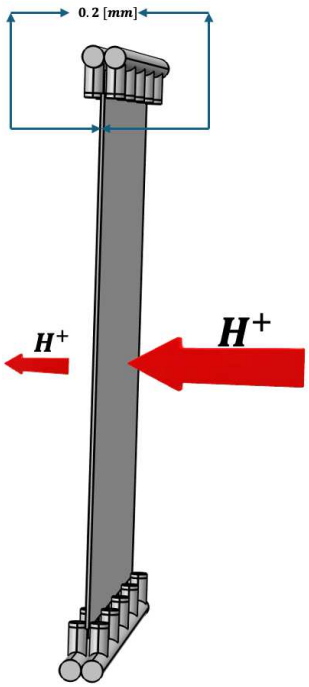

Figure 5.23 Membrane position between two compartments

Figure 5.24 illustrates the critical impact of membrane thickness on the system's performance, highlighting how its reduction can substantially improve ionic conductivity and facilitate proton transfer, thereby optimizing the efficiency of the electrochemical process.

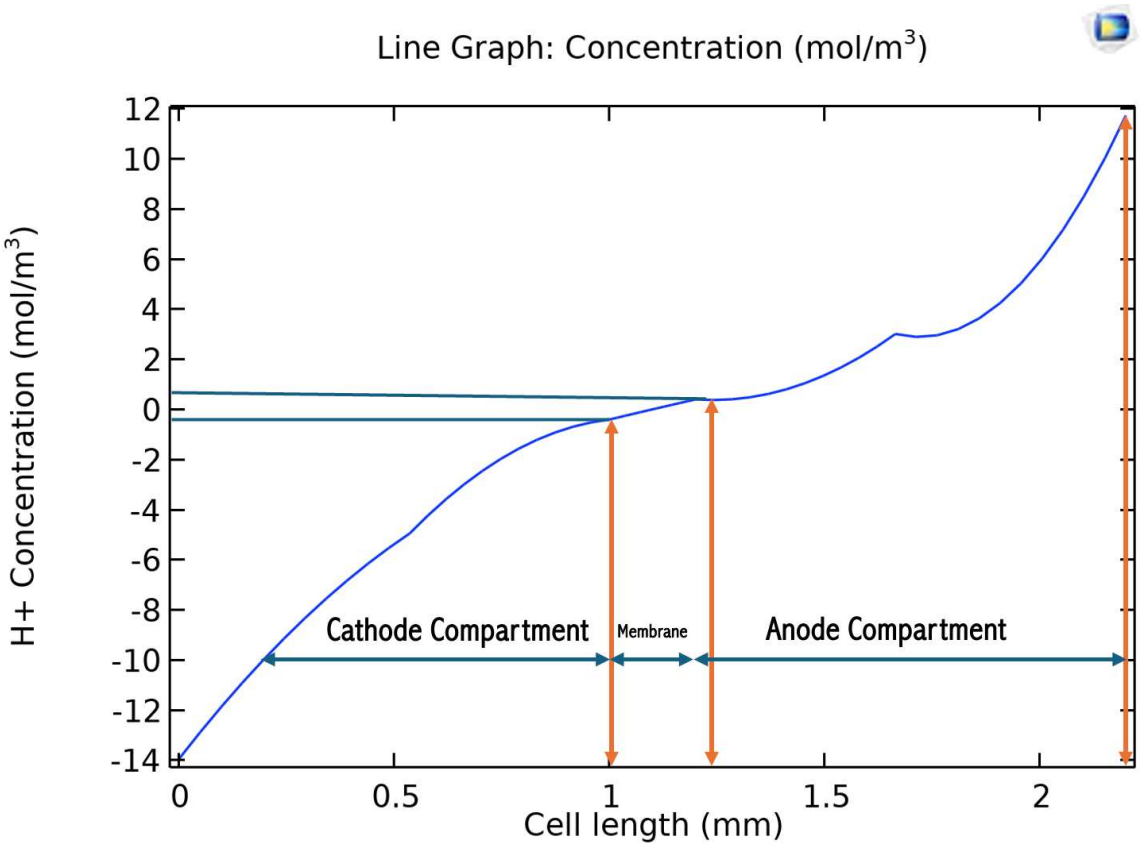

Figure 5.24 H+ concentration gradient as a function of cell length

In figure 5.22, a significant concentration gradient across the membrane is observed, indicating that proton exchange is limited. This gradient was visualized by the sharp decrease in concentration within the membrane area, suggesting that the thicker membrane poses a greater resistance to proton flow, which could lead to less efficient product distribution. In contrast, figure 5.24 shows a much smoother transition in proton concentration across the membrane area. This suggests a more efficient proton exchange, likely due to the thinner membrane providing less resistance and the improved reactant distribution. Consequently, this would facilitate a better generation of the product, CO, as the protons can more readily reach the cathode compartment where they participate in the reaction to form CO. Thickness reduction also led to the variations in electrolyte current distribution along the cell length, as depicted in Figure 5.25:

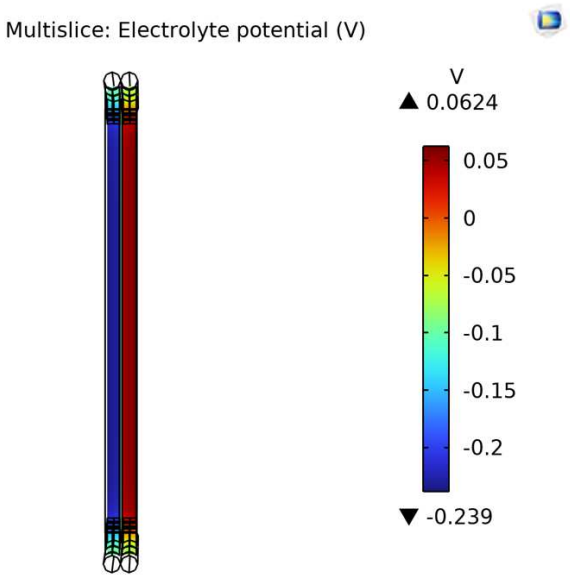

Figure 5.25 Visualization of Electrolyte Potential

When comparing the original cell with a 1mm membrane and a single inlet and outlet to a new version with multiple inlets and outlets and a thinner 0.2mm membrane, we see major differences in how the electrolyte potential spreads across the cell.

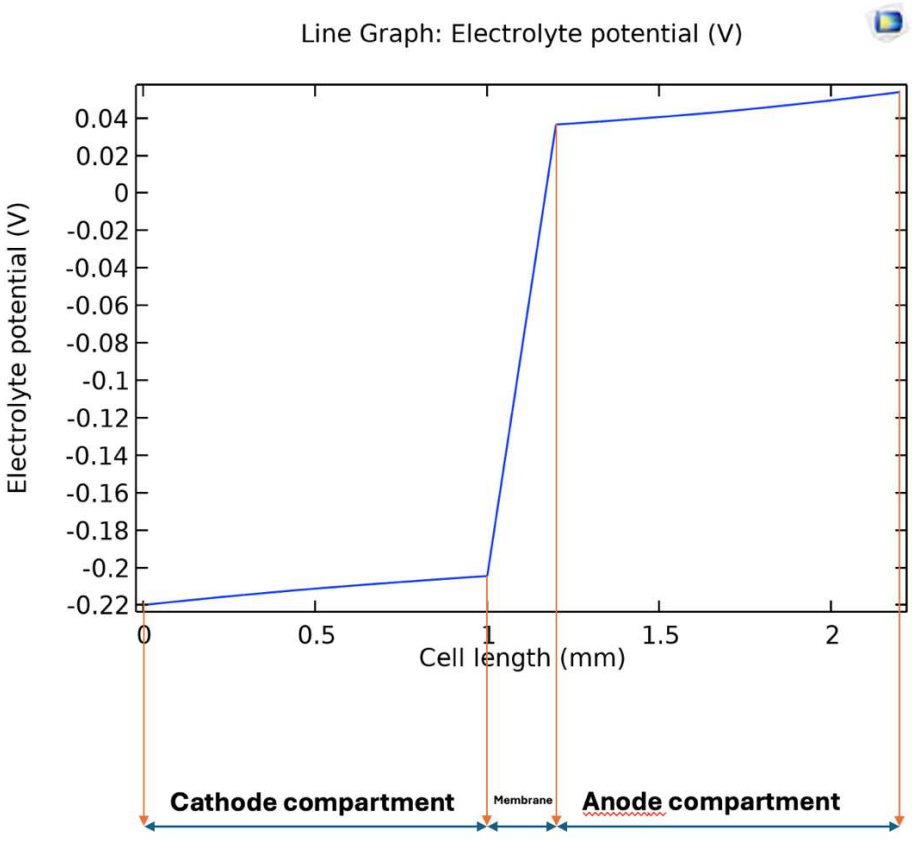

Figure 5.26 Electrolyte potential after reducing the membrane thickness

Refering to figure 5.10 and 5.26 with the decreased membrane thickness, there would be a shift in the electrolyte potential profile. The potential gradient across the membrane is steeper, as indicated by the more abrupt transition from the cathode to the anode in figure 5.26. This suggests that the reduced membrane thickness has effectively lowered the resistance to ion flow, thereby enhancing the cell's ionic conductivity. The electrolyte potential near the cathode compartment does not exhibit as low values as seen with the thicker membrane, which could be attributed to a more efficient ion migration through the thinner membrane.

Furthermore, figure 5.26 reveals that the potential distribution is more uniform along the length of the cell, possibly indicating a more homogeneous ion distribution and an overall more efficient electrochemical process. This uniformity could lead to improved performance characteristics such as increased power density and more rapid electrochemical kinetics, which are desirable for our application. In conclusion, the simulation demonstrated that membrane thickness significantly affects the resistivity and, consequently, the overall efficiency of the cell.

In the subsequent phase of this chapter, the outcomes of simulations involving a cell configuration with multiple inlets and outlets will be presented. This setup is designed to provide a more precise understanding of mass transfer effects on product distribution and selectivity, enabling a comprehensive comparison and informed selection of the optimal operating conditions.

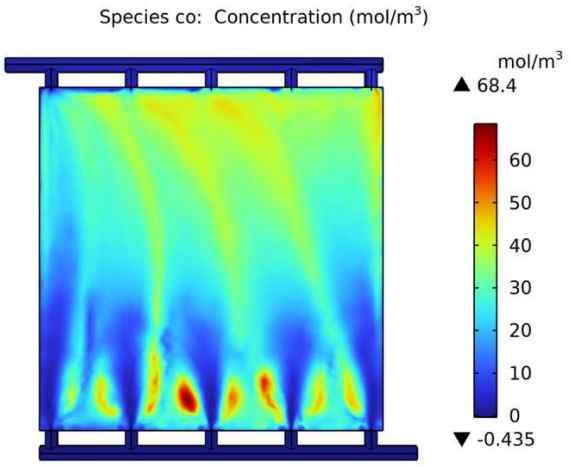

Figure 5.27 CO concentration gradient on cathode surface

Utilizing the principles of laminar flow physics with a measured velocity of 1.06 m/s, in conjunction with a cell configuration featuring multiple inlets and outlets, an enhanced distribution of reactants is achieved, and consequently, of the products within the cell, as depicted in Figure 5.27. While there are identifiable zones of stagnation, which align with the anticipated outcomes of fluid dynamic analysis, predominantly located at the bottom of the cell, the overall product distribution remains uniformly distributed across the entirety of the cell. This uniformity in distribution is indicative of efficient fluid dynamics and effective design parameters, which are critical for optimizing the cell's performance.

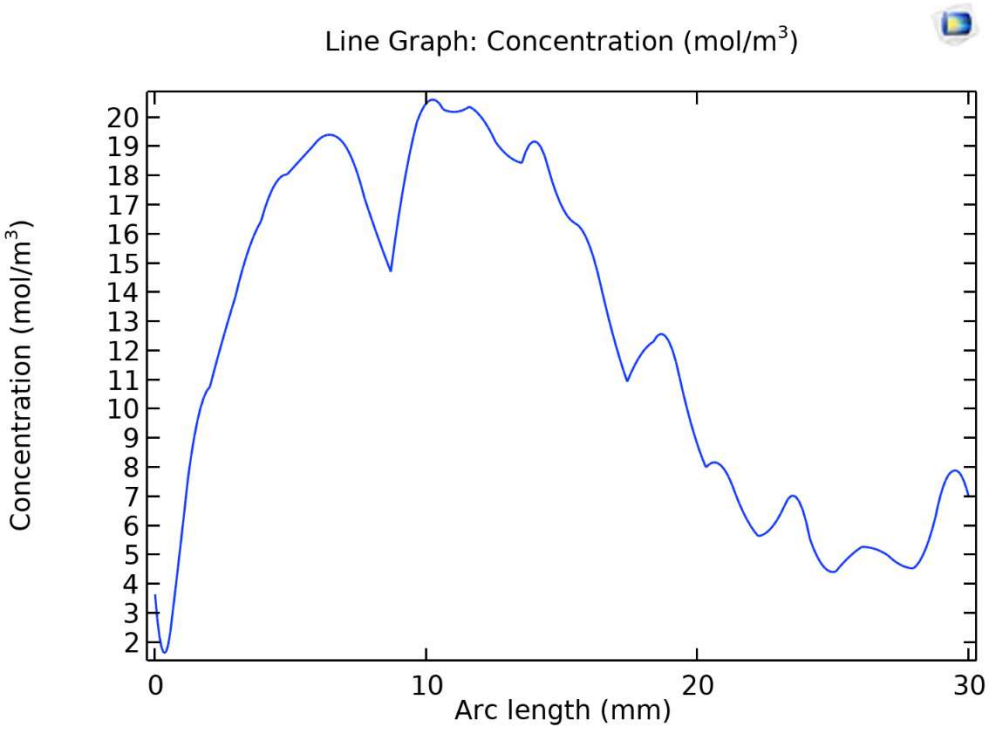

Figure 5.28 Concentration of carbon monoxide (CO) production as a function of the arc length

In Figure 5.28, the graph shows the spatial concentration profile of CO, along the cathode length away from the inlet channel. The observed diminution in concentration proximal to the inlet, particularly within the initial 0 to 0.1 mm segment, can be attributed to minimal fluid velocity adjacent to the wall, resulting in a reduced presence of reactants. As the distance from the inlet increases, there is a concomitant rise in CO concentration. This trend indicates the development of a concentration gradient within the cell. When placed together with the configuration of a cell equipped with a single inlet and outlet, the slight inflection in the

concentration curve suggests an alteration in the diffusion dynamics, reinforcing the presence of a concentration gradient in the electrochemical environment.

By examining the impact of fluid distribution changes caused by varying cell configurations, it is discovered that improved fluid distribution results in a higher concentration of the primary product, CO production. Consequently, the descision was made to illustrate the entire CO production process on the surface of the catalyst, subsequently comparing these results with CO production in a cell configuration featuring a single inlet and outlet.

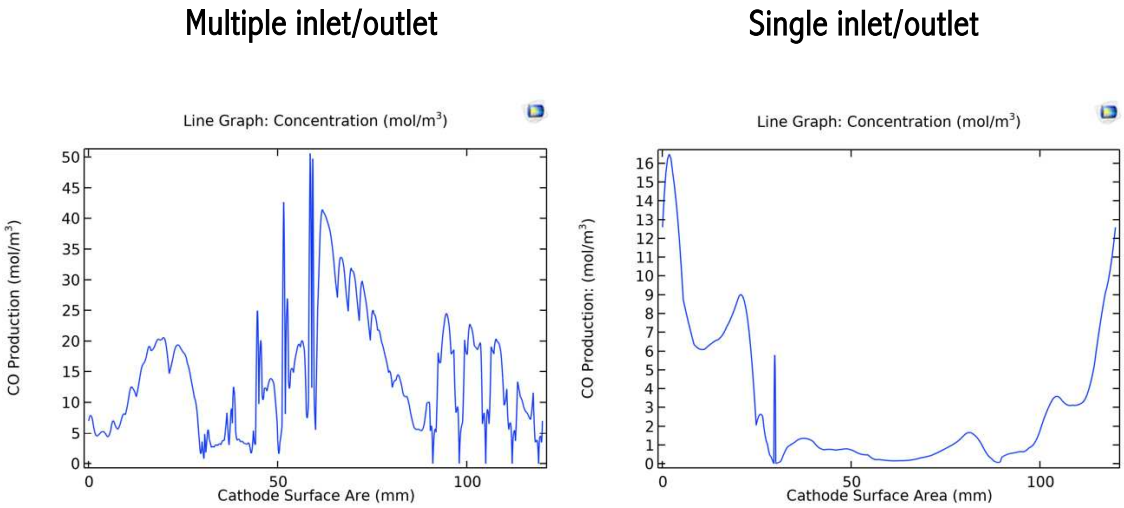

Figure 5.29 CO production comparison in single and multiple cell configurations

When comparing the simulation results of CO production across the entire cathode surface for different cell configurations, there are notable differences. The figure 5.29 single inlet and outlet shows a peak CO production concentration of just above 16 mol/m³. This configuration exhibits a steep initial rise followed by significant fluctuations, with the concentration dipping to nearly 0 mol/m³ before gradually increasing to a stable level of around 5 mol/m³ with minor fluctuations.

In contrast, the cell configuration with multiple inlets and outlets presents a much more variable pattern, with CO production concentrations reaching as high as nearly 50 mol/m³. The graph displays multiple sharp peaks and troughs, indicating a less stable CO production profile. The concentration fluctuates widely and more frequently than in the single inlet and

outlet configuration, suggesting that the multiple inlets and outlets setup might induce a more dynamic environment within the cathode surface area.

These results suggest that the configuration with multiple inlets and outlets has the potential to increase the maximum CO production but at the cost of greater variability and possibly less predictability in the production rates. The choice between these configurations would likely depend on the specific requirements of the process stability and the maximum production capacity desired.

Regarding the scond reaction happeing in our catalyst layer, a better hydrogen distribution is observed, as shown in figure 5.30:

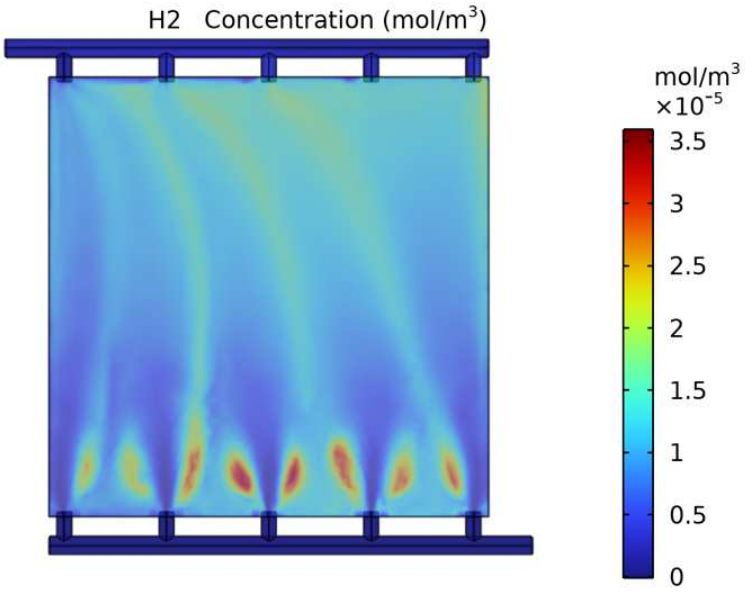

Figure 5.30 H_2 concentration gradient on cathode surface

Since the parameters and operating conditions have been tailored to maximize CO output, the lower observed levels of hydrogen in our cell is justified. As we can see from figure 5.30 in cell with multiple inlets and outles a better product distribution and less hydrogen production is observed compare to the cell configuration with single inlet and outlet.

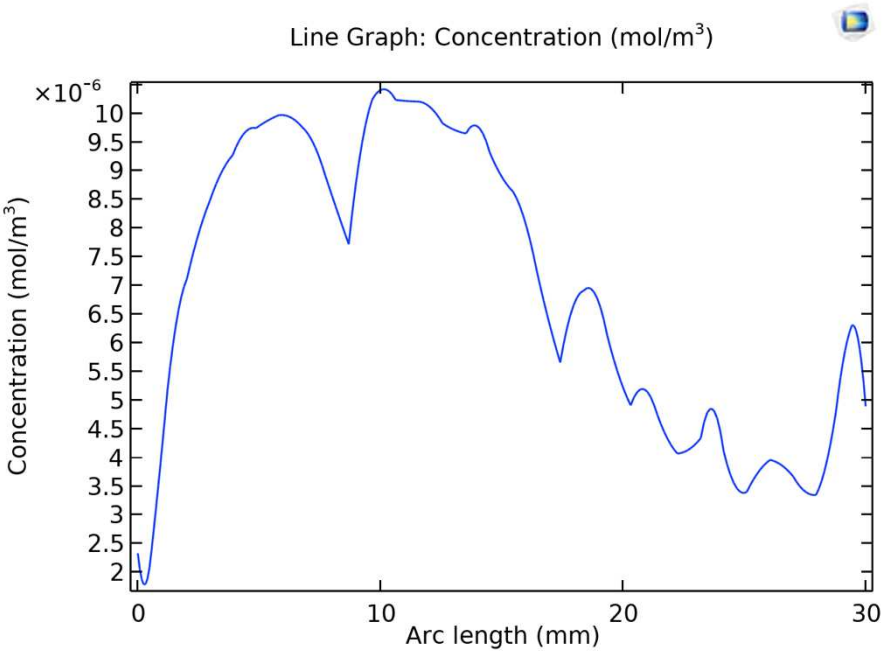

Figure 5.31 concentration of hydrogen (H_2) production as a function of the arc length

Figure 5.31 represents the cell with multiple inlets and outlets, shows a hydrogen concentration profile with significant fluctuations along the arc length. This suggests that the fuel cell design with multiple inlets and outlets leads to a more complex flow pattern, allowing for better mixing and distribution of hydrogen within the cell. The peaks and valleys in the concentration profile indicate regions where hydrogen is more prevalent, followed by areas where it is less so, which could be indicative of efficient utilization of reactants and distribution of hydrogen due to the multiple flow paths.

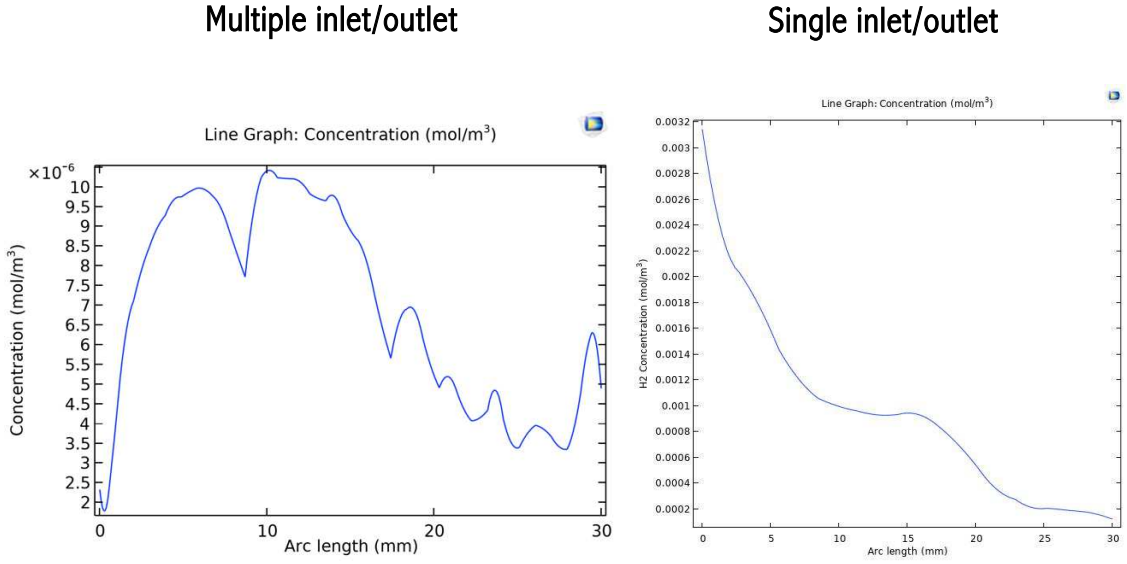

Figure 5.32 H_2 production comparison in single and multiple cell configurations

In the single inlet and outlet flow cell, depicted in the first graph, H_2 concentration decreases sharply as a function of the Y axis of the catalys away from the inlet, indicating a depletion of reactants as the flow progresses through the cell. This suggests that the reactants are not being utilized efficiently, possibly due to mass transport limitations and suboptimal mixing, which results in a decrease in hydrogen production along the flow path.

The cell with multiple inlets and outlets configuration showcases a more consistent hydrogen production profile characterized by periodic fluctuations in concentration across the arc length. Notably, the hydrogen concentrations in this configuration are generally lower than those observed in the single inlet and outlet setup. This phenomenon is attributed to the enhanced production of CO within the multi-inlet system under identical input conditions. The design of the multiple inlet and outlet system inherently favors the selectivity towards CO production over hydrogen.

6

Conclusion

This study focused on developing a model for the electrochemical reduction of ERC to CO using a silver electrode within an electrochemical cell. Key findings from this research are outlined below.

A major challenge in the ERC is achieving selectivity towards desired products. While numerous factors affect selectivity in electrochemical cells, the influence of fluid flow has been surprisingly understudied. This study explores the impact of fluid flow on selectivity by analyzing two cell designs (single vs. multiple inlets/outlets) with varying flow velocities.

Building upon the experimental work of a previous student at the University of Magdeburg in collaboration with the Max Planck Institute [38], this research addresses a previously unexplored aspect: the influence of fluid flow on selectivity. To investigate this effect, the cell geometry was modified and simplified to achieve two distinct fluid flow regimes: laminar and turbulent, at various velocities.

Two flow regimes were investigated: laminar and turbulent, at specific velocities. Both were applied to the single and multiple inlet/outlet cell configurations. The results identified the configuration with multiple inlets and outlets operated at 1.06 m/s as the most promising for further research. To ensure minimal stagnant zones and a uniform current distribution, the chosen cell configuration with multiple inlets/outlets at 1.06 m/s was further analyzed in COMSOL Multiphysics software. The software's Primary Current Distribution module,

simulating 3D current flow based on applied potential and electrolyte conductivity, was used. The results confirmed a uniform current distribution within the cell, allowing for subsequent analysis stages.

To get deeper into the complex processes within the electrochemical CO_2 reduction cell, the Tertiary Current Distribution physics module was incorporated into the COMSOL model. This module accounts for both electrode reactions and concentration gradients, providing a more comprehensive picture. By incorporating convection, migration, and diffusion into the model of a single inlet/outlet cell, we observed a uniform concentration of CO production along the catalyst surface, except for slow and stagnant regions at the center. The analysis also considered side reactions, including hydrogen (H_2) production and the counter electrode reaction, Oxygen production.

Following the same conditions, the cell with multiple inlets and outlets exhibited a better production distribution across the catalyst surface, as anticipated. Apart from the even production distribution, in the cell where a better mass transfer was observed the concentration of our product also was higher, and the reason is that a laminar and uniform distribution of the electrolyte ensures that reactants are more efficiently delivered to the catalyst surface. This minimizes concentration gradients within the cell, meaning that reactants (in this case, CO_2 and electrolyte ions) can reach the catalyst more evenly and reactions can occur more uniformly across the entire surface. Improved mass transport typically results in higher reaction rates and thus higher product generation. In addition, with a more uniform distribution of the electrolyte, the entire catalyst surface can participate more effectively in the reaction. Therefore, a uniform electrolyte distribution can help in maintaining optimal conditions for the electrochemical reactions, potentially lowering the overpotentials required for the CO_2 reduction to proceed. Lower overpotentials mean that the energy efficiency of the cell is improved, which can often lead to an increase in the selectivity and yield of the desired products.

The uniform distribution of the electrolyte also enables us to have a better control over the selectivity, because non uniform conditions can favor the formation of a wider range of products, due to variations in local pH, concentration, and electrical field. By ensuring a more

consistent environment, we favored the formation of specific products over others, thus seeing an increase in CO production in the cell with more uniformity.

Another important point is that, when we have non uniform fluid distribution inside a cell, reactant are depleted near the electrode surface, and products accumulate, creating a concentration gradient. This gradient can impede the electrochemical reaction, as the reduced availability of reactants slows down the reaction rate. Additionally, the accumulation of products can further hinder the reaction. This effect can lead to increased overpotentials, which are the extra voltages needed beyond the theoretical voltage to drive a reaction forward at a certain rate. On the other hand, achieving uniform distribution helps minimize the concentration gradient that led to concentration polarization.

In conclusion, obtaining the uniform fluid distribution inside the electrochemical cells ensure better product concentration and more control over selectivity.

7

Future Outlook

As mentioned in this study, to achieve a uniform distribution, the supplying parts were modified from single to multiple. However, for in-depth exploration, various geometric strategies, including the integration of grids or leveraging other fluid dynamics techniques, could be investigated to enhance fluid distribution further. Implementing such a system on an industrial scale necessitates meticulously designing the cell to ensure uniform fluid distribution, even at elevated flow rates. This approach is crucial for scaling up the technology while maintaining efficiency and effectiveness.

In addition, the effects of bubbles were neglected. Since the presence of bubbles alters the cell performance notably in 3 ways [59]: 1) bubbles attached to surface reduce the effective electrode area which is otherwise used for the electrochemical reaction. 2) Bubbles, once detached from the surface, act as flowing insulators, thereby increasing the ohmic drop. 3) Lastly, bubble growth and its detachment, in fact, causes micro-convection of electrolyte around it, it is another factor that has to be analyzed to have a better mass transport in the cell.

8

Bibliography

[1] Nasa Global Climate Change: https://climate.nasa.gov/vital-signs/carbon-dioxide/

[2] International Energy Agency, 2022, CO2 Emissions in 2022, https://iea.blob.core.windows.net/assets/3c8fa115-35c4-4474-b237-1b00424c8844/CO2Emissionsin2022.pdf

[3] Yosra Kotb, Seif-Eddeen, K. Fateen, Jonathan Albo,dand Ibrahim Ismail. 2017, Modeling of a Microfluidic Electrochemical Cell for the Electro Reduction of CO_2 to CH_3OH, https://www.researchgate.net/publication/320326227_Modeling_of_a_Microfluidic_Electrochemical_Cell_for_the_Electro-Reduction_of_CO_2_to_CH_3_OH

[4] A device that converts carbon monoxide into carbon dioxide through a chemical reaction between vaporous water and carbon monoxide according to the following equation: H2O+CO=CO2+H2. (https://www.sciencedirect.com/topics/chemistry/carbon-monoxide)

[5] Wikipedia, Electrochemical reduction of carbon dioxide (https://en.wikipedia.org/wiki/Electrochemical_reduction_of_carbon_dioxide)

[6] Dr. Colleen Spiegel, 2017, Alternative Liquid Fuel Types for Fuel Cells, https://www.fuelcellstore.com/blog-section/alternative-liquid-fuel-types-fuel-cells

[7] Xu Lu Xu Lu, 2023, Electrochemical conversion of high-pressure carbon dioxide https://physicsworld.com/a/electrochemical-conversion-of-high-pressure-carbon-dioxide/

[8] Dalei Sun, Xiaomin Xu, Yanling Qin, Prof. San Ping Jiang, Prof. Zongping Shao, 2019, Rational Design of Ag-Based Catalysts for the Electrochemical CO2 Reduction to CO (https://chemistryeurope.onlinelibrary.wiley.com/doi/full/10.1002/cssc.201902061?casa_tok

en=Xvk_smj3qZkAAAAA%3AZiKOEocCpc9mjp1xDwrrZrwj7qv1La_haqNpudaUevyYSO1foszcM4nlOyKkVoLLLx8abMYdhiq8Q)

[9] Wenjun Zhang 1, Yi Hu 1, Lianbo Ma 1, Guoyin Zhu 1, Yanrong Wang 1, Xiaolan Xue 1, Renpeng Chen 1, Songyuan Yang 1, Zhong Jin 1, 2018, Progress and Perspective of Electrocatalytic CO2 Reduction for Renewable Carbonaceous Fuels and Chemicals https://pubmed.ncbi.nlm.nih.gov/29375961/

[10] Paramita Saha, Sk Amanullah, and Abhishek Dey, 2022, Selectivity in Electrochemical CO_2 Reduction (https://pubs.acs.org/action/showCitFormats?doi=10.1021/acs.accounts.1c00678&ref=pdf)

[11] Rongzhong Jiang, Vijay S. Parameshwaran, Jonathan Boltersdorf, and David R. Baker, 2023, Copper-Nanowires Incorporated with Silver-Nanoparticles for Catalytic CO2 Reduction in Alkaline Zero Gap Electrolyzer (https://pubs.acs.org/action/showCitFormats?doi=10.1021/acsaem.3c01605&ref=pdf)

[12] Sichao Ma , Yangchun Lan , Gaby M. J. Perez, Saman Moniri, Prof. Paul J. A. Kenis, 2014, Silver Supported on Titania as an Active Catalyst for Electrochemical Carbon Dioxide Reduction(https://chemistryeurope.onlinelibrary.wiley.com/doi/full/10.1002/cssc.201300934)

[13] Lien-Chun Weng,ab Alexis T. Bell ORCID logo *ab and Adam Z. Weber ORCID logo *a, 2019, Towards membrane-electrode assembly systems for CO2 reduction: a modeling study† (https://pubs.rsc.org/en/content/articlelanding/2019/ee/c9ee00909d)

[14] Morgan M Monroe1,2,3, Peter Lobaccaro1,2, Yanwei Lum1,3 and Joel W Ager1,3,4, 2017, Membraneless laminar flow cell for electrocatalytic CO2 reduction with liquid product separation (https://iopscience.iop.org/article/10.1088/1361-6463/aa6359)

[15] J. Setschenow, 2017, Über die Konstitution der Salzlösungen auf Grund ihres Verhaltens zu Kohlensäure, https://www.degruyter.com/document/doi/10.1515/zpch-1889-0409/html?lang=en

[16] S. Weisenberger, A. Schumpe, 1996, Estimation of gas solubilities in salt solutions at temperatures from 273 K to 363 K, https://www.semanticscholar.org/paper/Estimation-of-gas-solubilities-in-salt-solutions-at-Weisenberger-Schumpe/73f9d6cece0fa907bbaaf6f33b4a8d12fae3e75a

[17] Brian A Rosen 1, Amin Salehi-Khojin, Michael R Thorson, Wei Zhu, Devin T Whipple, Paul J A Kenis, Richard I Masel, 2011, Ionic liquid-mediated selective conversion of CO_2 to CO at low overpotentials, https://pubmed.ncbi.nlm.nih.gov/21960532/

[18] Ana S. Reis Machado, Manuel Nunes da Ponte, 2018, CO2 capture and electrochemical conversion, https://www.sciencedirect.com/science/article/pii/S2452223617301207

[19] Manuel Alvarez-Guerra,*a Jonathan Albo,b Enrique Alvarez-Guerraa and Angel Irabiena, 2015, Ionic liquids in the electrochemical valorisation of CO2, https://pubs.rsc.org/en/content/articlelanding/2015/ee/c5ee01486g

[20] Hiroshi Hashiba†, Lien-Chun Weng‡§, Yikai Chen‖, Hiroki K. Sato†, Satoshi Yotsuhashi†, Chengxiang Xiang‖, and Adam Z. Weber,2018, Effects of Electrolyte Buffer Capacity on Surface Reactant Species and the Reaction Rate of CO2 in Electrochemical CO2 Reduction, https://pubs.acs.org/doi/full/10.1021/acs.jpcc.7b11316

[21] Akira Murata, 1991, Product Selectivity Affected by Cationic Species in Electrochemical Reduction of CO 2 and CO at a Cu Electrode, https://www.researchgate.net/publication/244711299_Product_Selectivity_Affected_by_Cationic_Species_in_Electrochemical_Reduction_of_CO_2_and_CO_at_a_Cu_Electrode

[22] Michael R. Thorson, Karl I. Siil, Paul J.A. Kenis, 2013, Effect of cations on the electrochemical conversion of CO2 to CO, https://experts.illinois.edu/en/publications/effect-of-cations-on-the-electrochemical-conversion-of-cosub2sub-

[23] Michael Filippi, Tim Möller, Liang Lianga and Peter Strasser, 2023, Understanding the impact of catholyte flow compartment design on the efficiency of CO2 electrolyzers, https://pubs.rsc.org/en/content/articlelanding/2023/ee/d3ee02243a

[24] Allen J. Bard, Larry R. Faulkner, 2000, Electrochemical Methods: Fundamentals and Applications, 2nd Edition, https://www.wiley.com/en-us/Electrochemical+Methods:+Fundamentals+and+Applications,+2nd+Edition-p-9780471043720

[25] Thomas F. Fuller, J. N. H, 2018, Electrochemical Engineering, https://www.wiley.com/en-us/Electrochemical+Engineering-p-9781119004257.

[26]AlanCWest.2012,ElectrochemistryandElectrochemicalEngineering:AnIntroduction.ColumbiaUniversity, 2013.)

[27] Qingzhen Wang, Bin Liu, Shujie Wang and Jinlong Gong, 2023, Highly selective photoelectrochemical CO2 reduction by crystal phase-modulated nanocrystals without parasitic absorption, https://www.pnas.org/doi/10.1073/pnas.2316724121

[28] Frank J Millero, Taylor B Graham, Fen Huang, Héctor Bustos-Serrano, and Denis Pierrot, 2006, Dissociation constants of carbonic acid in seawater as a function of salinity and temperature,https://www.sciencedirect.com/science/article/abs/pii/S0304420305001921

[29] Kai G Schulz, Ulf Riebesell, Bjoern Rost, Silke Thoms, and RE Zeebe, 2006, Determination of the rate con- stants for the carbon dioxide to bicarbonate inter-conversion in pH-buffered seawater systems https://epic.awi.de/id/eprint/13960/1/Sch2006g.pdf

[30] George Keith Batchelor. 2000, An introduction to fluid dynamics. https://elmoukrie.files.wordpress.com/2022/04/g.-k.-batchelor-an-introduction-to-fluid-dynamics-cambridge-university-press-2000.pdf

[31] Nitish Vinay Gadgil ,2018, Modeling a Flow-Cell for Electrochemical Reduction of Carbon Dioxide to Formate
file:///Users/arash%20akbari/Downloads/MSc_Thesis_Nitish_Gadgil%20(6).pdf

[32] von L Graetz Annalena882, . Ueber die wärmeleitungsfähigkeit von flüssigkeiten https://onlinelibrary.wiley.com/doi/10.1002/andp.18822540106

[33] David C. Bock, Christopher J. Pelliccione, Wei Zhang, Jiajun Wang, K. W. Knehr, Jun Wang, Feng Wang, Alan C. West, Amy C. Marschilok, Kenneth J. Takeuchi, and Esther S. Takeuchi, 2016, Dispersion of Nanocrystalline Fe3O4 within Composite Electrodes: Insights on Battery-Related Electrochemistry, https://pubs.acs.org/doi/full/10.1021/acsami.6b01134

[34] David C. Wilcox,2006, Turbulence Modeling for CFD, Third Edition
https://cfd.spbstu.ru/agarbaruk/doc/2006_Wilcox_Turbulence-modeling-for-CFD.pdf

[35] Bo Zhao, Wei Long , Rong Zhou, 2021, A convective analytical model in turbulent boundary layer on a flat plate based on the unifying heat flux formula (https://www.sciencedirect.com/science/article/abs/pii/S1290072920312278)

[36] George Keith Batchelor. 2000, An introduction to fluid dynamics. https://elmoukrie.files.wordpress.com/2022/04/g.-k.-batchelor-an-introduction-to-fluid-dynamics-cambridge-university-press-2000.pdf

[37] Study and Study Step Types, COMSOLhttps://doc.comsol.com/5.5/doc/com.comsol.help.comsol/comsol_ref_solver.27.010.html

[38] Christoph Blümner, 2023, Exploring the effects of mass transport on the efficiency of CO2 electrolysis using a flow cell setup, Master Thesis.

[39] Electrochemistry Module Model Electroanalysis, Electrolysis, and Electrodialysis, COMSOL https://www.comsol.com/electrochemistry-module

[40] Václav Uruba, 2018, On Reynolds number physical interpretation, https://www.researchgate.net/publication/326898812_On_Reynolds_number_physical_interpretation

[41] Stokes, George, 1851, On the Effect of the Internal Friction of Fluids on the Motion of Pendulums, https://mural.uv.es/daroig/documentos/stokes1850.pdf

[42] Kai G Schulz, Ulf Riebesell, Bjoern Rost, Silke Thoms, and RE Zeebe, 2006, Determination of the rate con- stants for the carbon dioxide to bicarbonate inter-conversion in pH-buffered seawater systems. https://www.sciencedirect.com/science/article/pii/S0304420305001684

[43]Dongwei Du, Rong Lan, John Humphreys, Sivaprakash Sengodan, Kui Xie, Huanting Wang, and Shanwen Tao, 2016, Achieving both high selectivity and current density for CO2 reduction to formate on nanoporous tin foam electrocatalysts. https://chemistry-europe.onlinelibrary.wiley.com/doi/full/10.1002/slct.201600451

[44]JeremyTFeaster,ChuanShi,EtoshaRCave,ToruHatsukade,DavidNAbram,KendraPKuhl,Christo- pher Hahn, Jens K Nørskov, and Thomas F Jaramillo,2017, Understanding selectivity for the electrochemical reduction of carbon dioxide to formic acid and carbon monoxide on metal electrodes. https://pubs.acs.org/doi/10.1021/acscatal.7b00687

[45] Yoshio Hori and Shin Suzuki, 1983, Electrolytic-Reduction-of-Bicarbonate Ion at a Mercury Electrode, https://www.researchgate.net/profile/Yoshio-Hori/publication/244679180_Electrolytic_Reduction_of_Bicarbonate_Ion_at_a_Mercury_Electrode/links/5cd4209ea6fdccc9dd986084/Electrolytic-Reduction-of-Bicarbonate-Ion-at-a-Mercury-Electrode.pdf

[46] MarcoDunwell,QiLu,JeffreyMHeyes,JonathanRosen,JingguangGChen,YushanYan,FengJiao,and Bingjun Xu, 2017, The central role of bicarbonate in the electrochemical reduction of carbon dioxide on gold. https://pubs.acs.org/doi/10.1021/jacs.6b13287

[47] Jingjie Wu, Frank G Risalvato, Fu-Sheng Ke, PJ Pellechia, and Xiao-Dong Zhou, 2012, Electrochemical reduction of carbon dioxide I. Effects of the electrolyte on the selectivity and activity with Sn electrode. https://iopscience.iop.org/article/10.1149/2.049207jes

[48] Liu, Chong and Colón, Brendan C and Ziesack, Marika and Silver, Pamela A and Nocera, Daniel G, 2016, Water splitting–biosynthetic system with co2 reduction efficiencies exceeding photosynthesis. https://www.science.org/doi/10.1126/science.aaf5039

[49] [Avoiding negative concentrations. COMSOL URL https://www.comsol.com/support/knowledgebase/952/. accessed September 09, 2018.],

[50] Danckwerts Inflow Boundary Condition, COMSOL URL https://doc.comsol.com/5.6/doc/com.comsol.help.battery/battery_ug_chemsptrans.09.136.html

[51] Allen J. Bard, Larry R. Faulkner, 1980, Electrochemical Methods: Fundamentals and Applications, 2nd Edition, https://www.wiley.com/en-us/Electrochemical+Methods:+Fundamentals+and+Applications,+2nd+Edition-p-9780471043720

[52] G. K. BATCHELOR, F.R.S, 1967, AN INTRODUCTION TO FLUID DYNAMICS, https://elmoukrie.files.wordpress.com/2022/04/g.-k.-batchelor-an-introduction-to-fluid-dynamics-cambridge-university-press-2000.pdf

[53] LIDE DAVID, 1998, Chemistry and Physics,

[54] R Kortlever, KH Tan, Y Kwon, and MTM Koper, 2013, Electrochemical carbon dioxide and bicarbonate re- duction on copper in weakly alkaline media. https://link.springer.com/article/10.1007/s10008-013-2100-9

[55]SeunghwaLee,JoeyDOcon,YoungilSon,andJaeyoungLee, 2015, AlkalineCO2electrolysistowardselecti e and continuous HCOO−-production over SnO2 nanocatalysts. https://www.researchgate.net/publication/273352254_Alkaline_CO_2_Electrolysis_Towards_Selective_and_Continuous_HCOO_-_Production_over_SnO_2_Nanocatalysts

[56] Gadgil, Nitish, 2018, Modeling a Flow-Cell for Electrochemical Reduction of Carbon Dioxide to Formate, https://repository.tudelft.nl/islandora/object/uuid%3A885c941e-f98a-4761-9e09-c62071773af5

[57] Meenesh R. Singh, Jason D. Goodpaster, Adam Z. Weber, 2017, Mechanistic insights into electrochemical reduction of CO2 over Ag using density functional theory and transport models, https://www.pnas.org/doi/abs/10.1073/pnas.1713164114

[58] Richard E Zeebe and Dieter A Wolf-Gladrow, 2001, CO2 in seawater: equilibrium, kinetics, isotopes. Num- ber 65. https://sseh.uchicago.edu/doc/Zeebe_CO2_In_Seawater_Ch_1.pdf

[59] Helmut Vogt, 1983, Gas-evolving electrodes. In Comprehensive treatise of electrochemistry, https://link.springer.com/book/10.1007/978-1-4615-6690-8

[60] COMSOL https://doc.comsol.com/5.5/doc/com.comsol.help.cfd/cfd_ug_fluidflow_single.06.011.html

[61] Konderla, Vojtěch, 2022, Numerical modelling of a gas diffusion-based CO2 electrolyser with flowing catholyte, https://repository.tudelft.nl/islandora/object/uuid%3A1e62bbce-8c6c-4d83-819b-05eeadbdebdf